AD-A085 255 ARMY ENGINEER WATERWAYS EXPERIMENT STATION VICKSBURG--ETC F/G 18/3
FINITE-ELEMENT CALCULATIONS OF FOAM HEST 1.(U)
APR 80 J E WINDHAM
UNCLASSIFIED WES/MP/SL-80-1 NL

1 OF 2
AD
A085 255

LEVEL II

MISCELLANEOUS PAPER SL-80-1

FINITE-ELEMENT CALCULATIONS OF FOAM HEST 1

by

Jon E. Windham

Structures Laboratory
U. S. Army Engineer Waterways Experiment Station
P. O. Box 631, Vicksburg, Miss. 39180

April 1980
Final Report

Approved For Public Release; Distribution Unlimited

Prepared for Defense Nuclear Agency
Washington, D. C. 20305

Under DNA Subtask X99QAXSC062, Work Units 14 and 30, and
DNA H19HAXSX337, Work Unit 15

Destroy this report when no longer needed. Do not return it to the originator.

The findings in this report are not to be construed as an official Department of the Army position unless so designated by other authorized documents.

(14) WES/MP/SL-80-1

Unclassified
SECURITY CLASSIFICATION OF THIS PAGE (When Data Entered)

REPORT DOCUMENTATION PAGE

READ INSTRUCTIONS BEFORE COMPLETING FORM

1. REPORT NUMBER: Miscellaneous Paper SL-80-1
2. GOVT ACCESSION NO.: AD A085255
3. RECIPIENT'S CATALOG NUMBER:

(6) 4. TITLE (and Subtitle): FINITE-ELEMENT CALCULATIONS OF FOAM HEST 1.

(9) 5. TYPE OF REPORT & PERIOD COVERED: Final report. Oct 78-Feb 79

6. PERFORMING ORG. REPORT NUMBER:

(10) 7. AUTHOR(s): Jon E. Windham, Enrique

8. CONTRACT OR GRANT NUMBER(s):

9. PERFORMING ORGANIZATION NAME AND ADDRESS:
U. S. Army Engineer Waterways Experiment Station
Structures Laboratory
P. O. Box 631, Vicksburg, Miss. 39180

10. PROGRAM ELEMENT, PROJECT, TASK AREA & WORK UNIT NUMBERS: See Block 18

11. CONTROLLING OFFICE NAME AND ADDRESS:
Defense Nuclear Agency
Washington, D. C. 20305

(11) 12. REPORT DATE: April 1980

13. NUMBER OF PAGES: 116

14. MONITORING AGENCY NAME & ADDRESS (if different from Controlling Office):

(12) 121

15. SECURITY CLASS. (of this report): Unclassified

15a. DECLASSIFICATION/DOWNGRADING SCHEDULE:

16. DISTRIBUTION STATEMENT (of this Report):

Approved for public release; distribution unlimited.

(17) C062, X337

17. DISTRIBUTION STATEMENT (of the abstract entered in Block 20, if different from Report):

(16) X99QAXS, H19HAXS

18. SUPPLEMENTARY NOTES

The investigation reported herein was sponsored by the Defense Nuclear Agency (DNA) under Subtask X99QAXSC062, Work Unit 14, "Influence of Backfill on Structural Response," and Work Unit 30, "Shallow-Buried Structures." This report was published under DNA Subtask H19HAXSX337, Work Unit 15, "Buried Structures."

19. KEY WORDS (Continue on reverse side if necessary and identify by block number)

Backfills	Shallow buried structures
Finite element method	Simulation
Foam HEST I	Soil-structure interaction
HE explosions	Underground tests

62 ... 14

20. ABSTRACT (Continue on reverse side if necessary and identify by block number)

The results of analytical studies are presented in which the HONDO dynamic finite-element (FE) code was used to perform (1) a two-dimensional (2D), plane-strain calculation of the Foam HEST 1 test event, (2) a second 2D calculation identical with the first except that the backfill properties were changed from those of the sand used in Foam HEST 1 to those of a hypothetical low-strength clay, and (3) companion 1D calculations for a section through the backfill, a section through the center of the roof, and a section through

(continued)

DD FORM 1 JAN 73 1473 EDITION OF 1 NOV 65 IS OBSOLETE

Unclassified
SECURITY CLASSIFICATION OF THIS PAGE (When Data Entered)

411415

20. ABSTRACT (Continued)

the sidewall of the structure.

For locations in the backfill above and/or well away from the structure, vertical stress-time histories from the 2D calculation were in good agreement with those measured by the vertically-oriented stress gages in Foam HEST 1. The calculation also did a good job of replicating the intense 1-ms-duration initial loading pulse on the center of the roof as well as the early-time roof loading near the sidewalls.

Early-time particle velocity comparisons in the sand backfill were reasonably good, but the measurements after about 5 ms appear to have been significantly influenced by relatively compressible native soil materials beneath the backfill which were not modeled as such in the calculation. The calculated displacement of the center of the roof agrees very well with the measured response up to 8 ms; however, the calculated peak displacement was 3.4 cm at 12 ms, while the measured peak was approximately 20 cm at 35 ms.

The peak stress and impulse delivered to the center of the roof were higher for the clay backfill calculation than for the sand backfill calculation, Stress and impulse over the sidewall, however, were greater for the sand backfill case. The maximum relative deflection of the center of the roof for the clay backfill was 3.2 cm and occurred at 8.5 ms, while that for the sand was only 0.6 cm and occurred at 3.2 ms.

For shallow depths in the backfill, the agreement between 1D and 2D calculations of vertical stress was excellent for both sand and clay; for deeper locations in the clay, the 2D calculation histories were significantly altered by waves coming through the native soil ahead of those traveling directly through the backfill. For a 1D section through the center of the roof, stresses computed in both the sand and the clay backfills were in excellent agreement with the 2D results for at least 3 ms. For locations near the structure corners, however, results from 1D calculations can be misleading.

PREFACE

The investigation reported herein was sponsored by the Defense Nuclear Agency (DNA) under Subtask X99QAXSC062, Work Unit 14, "Influence of Backfill on Structural Response," and Work Unit 30, "Shallow-Buried Structures." This report was published under DNA Subtask H19HAXSX337, Work Unit 15, "Buried Structures."

The study was conducted by Dr. Jon E. Windham of the Geomechanics Division (GD), Structures Laboratory (SL), U. S. Army Engineer Waterways Experiment Station (WES), during the period October 1978-February 1979. Mr. John O. Curtis, GD, performed the calculations reported herein. The work was under the supervision of Dr. J. G. Jackson, Jr., Chief, GD. Chief of SL was Mr. Bryant Mather.

COL J. L. Cannon, CE, and COL N. P. Conover, CE, were Commanders and Directors of WES during the investigation and publication of this report. Mr. F. R. Brown was Technical Director.

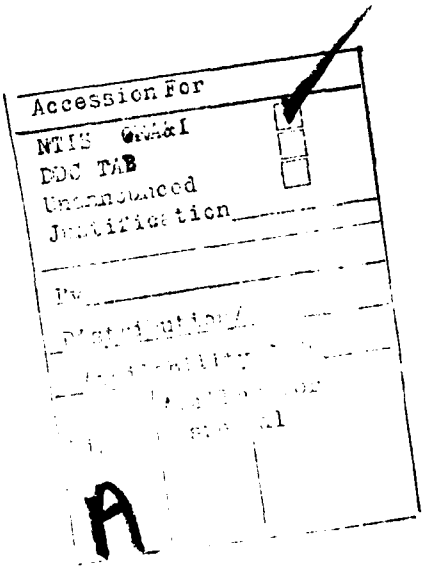

CONTENTS

LIST OF ILLUSTRATIONS

LIST OF TABLES

CONVERSION FACTORS, INCH-POUND TO METRIC (SI)
UNITS OF MEASUREMENT

Inch-pound units of measurement used in this report can be converted to metric (SI) units as follows:

Multiply	By	To Obtain
feet	30.48	centimetres
feet	0.3048	metres
feet per millisecond	0.3048	metres per millisecond
inches	2.54	centimetres
inch-pounds (force)	0.1129848	newton-metres
pounds (force)	4.448222	newtons
pounds (force) per square inch	6.894757	kilopascals
pounds (mass) per cubic foot	0.01601846	grams per cubic centimetre

FINITE-ELEMENT CALCULATIONS OF FOAM HEST 1

CHAPTER 1

INTRODUCTION

1.1 BACKGROUND

The Structures Laboratory of WES conducted Foam HEST 1, a high-explosive test of a shallow-buried, rectangular box structure, at a remote site near Fort Polk, Louisiana.[1] The test configuration is shown in Figure 1.1. The instrumentation locations for the test and additional structural details are shown in Figure 1.2. The backfill material was a dry, compacted commercial sand. The peak pressure in the cavity ranged from 1500 to 2400 psi* (103.4 to 165.5 bars) and resulted in a residual deflection of the center of the roof of 1/2 inch (1.27 cm) with respect to the corners of the structure.

The backfill/roof interface pressures measured by gages IF-1, IF-2, and IF-3 were particularly interesting. These gages measured the vertical stress in the soil directly above and adjacent to the structure roof; the measurements are shown in Figure 1.3. The maximum stresses for all three gages occur at essentially the same time, but after approximately 1 ms the stress over the center of the structure (IF-2) drops to 100 psi (6.9 bars) or less while the stresses measured over the roof near the sidewalls (gages IF-1 and IF-3) remain at the 300- to 900-psi (20.7- to 62.1-bar) level.

Two possible explanations were offered for this decrease in stress over the center of the roof span. The first explanation is that as the center of the roof deflects downward more than the sidewalls of the structure, vertical load is transferred from the area over the center of the roof span to the area over the sidewalls by arching. Since arching is predominantly a shear-related phenomenon, the time required to effect this load transfer is probably associated with the shear-wave velocity of the soil above the roof of the structure. The P-wave velocity of the backfill around the structure is approximately 1.6 feet/msec (0.5 metres/ms). Shear waves can generally be assumed to travel at one-half

* A table of factors for converting inch-pound units of measurement to metric (SI) units is presented on page 8.

the P-wave velocity; thus it would take an S-wave approximately 2.5 msec to travel the 2-foot distance from the center of the roof to the inside edge of the structure wall. But, as shown in Figure 1.3, the decrease in stress over the center of the roof has occurred as early as 0.7 msec after the peak stress occurs. Therefore, there is a question as to whether or not the observed stress decrease at this early time is due to arching.

A second explanation for the decrease in stress over the roof relates to one-dimensional (1D) wave-propagation phenomena or multiple reflection and refraction of waves trapped in the concrete roof slab between the soil backfill above and an air cavity below. The section through the center of the roof consists of 2.0 feet (0.61 metre) of sand over 0.5 foot (15.2 centimetres) of concrete over a free surface, i.e., air. Stress initially propagates from the blast-loaded surface through the sand and the concrete as a compression wave, hits the free surface at 2.5 feet (0.76 metre), and reflects upward as a tension wave (i.e., a relief of compressive stress), thereby reducing the stress over the center of the structure. By contrast, the section through the sidewall consists of 2 feet (0.61 metre) of sand over 5 feet (1.52 metres) of concrete which, in turn, rests on more soil. Since there is no free surface immediately below the interface to return a tensile wave, the compressive stress in the soil over the concrete remains relatively high for a longer period of time.

A series of 1D computer code calculations was conducted to investigate the postulated explanations.[2] The conclusions from this study were that 1D wave propagation can reasonably account for the phenomena seen in gages IF-1, IF-2, and IF-3, including the decrease in stress over the center of the structure up to a time of about 3 msec, but cannot account for either (1) the continued high stress (300-900 psi) maintained in the area above and near sidewalls or (2) the continued absence of stress at the center of the roof after a time of 3.5 msec. There is a possibility, therefore, that the loading on, and hence the response of, the structure is significantly influenced by both "late-time" effects produced by soil arching and "early-time" effects produced by wave interactions between materials with different impedances.

Assuming that the late-time buildup of stress over the structure corners and the absence of stress over the center of the roof were due to arching, the question is raised: What would the late-time stress distribution have been if a low shear strength clay backfill had been used in lieu of the relatively high shear strength sand backfill? It was postulated that less load would have been transferred away from the center of the roof.

1.2 PURPOSE AND SCOPE

Two 2D dynamic finite-element (FE) and six 1D dynamic FE calculations were performed with the HONDO code[3,4,5] to analytically assess the loads transmitted to the structure for the Foam HEST 1 environment. Calculation details, including the surface overpressure loading, material models, FE grid, time step and frequency transmission, etc., are given in Chapter 2. The first 2D calculation was a calculation of the Foam HEST 1 test and was conducted primarily to establish credibility of the calculation technique. The calculation results are compared with those from the experiment in Chapter 3. The second was a similar calculation, except that properties of a low shear strength clay backfill were substituted for those of the sand backfill actually used in the test. The stresses produced in the backfill and the loads transmitted to the structure are compared for these two calculations in Chapter 4. Three companion 1D code calculations were made for each 2D calculation in an attempt to separate 1D (early-time wave-propagation) and 2D (late-time) phenomena. The 1D calculations were conducted for a section through the backfill, a section through the center of the roof, and a section through the sidewall of the structure; results are given in Chapter 5.

Appendix A describes the analyses used to determine properties of the concrete structure for the 2D calculations. The results of a testing program to determine the properties of the soil materials and the properties recommended for use in the 2D calculations are presented in Appendix B. Cap model fits to these recommended properties are presented in Appendix C.

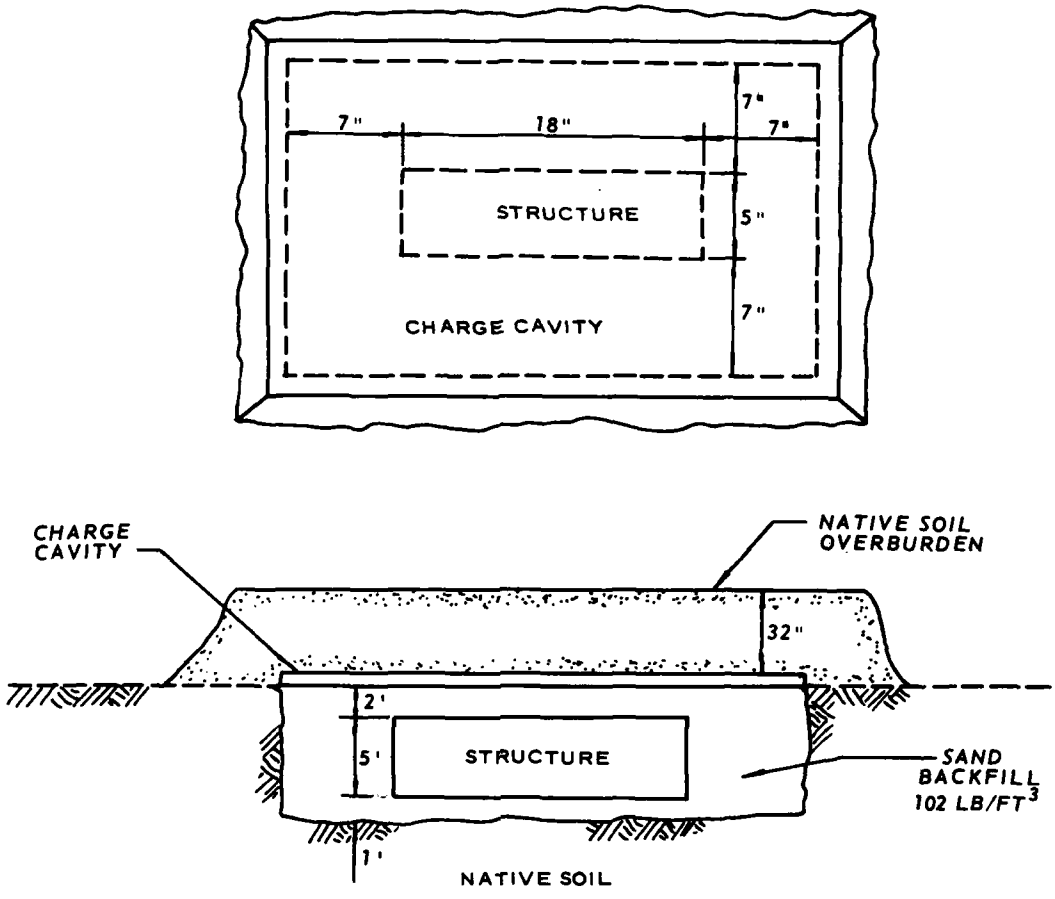

Figure 1.1 Foam HEST 1 test configuration.

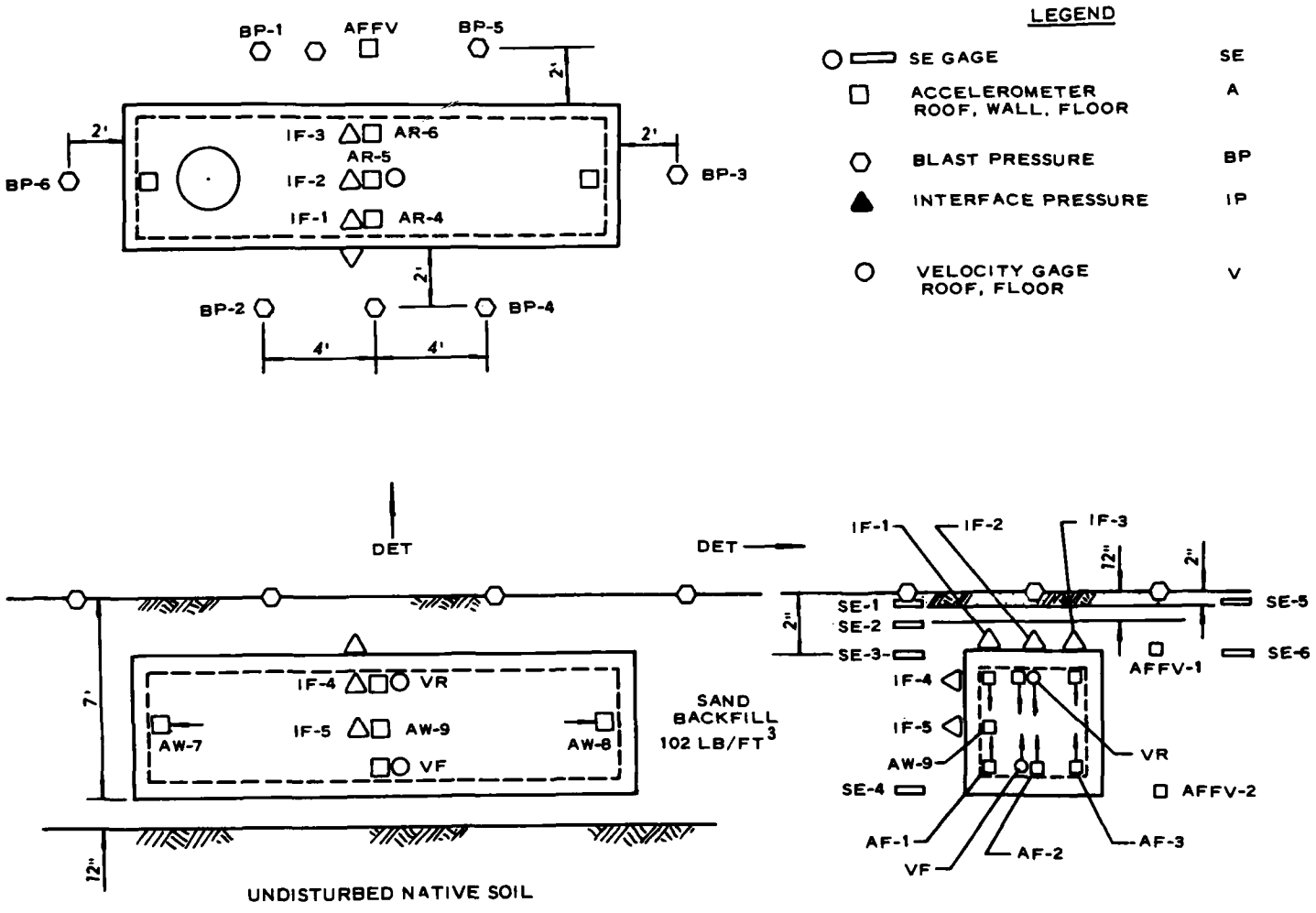

Figure 1.2 Structure details and instrumentation layout.

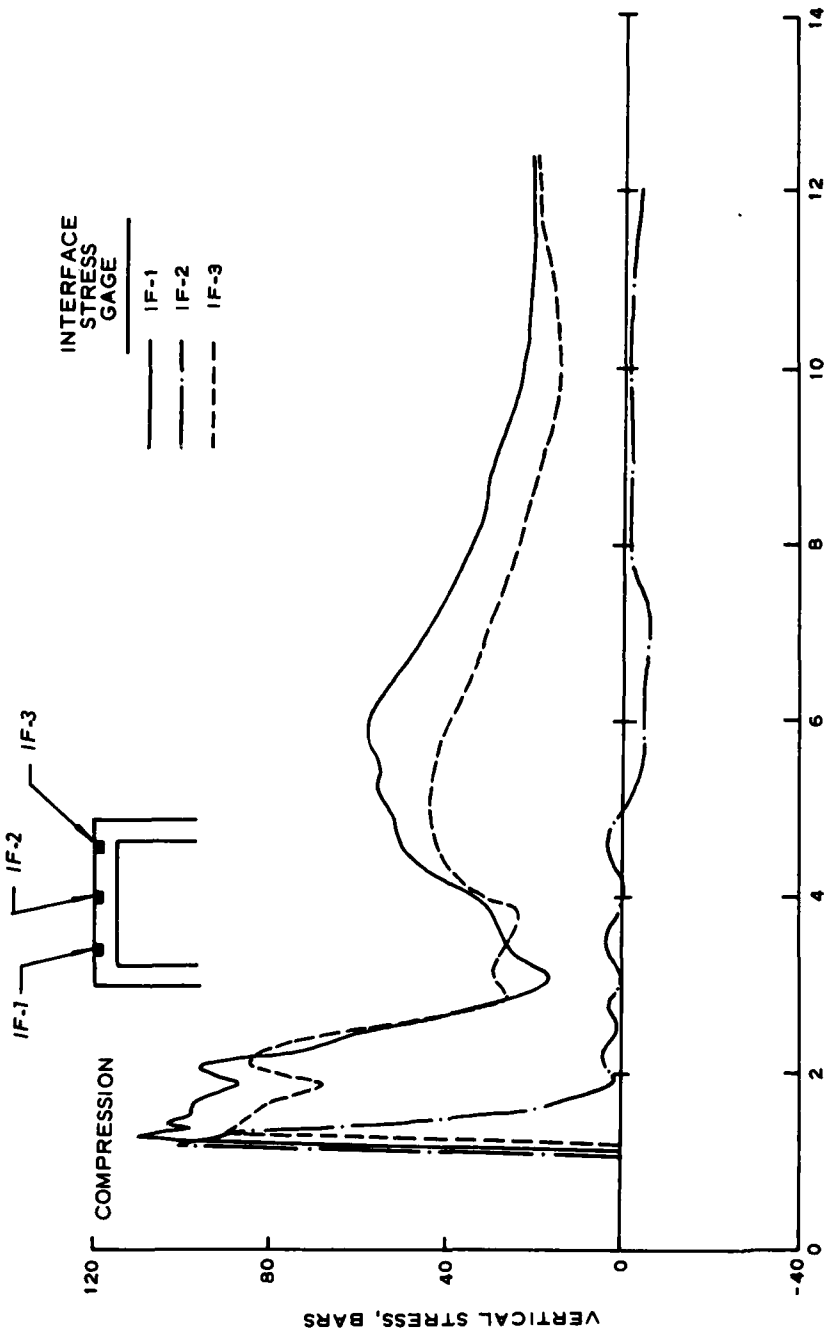

Figure 1.3 Stress-time histories from interface stress gages on roof.

CHAPTER 2

DESCRIPTION OF THE CALCULATIONS

2.1 FINITE-ELEMENT GRID

All calculations were performed on a CDC 7600 computer with the HONDO dynamic FE code. The FE grid that was employed in the 2D problems is shown in Figure 2.1 and consisted of 5316 constant-strain rectangular elements. The problem was assumed to be symmetric about a vertical centerline through the structure; therefore, only half of the problem was calculated. A boundary condition of radial displacements equal to zero was applied at the axis of symmetry. The elements located in the backfill directly above the structure are 1.0-inch (2.54-centimetre) square elements. The elements located in the remainder of the backfill and in the structure are 1.5-inch (3.81-centimetre) square elements. The elements located in the free-field are 6-inch (15.24-centimetre) square elements. Slide lines were used along the interfaces where mismatches in elements occurred. The slide lines were tied; i.e., no slip was allowed along the slide lines. The grid was chosen because of the desire for fine resolution. The FE grids for the 1D problem were based on vertical sections through the 2D grid, as shown in Figure 2.2.

2.2 SURFACE OVERPRESSURE

The surface overpressure was taken as an average of that measured by blast pressure gages BP-2 and BP-3 in the Foam HEST 1 test. The maximum pressures measured by these gages were 103.3 and 137.9 bars, respectively; a third airblast gage, BP-5, recorded a peak pressure of 165.5 bars but was not used in these analyses. The airblast applied during the Foam HEST 1 test was actually traveling across the backfill section at 20 feet/ms (6.1 metres/ms). The surface loading was applied as a standing overpressure-time relation in the calculations and is shown in Figure 2.3. This overpressure-time history was applied uniformly at the surface of the backfilled area shown in Figure 2.1. The rise time t_r to a peak stress of 120 bars was 0.14 ms, dictating a

loading rate of 857 bars/ms. The oscillations after the first peak are due to reflections in the HEST cavity. The duration of each of the calculations was 15 ms. At 15 ms the surface overpressure from the airblast input was approximately 6 bars.

2.3 MATERIAL PROPERTIES FOR STRUCTURE

The structure is covered by 2 feet (0.61 metre) of backfill and is supported on a 1-foot (0.30-metre) layer of backfill at a depth of 7 feet (2.13 metres); the square structure has outside dimensions of 5 feet (1.52 metres). Its roof and floor are 6 inches (15.24 centimetres) thick. The actual structure in the Foam HEST 1 test had outside dimensions of 4.93 feet (1.5 metres) and wall thicknesses of 5.6 inches (14.22 centimetres). The exterior structure elements are treated as being fully bonded to those of the backfill. The structure is treated as an elastic-plastic material with a modulus of elasticity (E) of 4.2×10^6 psi (2.9×10^5 bars) and a Poisson's ratio ν of 0.25. The limiting value of elastic stress f_y is 3500 psi (241 bars). Appendix A presents the results of analyses to determine the properties of the structure. The value of E (2.9×10^6 bars) was made compatible with a natural period of 6.7 ms measured in a forced vibration test of the structure in an uncovered condition.[6] The yield value (241 bars) was selected to correspond with the ultimate thrust and moment conditions at failure from a static test on a structure one-half the size of the one tested in the Foam HEST 1 test.[7] A strain-hardening parameter of 1000 psi (69 bars) was used in the plastic region to minimize numerical instability problems.

2.4 RECOMMENDED SOIL PROPERTIES

The commercial sand used as backfill in the Foam HEST 1 test classifies as a poorly graded sand, SP, according to the Unified Soil Classification System.[9] The average dry unit weight and water content after placement were 1.63 gm/cc and 3.2 percent, respectively. Uniaxial strain tests with loading rates of approximately 0.002 bar/ms (static),

15 bars/ms, and 295 bars/ms were conducted on this sand. No appreciable increase in stiffness was observed for specimens tested at loading rates of 15 bars/ms. However, when specimens were subjected to loading rates of 295 bars/ms, the stiffness of the stress-strain relation increased by a factor of 4 or more. A series of 1D calculations was conducted for a section through the structure roof using the surface airblast shown in Figure 2.2 and the UX stress-strain relations from the various laboratory tests. The calculated vertical stress delivered to the roof of the structure was compared with that measured by interface stress gage IF-2. None of the UX stress-strain relations gave good results. The best agreement between calculated and measured results was obtained when a linear UX stress-strain loading relation with a modulus of 62 ksi (4278 bars) was used to represent the sand backfill. This modulus was calculated from times of arrival on the SE gages which indicated the initial stress was traveling at a speed of 1.65 feet/ms (0.5 metre/ms). Therefore, a UX stress-strain relation with a modulus of 62 ksi (4278 bars/ms) was recommended for the sand backfill.

Undisturbed samples of the native site materials adjacent to and beneath the structure excavation were not available; properties for these regions of the calculations were thus assumed to be identical to those of the sand backfill. The backfill properties for the hypothetical clay calculations were based on backfill encountered in Project HARD PAN. The HARD PAN backfill classifies as a plastic clay (CH) according to the Unified Soil Classification System; compaction to a dry density of 1.54 gm/cc at a water content of 20.7 percent requires about 97 percent of Standard Proctor effort. Available test data on the HARD PAN backfill[10] and other clay data with relevant rate effects information[11] were used to develop the clay backfill property recommendations.

The test data and analyses used to develop property recommendations for the three soil materials described above are documented in Appendix B.

2.5 SOIL MATERIAL MODELS

Mechanical response of the soil materials was simulated by a nonlinear elastic/nonideally plastic (cap) model.[8] The equations are given in Appendix C along with coefficient values used to fit the model to the sand and clay backfills. A comparison of UX stress-strain relations generated with the model for these two materials is shown in Figure 2.4. Initial constrained moduli from the fits are 4262 and 940 bars for the sand and clay, respectively. Wet density values of 1.63 and 1.54 gm/cc were inadvertently programmed in lieu of the recommended values of 1.69 and 1.86. Initial P-wave arrivals at various nodes in the calculations are thus based on C_P values of 1.678 feet/ms for the sand and 0.811 feet/ms for the clay. UX stress paths are compared in Figure 2.5. Initial shear moduli are 1174 and 182 bars so S-wave arrivals in the calculations are associated with C_S values of 0.880 feet/ms for the sand and 0.357 feet/ms for the clay. Failure surfaces derived from model simulations of TX shear tests are compared in Figure 2.6. The sand can sustain a maximum principal stress difference of approximately 70 bars under a mean normal stress of 100 bars, whereas the maximum principal stress for the clay can never exceed 10 bars.

2.6 TIME INCREMENT AND FREQUENCY TRANSMISSION

Each calculation was run for 1500 time steps of 0.01 ms each. This time step was chosen to satisfy the Courant criteria* and was controlled by the minimum FE dimension and P-wave velocity within the concrete structure. The lowest frequencies that can be fully transmitted are given by the reciprocal of the airblast loading pulse duration, i.e., 1/15 ms or 66.7 Hz. The lowest frequency for a symmetric structure mode in the uncovered condition was determined to be 150 Hz by a forced

---

* $$\Delta t \leq \frac{\Delta X_{min}}{C_{P_{max}}} \leq \frac{0.125 \text{ feet}}{12.4 \text{ feet/ms}} = 0.01008 \text{ ms}.$$

vibration test[6] and by a 2D modal analysis.* The indication from previous calculations of this type is that the effect of embedment of a structure has a very minimal effect on the frequency response of a structure.[12] Thus, the duration of the calculations was long enough to permit peak displacement responses in the lowest mode of the system.

The highest frequencies that can be fully transmitted cannot exceed the reciprocal of the loading rise time, i.e., 1/0.14 ms or 7140 Hz. As a practical matter, however, credible frequencies probably did not exceed one-half of this value or approximately 3500 Hz. The FE grid for the backfill material above the structure can transmit frequencies up to 6300 Hz based on the formula

$$f_{max} = \frac{C_{P_{min}}}{\pi \Delta X_{max}} \qquad (2.1)$$

By similar calculation the clay backfill above the structure can transmit frequencies up to 3200 Hz. Thus the cutoff frequencies for calculating the response of the roof were assumed to be on the order of 3500 Hz for the sand backfill calculation and 3200 Hz for the clay backfill calculation. The sand and clay backfills on the sides and beneath the structure can transmit frequencies of 4200 Hz and 2140 Hz, respectively, and the free-field material can transmit frequencies of 1050 Hz. The wave speeds and frequency contents for the various zones are shown in Table 2.1.

The modal analyses presented in Appendix A gave a 10th-mode frequency of 882.3 Hz. Thus, the calculations were judged to have a sufficient range of frequency response to permit an adequate assessment of the stress and motion patterns that would occur within the structure/backfill system under the Foam HEST 1 airblast loading environment. Based on the wave speeds given in Table 2.1, reflections from the bottom boundary reached the bottom of the structure at times of approximately

---

* See Appendix A.

7.5 and 9.4 ms in the sand and clay backfill calculations, respectively. Although the quantitative effect of these boundary reflections is difficult to assess and will differ depending on output type, time, and location, any comparisons at times later than those indicated above should be made with some caution.

Table 2.1 Wave Speeds and Frequency Content

Material Type	Initial Loading P-wave Velocity C_{P_i} ft/ms	Maximum P-wave Velocity $C_{P_{max}}$ ft/ms	Initial Loading S-wave Velocity C_{S_i} ft/ms	Maximum S-wave Velocity $C_{S_{max}}$ ft/ms	Frequency Content* Preserved		
					1.0-in. Element Hz	1.5-in. Element Hz	6-in. Element Hz
Sand backfill	1.68	4.05	0.88	2.37	6300	4200	1050
Clay backfill	0.81	5.97	0.36	0.36	3200	2140	1050+
Undisturbed soil	1.68	4.05	0.88	2.37	6300	4200	1050
Concrete	12.4	12.4	7.20	7.20	--	13000	--

* $$f_{max} = \frac{C_{P_{min}}}{\pi \Delta X_{max}} .$$

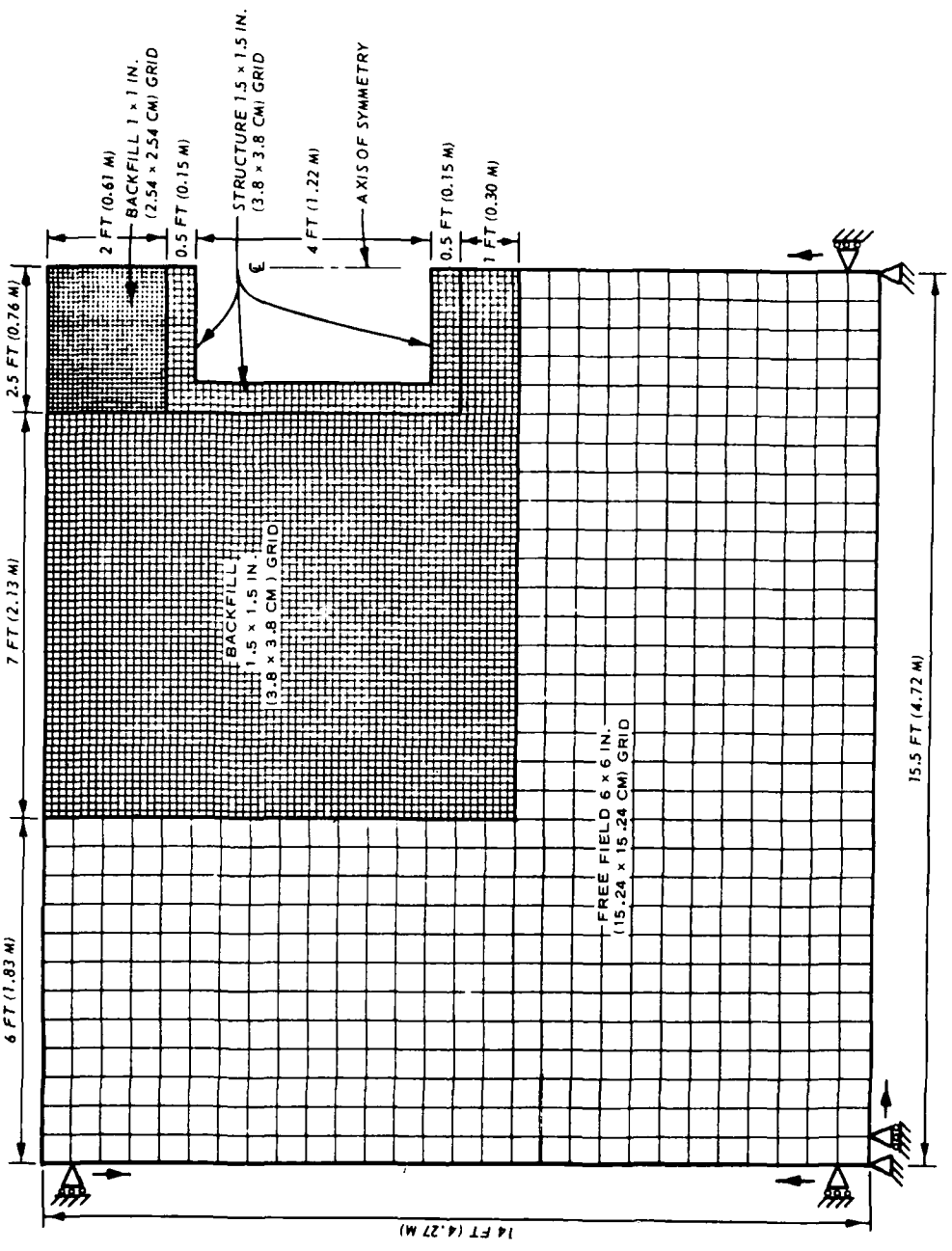

Figure 2.1 Geometry for 2D finite-element calculations.

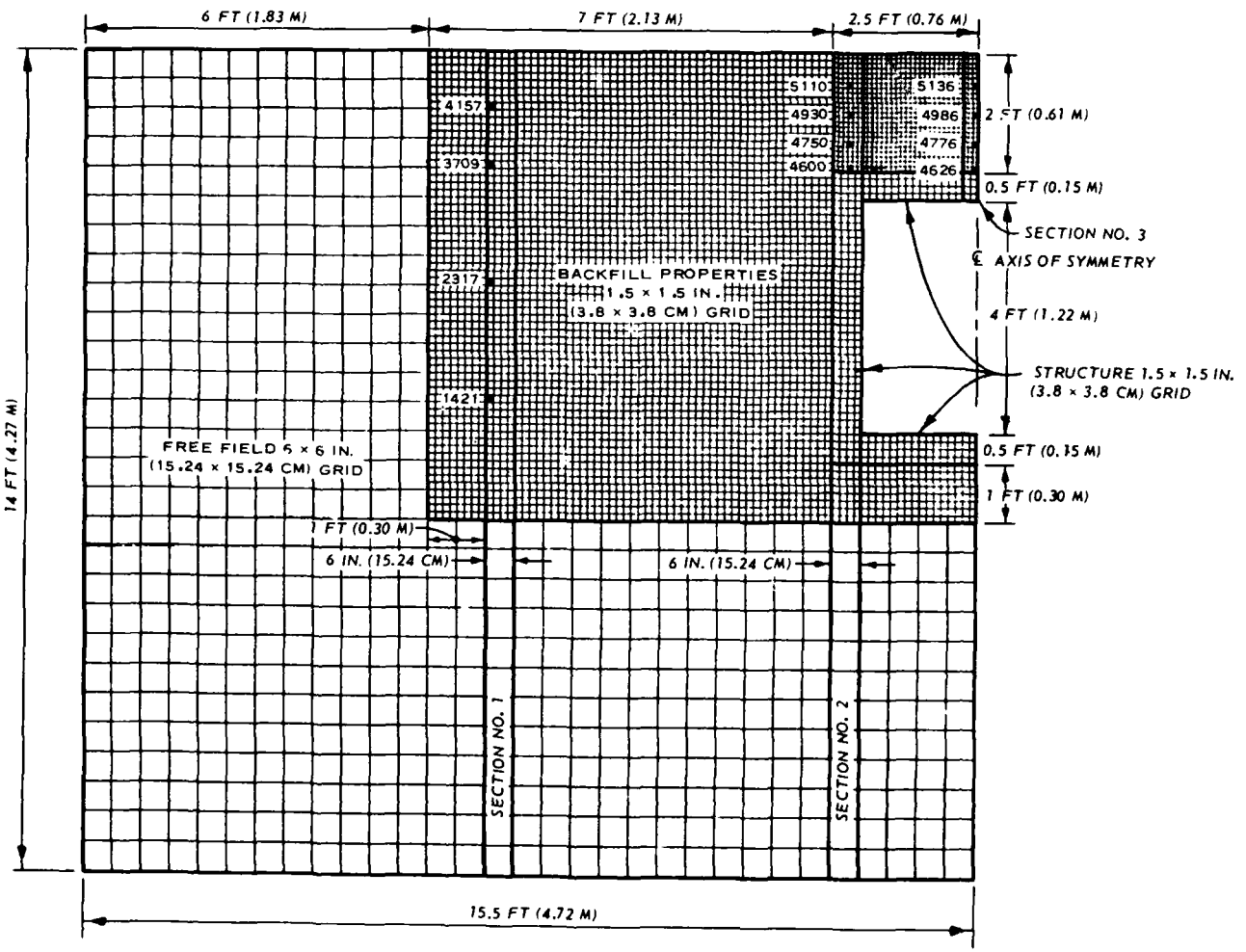

Figure 2.2 Geometry for 1D calculations and locations with respect to 2D finite-element geometry.

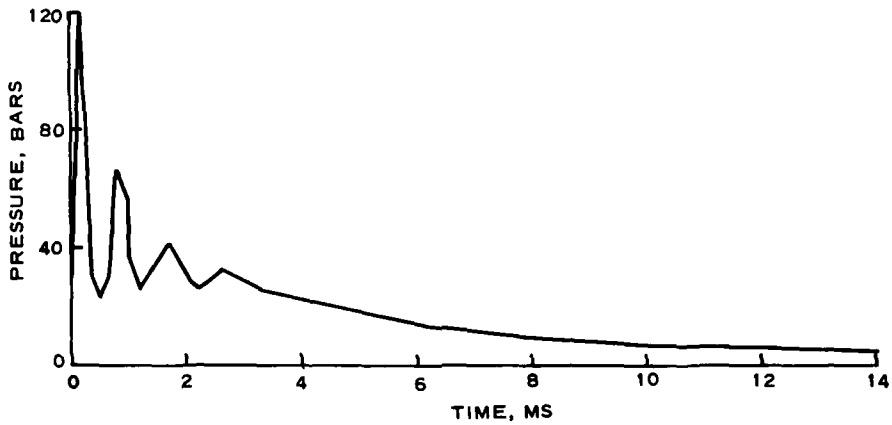

Figure 2.3 Airblast loading for calculations.

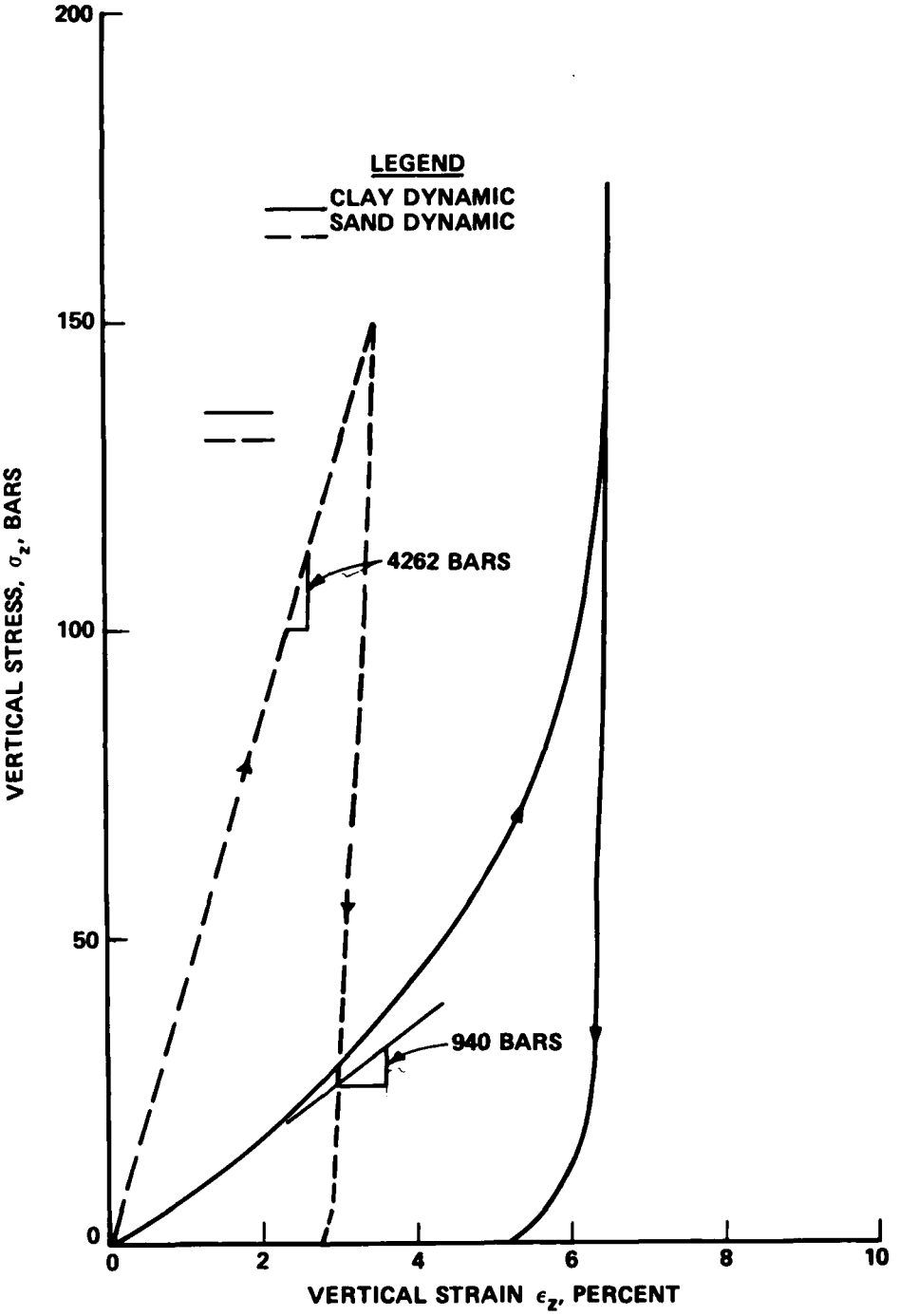

Figure 2.4 Comparison of the UX stress-strain curves for clay and sand produced by the constitutive model.

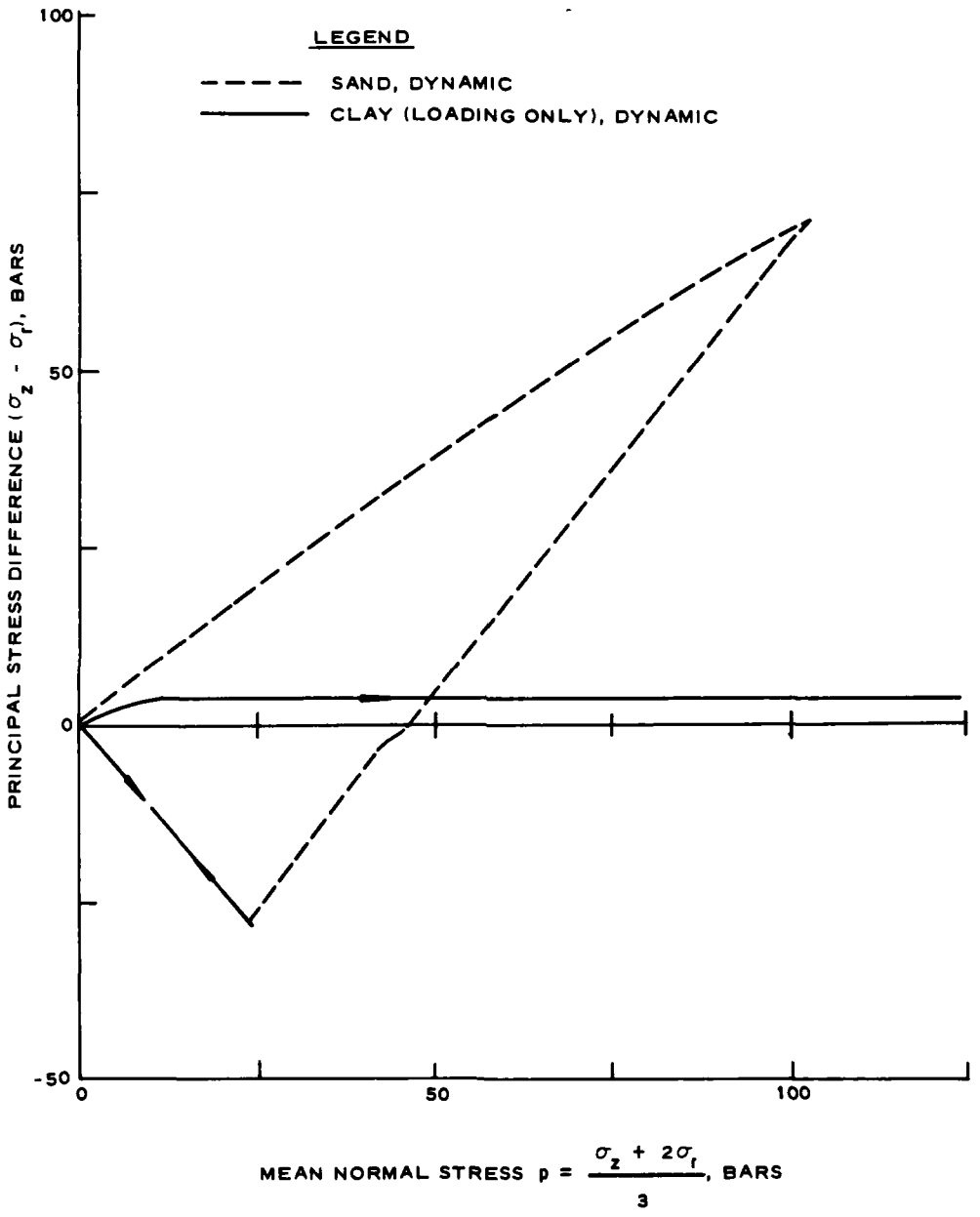

Figure 2.5 Comparison of the UX stress paths for clay and sand produced by the constitutive model.

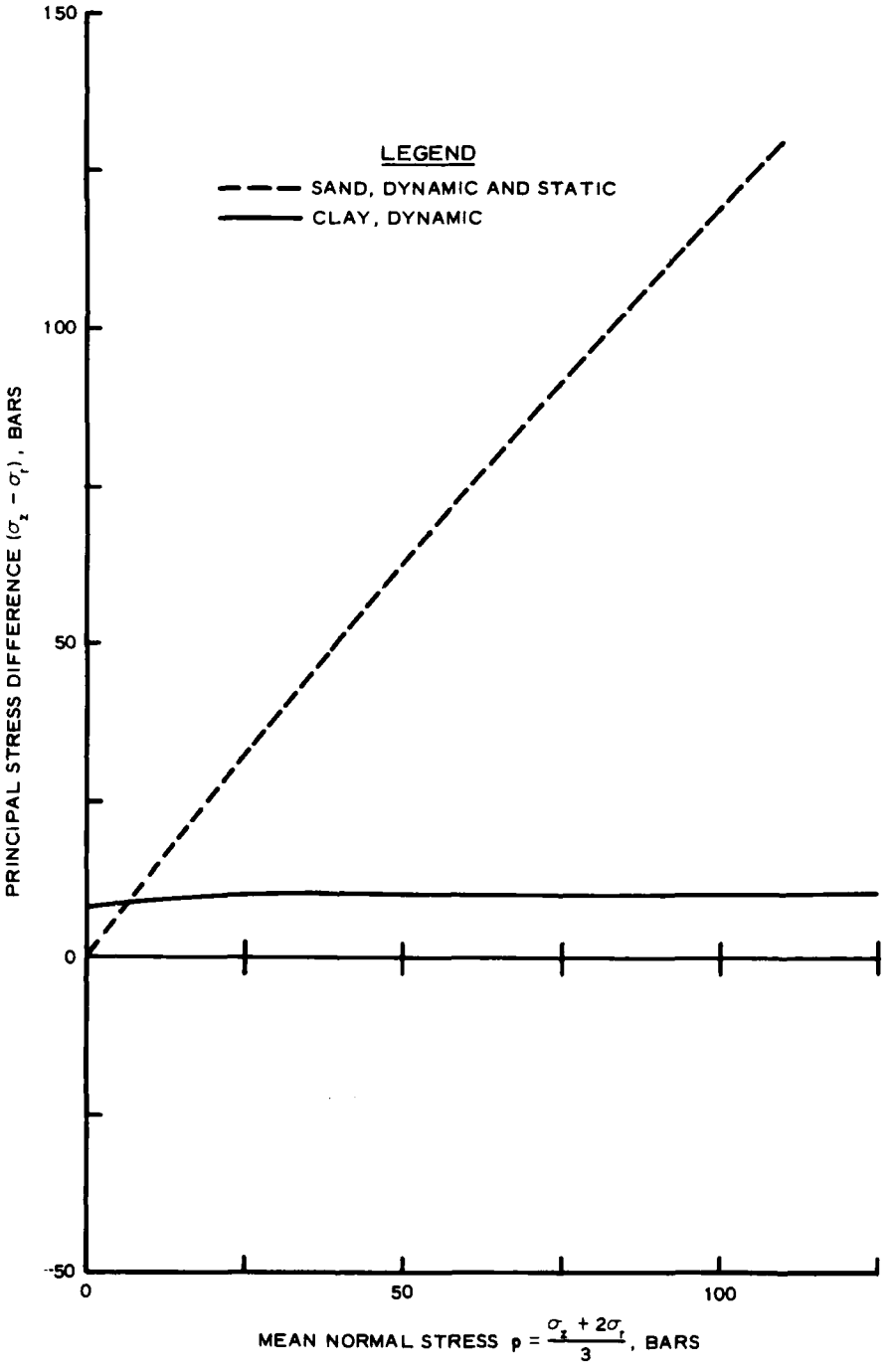

Figure 2.6 Comparison of the TX failure surfaces for clay and sand produced by the constitutive model.

CHAPTER 3

COMPARISON OF FOAM HEST 1 CALCULATION WITH EXPERIMENTAL RESULTS

The results from the 2D calculation of Foam HEST 1 are compared in this chapter with the experimental results. As discussed in Section 2.6, artificial boundary reflections may have influenced the calculational results after about 8 ms; the comparisons shown in this chapter are limited, therefore, to this period of time.

3.1 STRESS-TIME HISTORY COMPARISONS

A comparison of the vertical stress-time history at a location 2 feet (0.61 metre) below the ground surface and 6 feet (1.83 metres) horizontally from the structure is presented in Figure 3.1. The comparison of the calculated and measured arrival times and general character of the stress-time histories are excellent. The measured peak stress of 68 bars is approximately 40 percent higher than that calculated. This 40 percent difference in calculated and measured peak stresses is within the range of overregistration previously observed in SE gage measurements.[13] Or the difference may be associated with the surface overpressure. The maximum airblast pressure in the calculation was 120 bars (1740 psi). The peak airblast pressure measurements made for the Foam HEST 1 event, however, ranged from 103.4 bars to 165.5 bars (1500 to 2400 psi).[1] If an applied airblast loading with a larger peak pressure had been used, the agreement would have been much better.

Figure 3.2 shows a comparison of calculated and measured vertical stresses at the 1-foot (0.30-metre), 2-foot (0.61-metre), and 7-foot (2.13-metre) depths at a horizontal distance of 2 feet (0.61 metre) from the structure sidewall. The arrival-time agreement is very good at the 0.30- and 0.61-metre depths. However, at the 2.13-metre depth the vertical stress is arriving much faster in the calculation than in the experiment and sooner than possible if traveling only through backfill with a wave speed of 1.68 feet/ms (0.51 metre/ms). The calculated time of arrival is 2.8 ms and coincides with the time that is required for a

stress wave to travel vertically through 2 feet of backfill above the structure at 1.68 feet/ms, 5 feet of concrete (i.e., through the sidewall) at 12.4 feet/ms, and horizontally through 2 feet of backfill at 1.68 feet/ms. The initial vertical stress produced in the calculation was caused by a Poisson effect upon this horizontal stress wave. Since an SE gage only measures stress in one direction, the first significant signal sensed by the vertically-oriented gage occurred at 4.2 ms, which corresponds with the time required for a 1.65-foot/ms wave to travel 7 feet.

The vertical stress measured on the center of the structure roof (gage IF-2) is compared with the calculated stress in Figure 3.3. Although the calculated peak stress is again less than the measured peak, overall agreement between measured and computed results is very good. The measured stress goes to zero at approximately 5.15 ms while the calculated stress remains constant at approximately 6 bars after this time, which generally agrees with the airblast overpressure during this period of the calculation. This difference between the measured and calculated stresses after the first pulse, i.e., after 2 ms, is probably due to the fact that the soil was bonded to the concrete in the calculation while the soil is free to separate in the experiment.

A comparison of the vertical stresses measured near the sidewalls by roof interface stress gages IF-1 and IF-3 and calculated at the same location (Element 4604) is shown in Figure 3.4. The calculated maximum stress is less than the measured stresses; possible causes for this have already been discussed. The character of the calculated and measured stress-time histories is the same up to a time of 2.3 ms but is distinctly different after this time; the causes for this late-time difference in wave character are not readily apparent.

3.2 MOTION-TIME HISTORY COMPARISONS

Acceleration measurements were made in the sand backfill 2 feet from the sidewall of the structure at depths of 2 feet and 7 feet by accelerometers AFFV-1 and AFFV-2, respectively. The velocity-time history determined by integrating the AFFV-1 record is compared for 8 ms of time in Figure 3.5 with the calculated velocity-time history for this location. The 40 percent difference between the measured peak particle velocity and the calculated peak is consistent with the peak stress comparisons for the 2-foot depth previously shown in Figures 3.1 and 3.2; this suggests that underprediction of the peak surface overpressure applied in the calculation may be responsible for the discrepancy rather than overregistration of the stress gages placed in the experiment.

Figure 3.6 shows velocity comparisons for the 7-foot depth. The measured velocity starts to decay after its initial peak but then indicates a second downward surge. The timing of this surge appears to correlate with a tensile relief wave generated at the bottom of the 8-foot-deep excavation by a material with a lower impedance than the sand backfill. The sharp decay in the record for SE gage 4 at this same time (see Figure 3.2) tends to confirm this hypothesis as does the sharp velocity increase noted in Figure 3.5 at 7 ms, about the right time for this relief wave to reach the 2-foot depth. Reflections off the floor of the excavation were not produced in the calculation since the properties of the undisturbed soil materials surrounding the excavation were assumed to be identical to those of the sand backfill.

Displacement comparisons also support the "soft foundation" hypothesis. For example, accelerometer data indicate a maximum displacement of approximately 18 cm at the 2-foot depth and in excess of 12 cm at the 7-foot depth, whereas the calculation depicted maximum displacements of approximately 2.5 cm and 2 cm at these depths. The downward displacements in the calculation reached a maximum at 12-13 ms while those from the doubly integrated accelerometers maximized at times of 40 ms or greater.

Figure 3.7 compares the calculated downward displacement of the center of the roof of the structure with the displacement obtained by doubly integrating accelerometer AR-5 for 8 ms. The calculated and measured displacements agree very well up to this time; however, the calculated displacement reached a maximum of 3.4 cm at 12 ms while the measured maximum displacement was approximately 20 cm at 35 ms. Figure 3.8 compares the calculated deflection of the center of the roof with the calculated deflection of the bottom corner of the structure. The calculated maximum relative deflection between these two points was 0.6 cm and occurred at a time of 3.2 ms. Based on accelerometer measurements located near the two bottom corners (AF-1 and AF-3) and at the center of the roof (AR-5), the maximum relative deflection was 3.8 to 7.6 cm and occurred at a time of 25 to 35 ms. The posttest relative deflection was measured as 1.27 cm.

Although the FE calculation was not designed to simulate structural loadings and response beyond a time of approximately 8 ms, the obviously large discrepancies between calculated and measured maximum motions at later times indicate that more attention should have been given to the properties used to describe the undisturbed soil materials beneath the excavation. A better model for the reinforced concrete structure would probably help also, but neither the problem nor the solution is as obvious as with the native soils

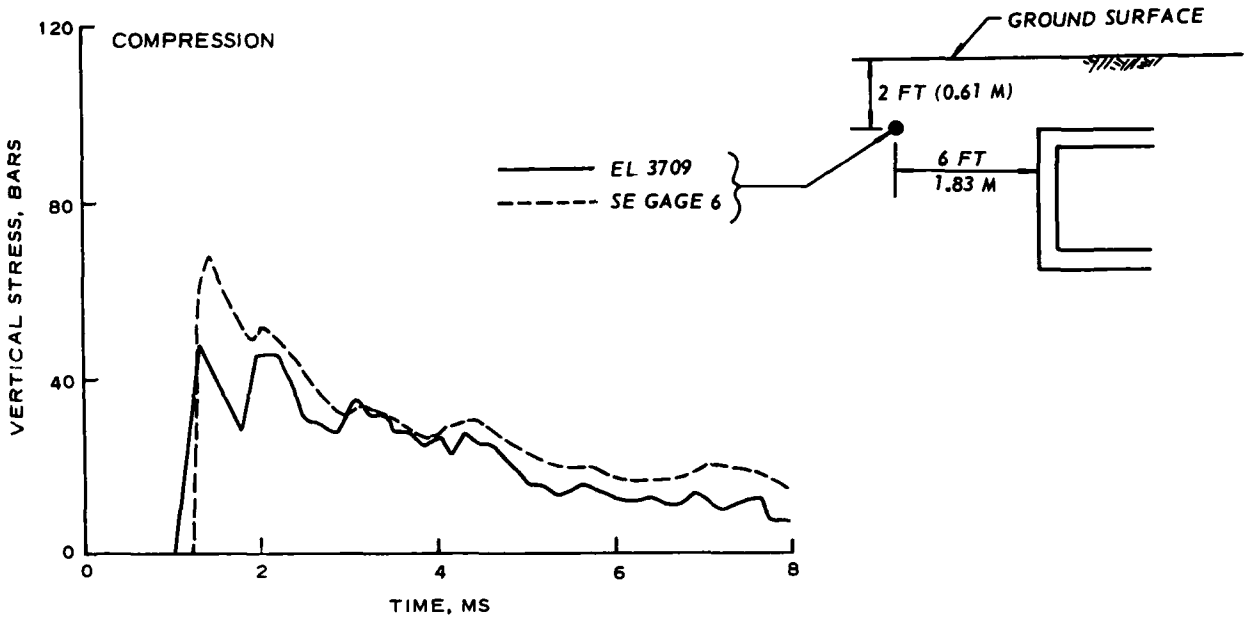

Figure 3.1 Comparison of measured and calculated vertical stress-time histories in the sand backfill at the 2-foot (0.61-metre) depth and 6 feet (1.83 metres) horizontally from the structure.

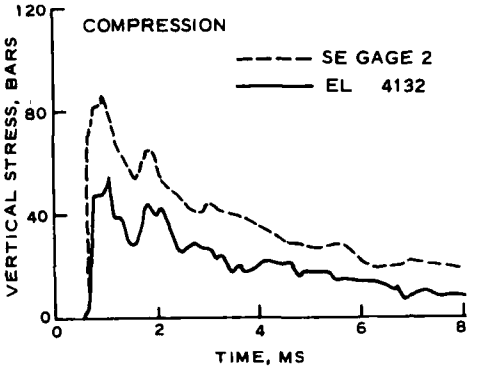

a. 1 FT (0.3 M) DEPTH

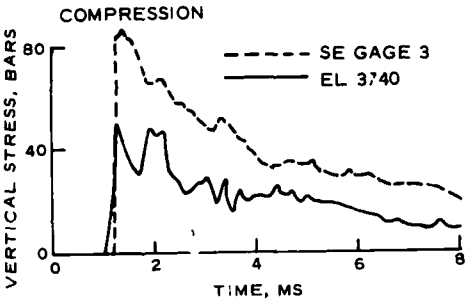

b. 2 FT (0.61 M) DEPTH

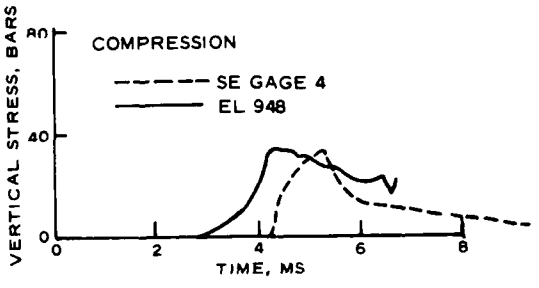

c. 7 FT (2.13 M) DEPTH

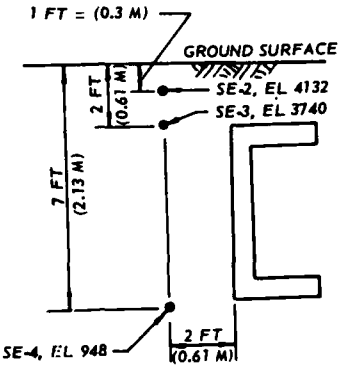

Figure 3.2 Comparison of calculated and measured vertical stress-time histories in the sand backfill at locations 2 feet (0.61 metre) horizontally from the structure and at depths of 1 foot (0.30 metre), 2 feet (0.61 metre), and 7 feet (2.13 metres).

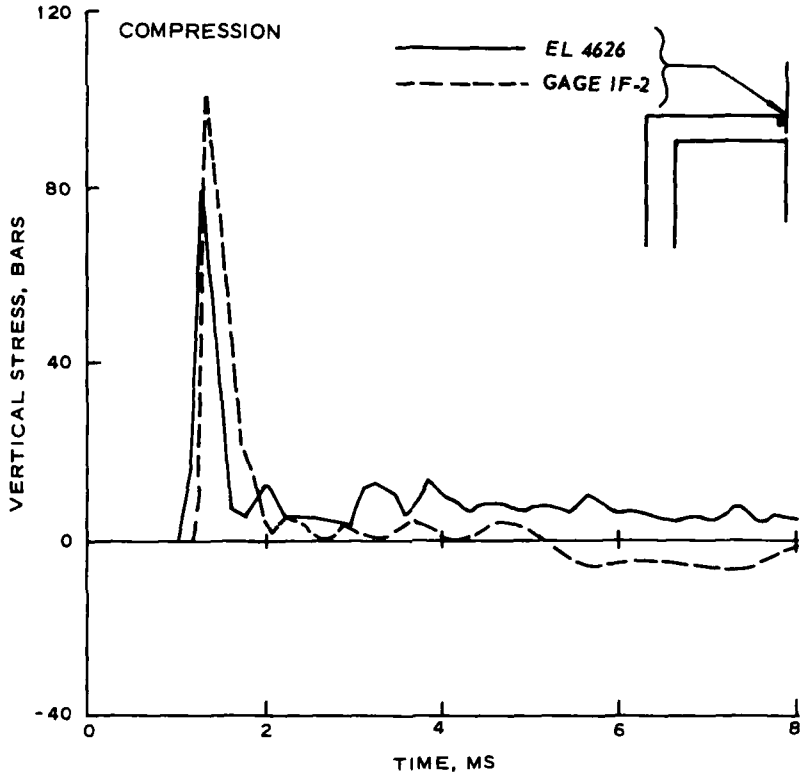

Figure 3.3 Comparison of calculated and measured vertical stress-time histories at the center of the structure roof.

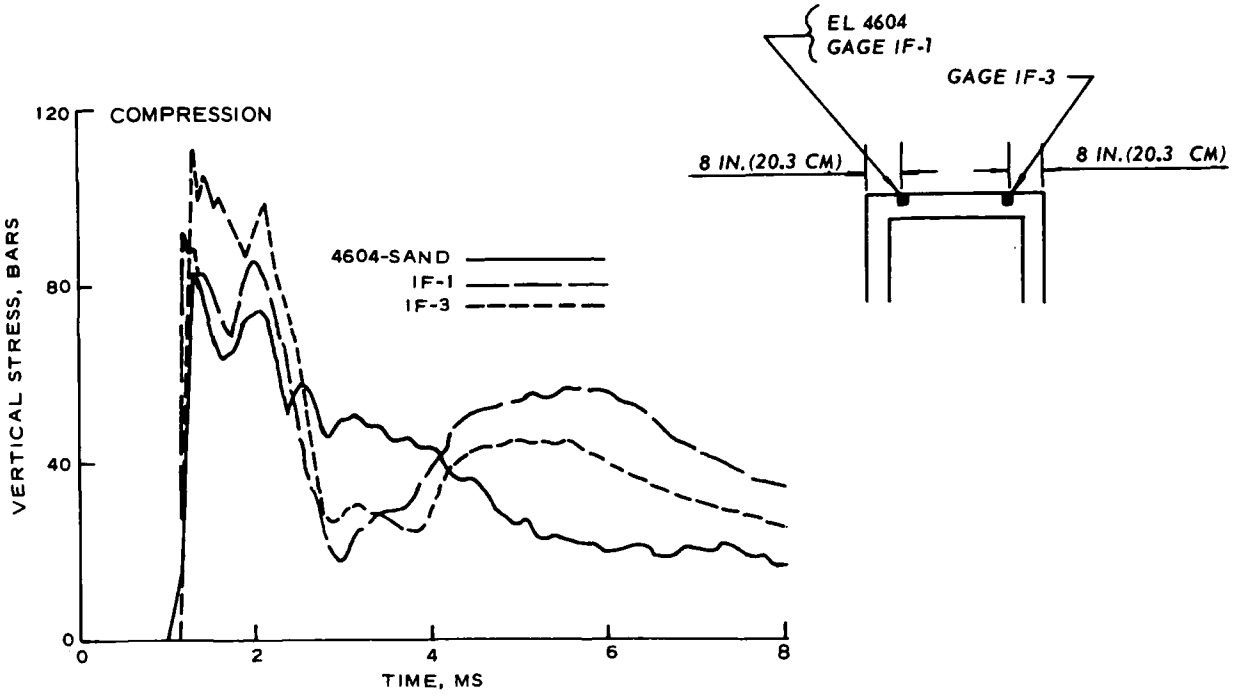

Figure 3.4 Comparison of calculated and measured vertical stress-time histories on the structure roof at locations 8 inches (20.3 cm) from the corner of the structure.

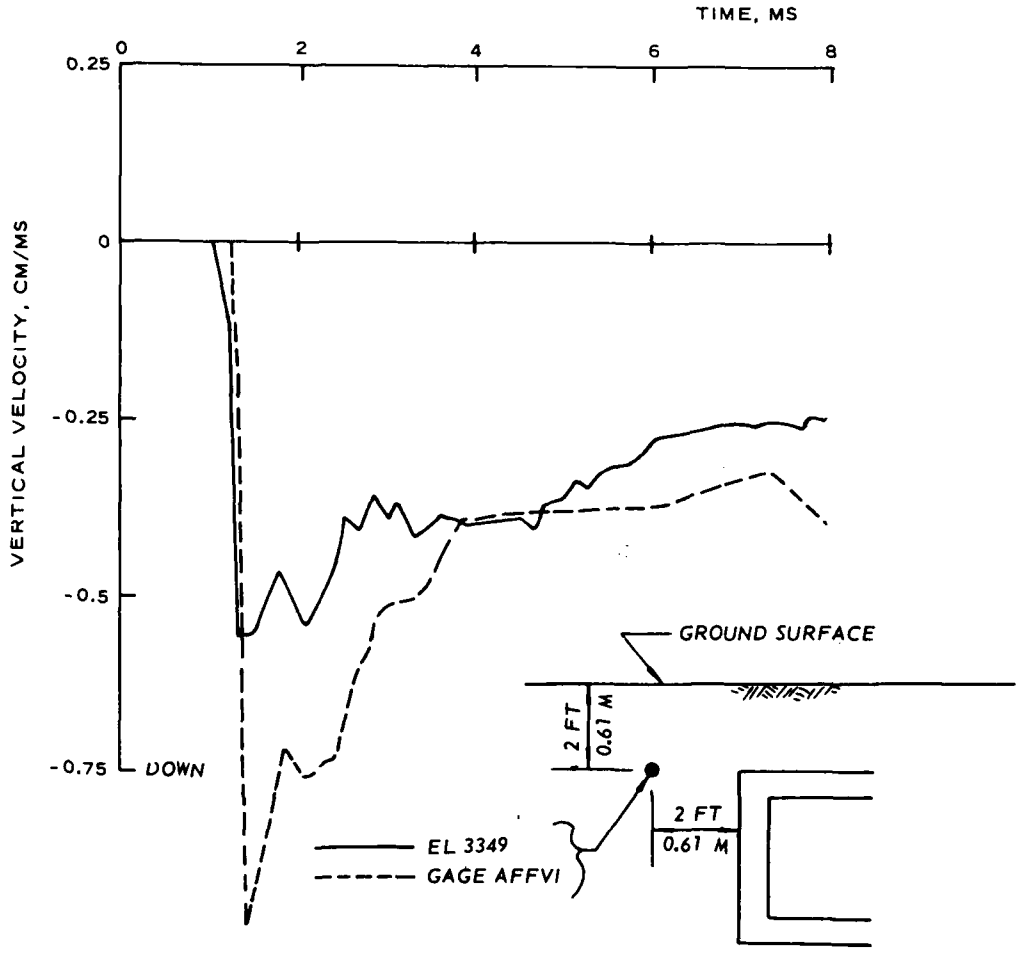

Figure 3.5 Comparison of calculated and measured vertical velocity-time histories in the sand backfill at the 2-foot (0.61-metre) depth.

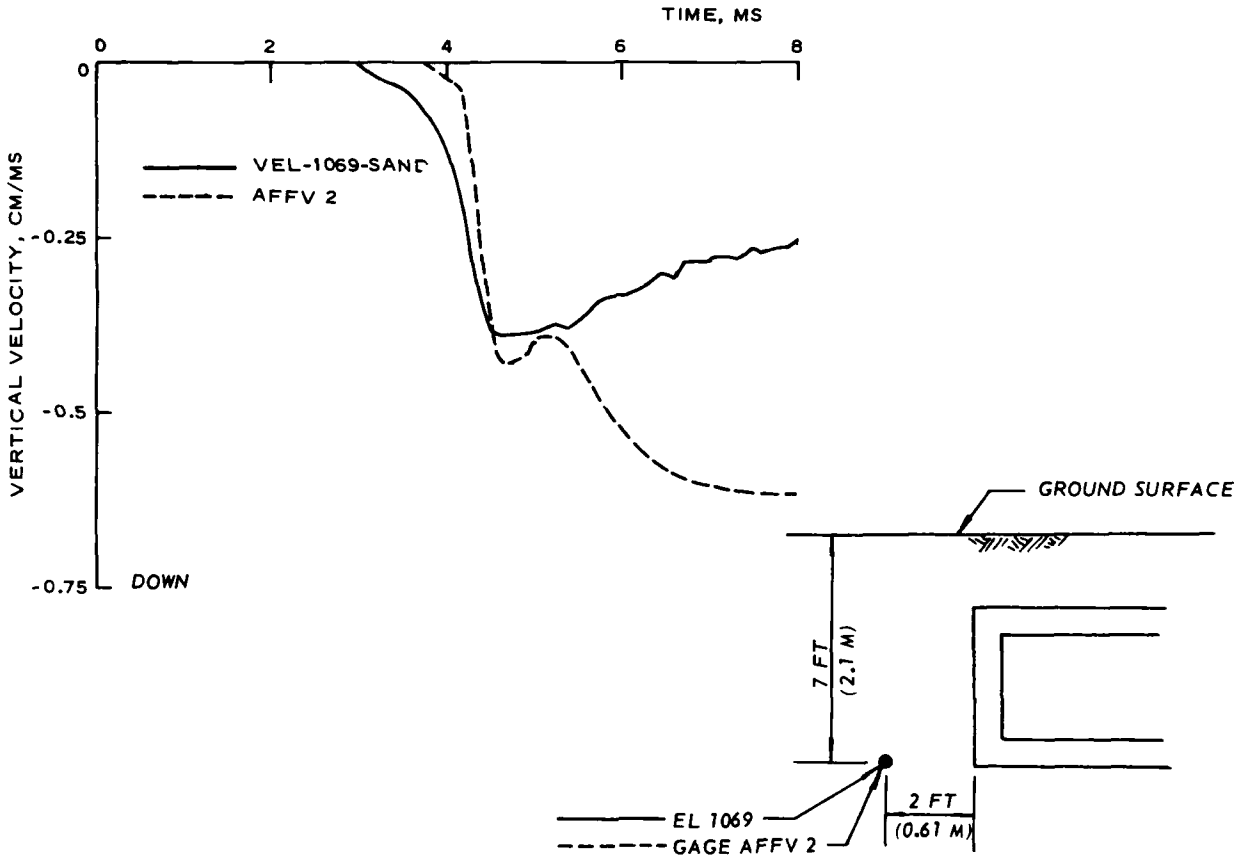

Figure 3.6 Comparison of the calculated and measured vertical velocity-time histories in the sand backfill at the 7-foot (2.1-metre) depth.

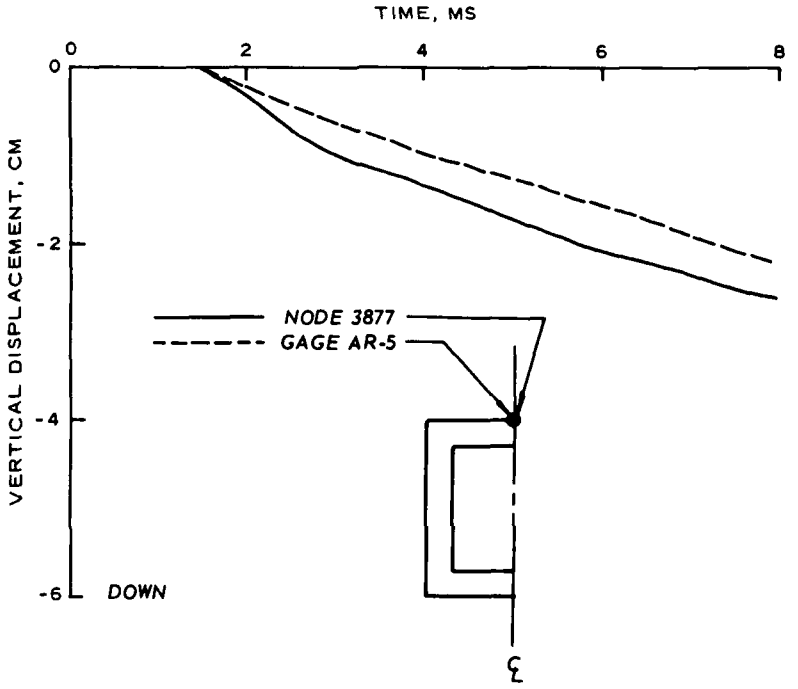

Figure 3.7 Comparison of calculated and measured deflection of the center of the roof at early times.

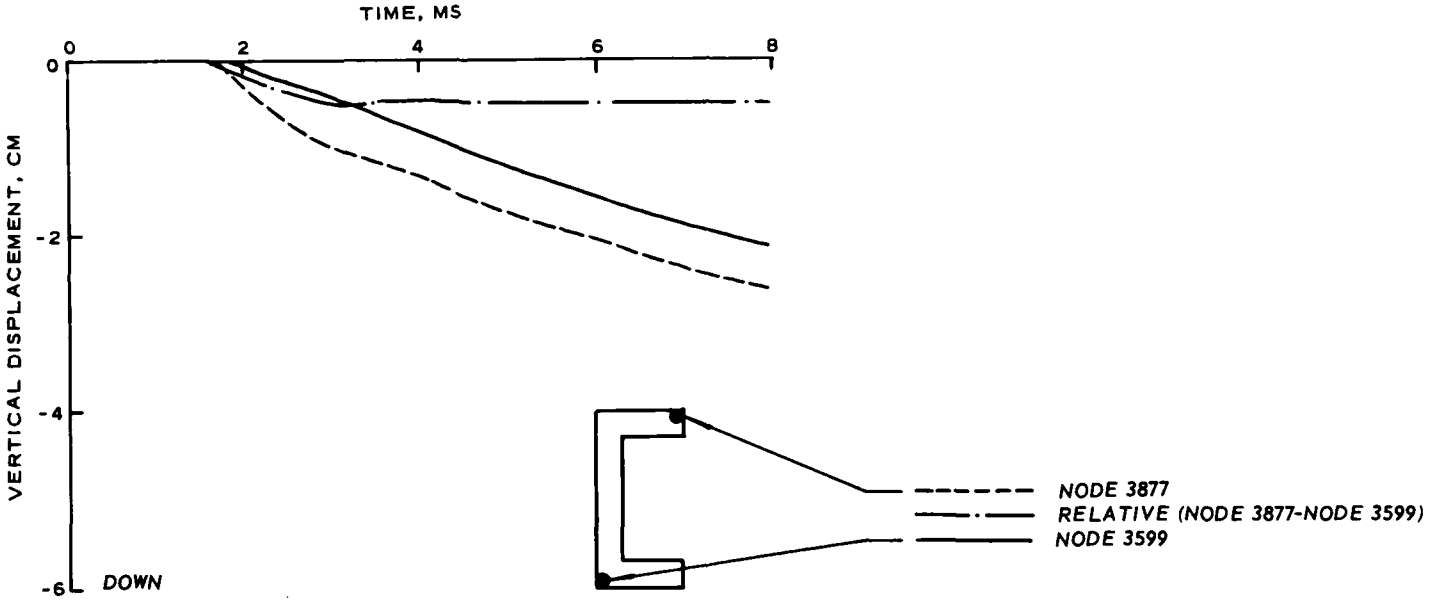

Figure 3.8 Calculated deflection of the center of the roof, the bottom corner of the structure, and relative deflection of the center of the roof.

CHAPTER 4

EFFECT OF CLAY VERSUS SAND BACKFILL ON LOADS TRANSMITTED TO THE STRUCTURE

In order to determine the effect of varying the shear properties of the backfill material on the loads transmitted to the structure roof, the previously described 2D calculation of Foam HEST 1 was repeated identically except that the properties of the backfill zone were changed from those of a high shear strength frictional material (sand) to those of a low shear strength cohesive material (clay). Comparisons of the cap model fits to the UX stress-strain, UX stress-path, and TX failure properties for the sand and clay backfills are shown in Figures 2.4, 2.5, and 2.6, respectively.

4.1 STRESS- AND MOTION-TIME HISTORIES

Figure 4.1 presents a comparison of vertical stress-time histories for points located 2 feet (0.61 metre) from the structure sidewall and at depths of 1 foot (0.30 metre), 4.5 feet (1.4 metres), and 7 feet (2.1 metres). The arrival times at each depth are greater and the peak stresses are less for the clay backfill than for the sand backfill. For both cases, first arrivals at 1 foot are obviously waves through the soil backfill. At 4.5 feet, however, horizontal stresses radiating from the structure arrive about 0.1 ms earlier for the sand and 0.4 ms for the clay than vertical stresses traveling directly through the backfill. At 7 feet, the influence of the structure on both the arrival times and the rise times of the stress waves is quite pronounced.

Figure 4.2a compares the vertical stress-time histories for Element 4626 located just above the center of the structure roof. Although the stresses in the sand backfill were higher than those in the clay, the peak stress on the roof is higher for the clay calculation. And as can be seen in Figure 4.2b, the impulse delivered to the center of the structure roof is higher for the clay calculation than for the sand

calculation. Relative deflections between the center of the roof and the bottom corner of the structure are compared in Figure 4.2c; the maximum relative deflection of the roof for the clay backfill case is 3.2 cm and occurs at a time of 8.5 ms while that for the sand is 0.6 cm and occurs at 3.2 ms.

Vertical stress- and impulse-time histories at a point above the sidewall of the structure are compared for the two calculations in Figure 4.3. Both were greater for the sand backfill case; just the opposite was true for the center of the roof. Since the two calculations were the same except for the properties of the backfill material, the differences noted in the pattern of stress and impulse distribution on the roof must result solely from the change in backfill.

Roof stress distribution patterns are further defined in Figures 4.4 through 4.9, which present stress-time histories for six locations along the structure roof. All output locations are 1/2 inch above the roof of the structure and are located at 6-inch (15.2-cm) intervals from the outside corner of the structure (el 4597) to the center of the roof (el 4626). Figures 4.4 and 4.5 present vertical stress-time histories, Figures 4.6 and 4.7 present horizontal stress-time histories, and Figures 4.8 and 4.9 present shear stress-time histories from the sand and clay calculations, respectively.

The vertical stress histories from the sand calculation (Figure 4.4) are quite different from the horizontal stress histories (Figure 4.6), whereas the horizontal stress-time histories from the clay calculation (Figure 4.7) are quite similar to the vertical stress-time histories (Figure 4.5). This is reasonable since the failure envelope for the clay allows a maximum stress difference of only 10 bars. The ability of the sand to support larger shear stresses than the clay is evident from Figures 4.8 and 4.9, i.e., the shear stresses over the corner of the structure reach a maximum value of approximately 32 bars in the sand but never reach a value greater than 6 bars at any location in the clay.

4.2 STRESSES ON STRUCTURE ROOF AT EARLY TIMES

Figure 4.10 presents isochrones of horizontal stress, vertical stress, and shear stress for the row of elements just above the roof at times of 1.2, 1.35, 1.5, and 1.65 ms after the start of the sand calculation. The airblast loading arrives at this row of elements at 1.14 ms. The plots at 1.2 and 1.35 ms show that the roof is being loaded initially by approximately a plane wave; the shear stresses at 1.2 ms are essentially zero and at 1.35 ms are less than 2 bars. At 1.5-ms, the horizontal and vertical stresses have increased over the sidewall but have decreased sharply over the center of the roof. The shear stress at this time is zero above the center of the roof and approximately 14 bars in the vicinity of the sidewall. The trend continues to 1.65 ms, when the vertical stress has decreased to approximately 6 bars above the center of the roof and the shear stress has increased to 23 bars near the sidewall.

Figure 4.11 presents horizontal, vertical, and shear stresses for the row of elements just above the roof at times of 2.4, 2.55, 2.7, and 2.85 ms after the start of the clay calculation. First arrival at these elements occurs at 2.37 ms. At 2.4 ms the horizontal and vertical stresses are fairly uniform across the roof with a slight increase over the corner. At 2.55 ms the horizontal and vertical stresses over the center half of the roof have increased to approximately 95 and 100 bars, respectively, while those above the corner are approximately 60 bars. At 2.7 ms the horizontal and vertical stresses near the corner oscillate around 60 bars while those over the center portion of the roof are decreased to 58 and 60 bars, respectively. At 2.85 ms the stresses over the corner remain at the 60-bar level while the stresses over the center of the roof have decreased to approximately 30 bars. The shear stresses at all four times are very low with a slight buildup over the corner that increases with time.

4.3 NORMAL STRESSES AROUND STRUCTURE AND NEUTRAL AXIS DEFLECTIONS AT LATE TIMES

Instantaneous snapshots or isochrones of normal stress around the exterior of the structure and the deflected shape of the structure are shown in Figure 4.12 for times of 5, 10, and 15 ms. The stresses around the structures at late times are more uniform in the clay calculation whereas in the sand calculation they still tend to concentrate near the corners. This is especially true near the top of the sidewall, which indicates that the roof is being given some in-plane support. The neutral axis deflections for the roof, floor, and sidewalls are greater for the clay backfill case than for the sand backfill case, as shown in the figure.

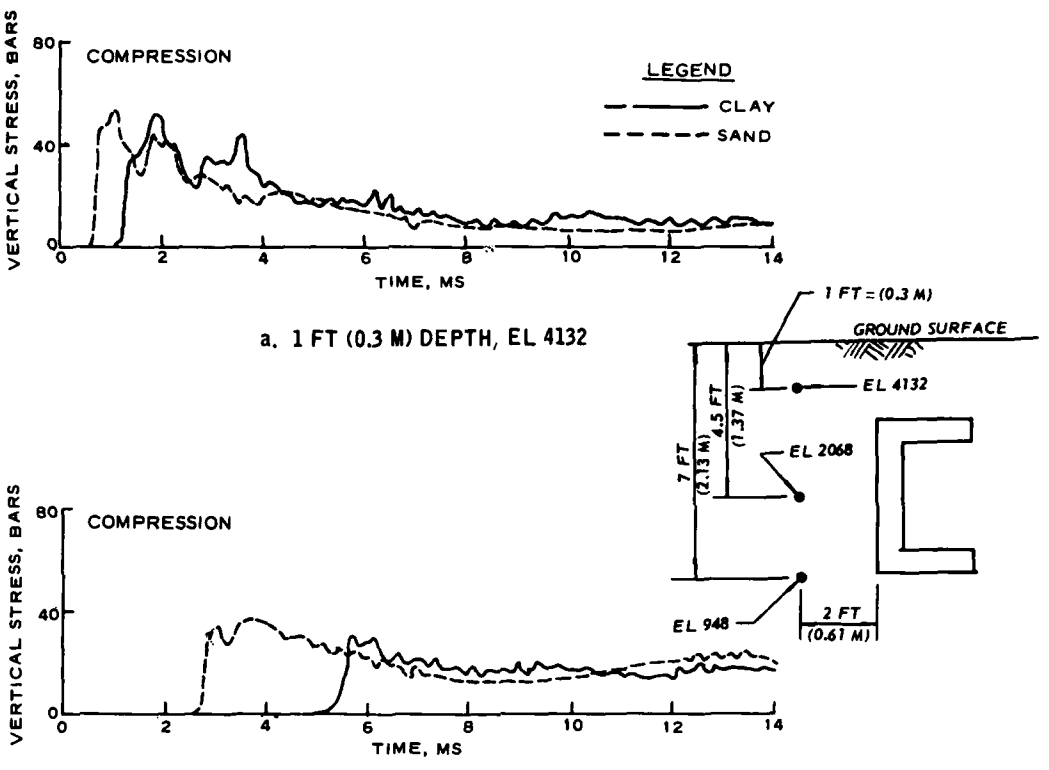

Figure 4.1 Vertical stress-time histories in the clay and sand backfill at the 1-foot (0.30-metre), 2 foot (0.61-metre), and 7-foot (2.1-metre) depths.

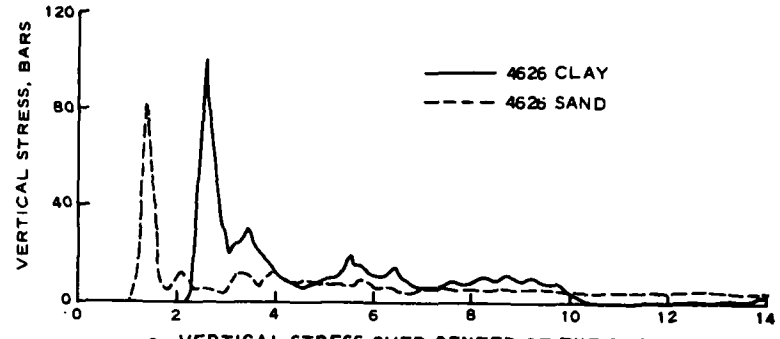

a. VERTICAL STRESS OVER CENTER OF THE ROOF

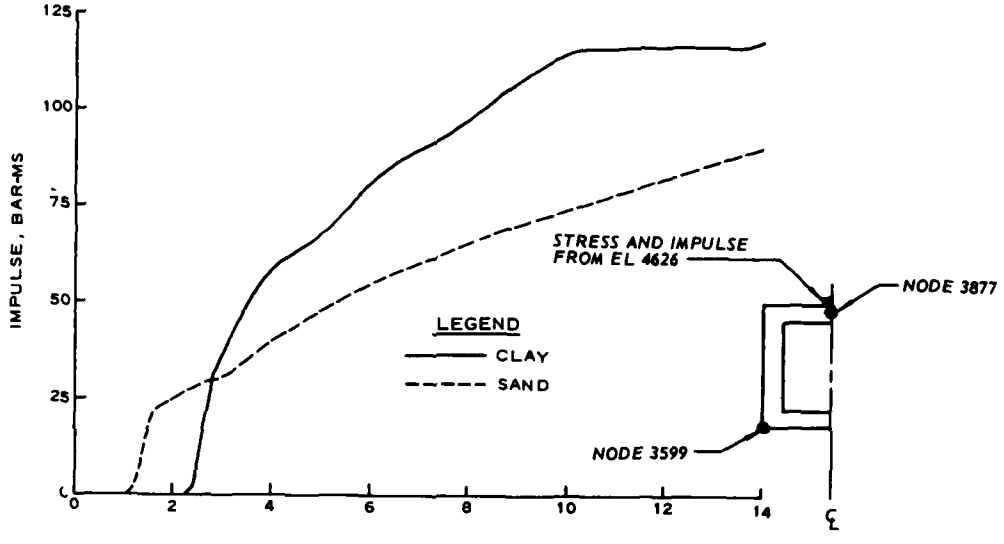

b. IMPULSE DELIVERED TO THE CENTER OF THE ROOF

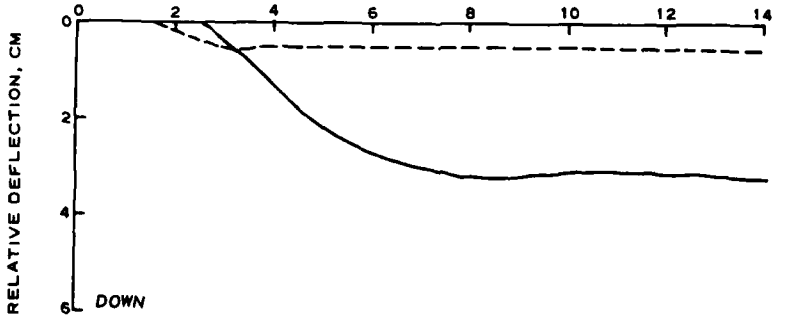

c. RELATIVE DEFLECTION (NODE 3877-NODE 3599) OF THE CENTER OF THE ROOF

Figure 4.2 Vertical stress and impulse delivered to and relative deflection of the center of the roof (clay versus sand backfill).

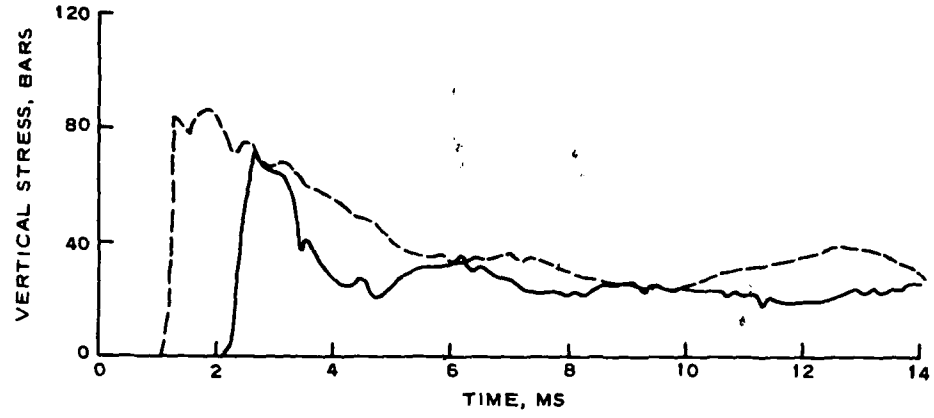

a. VERTICAL STRESS TIME HISTORY OVER CORNER

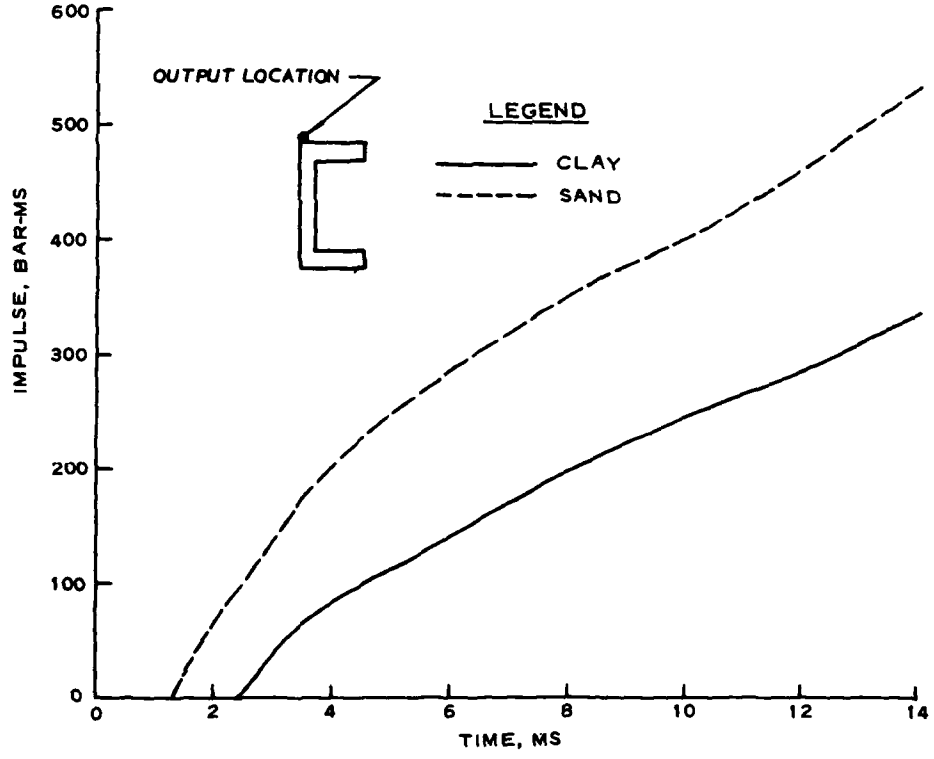

b. VERTICAL IMPULSE OVER CORNER

Figure 4.3 Vertical stress and impulse delivered to the corner of the roof (clay versus sand backfill).

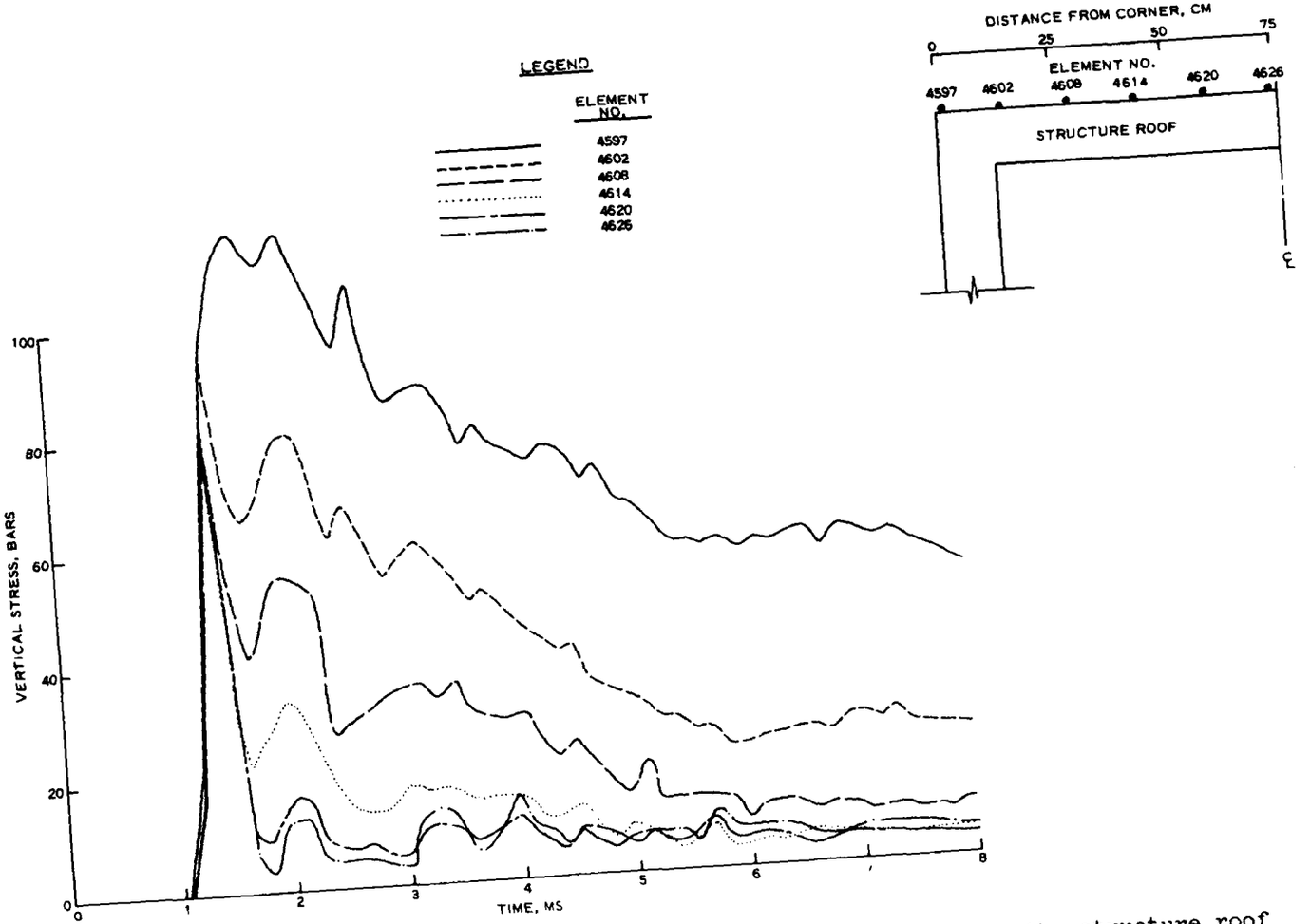

Figure 4.4 Vertical stress-time histories for six locations along the structure roof (sand backfill).

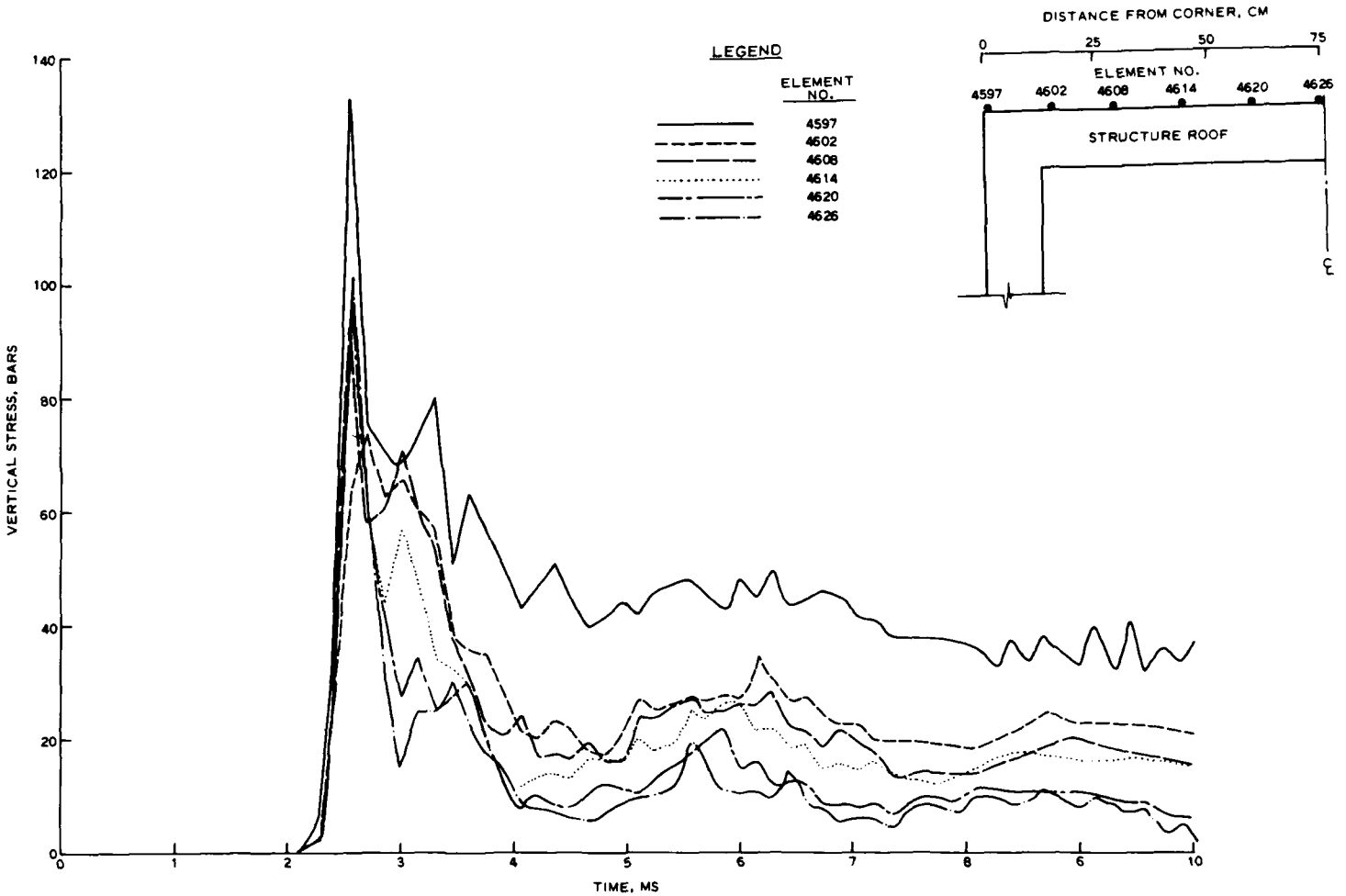

Figure 4.5 Vertical stress-time histories for six locations along the structure roof (clay backfill).

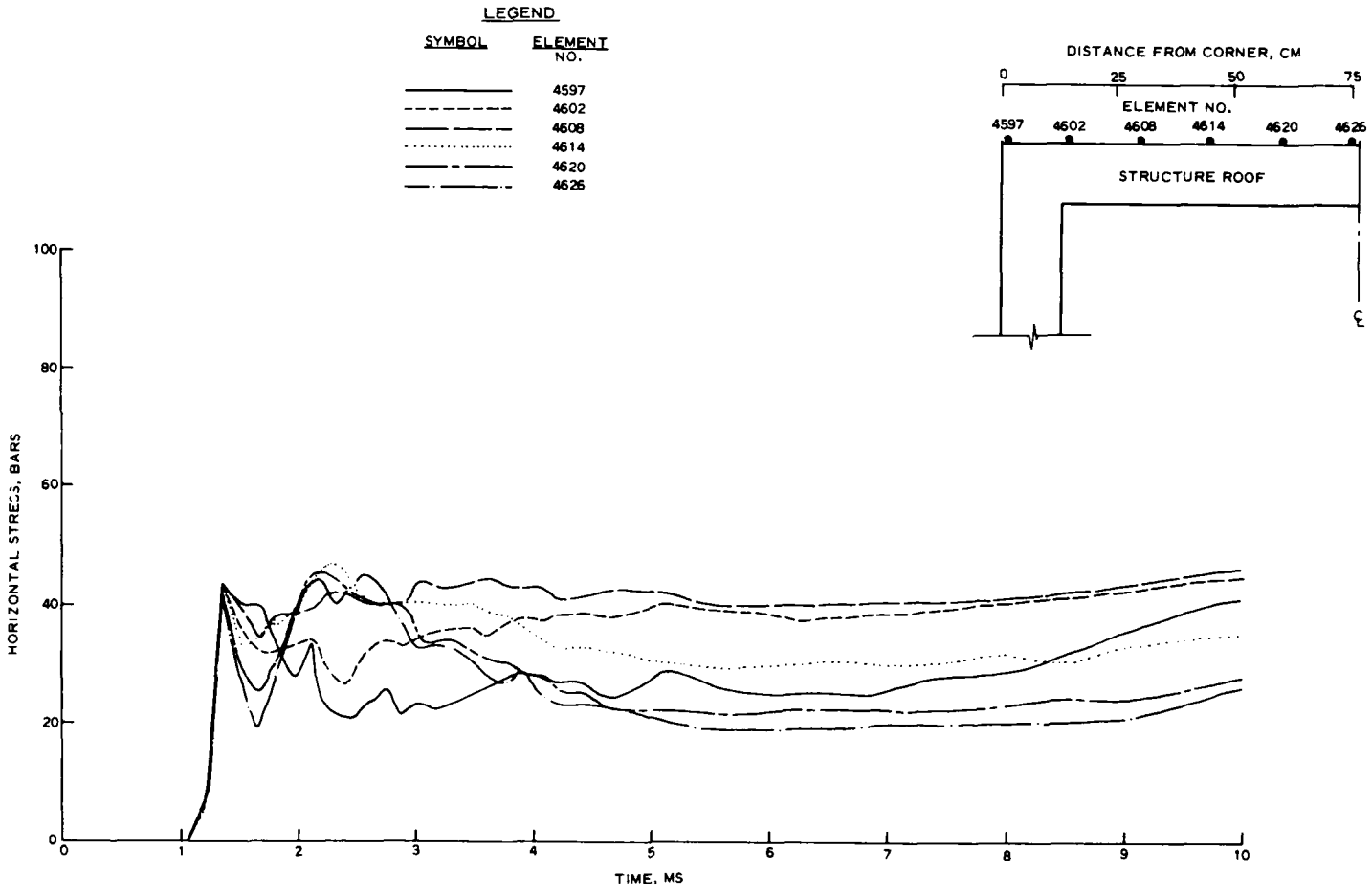

Figure 4.6 Horizontal stress-time histories for six locations along the structure roof (sand backfill).

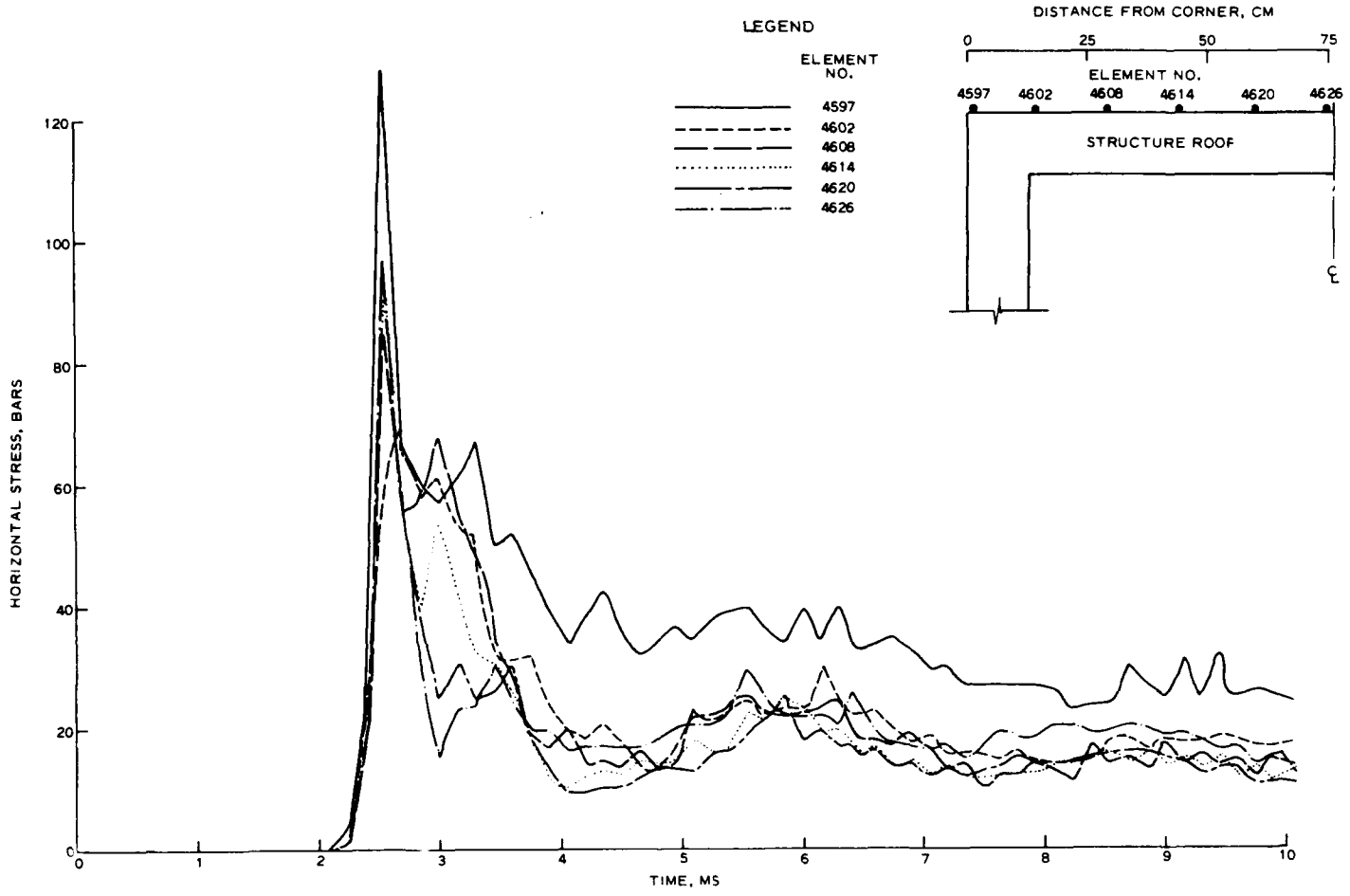

Figure 4.7 Horizontal stress-time histories for six locations along the structure roof (clay backfill).

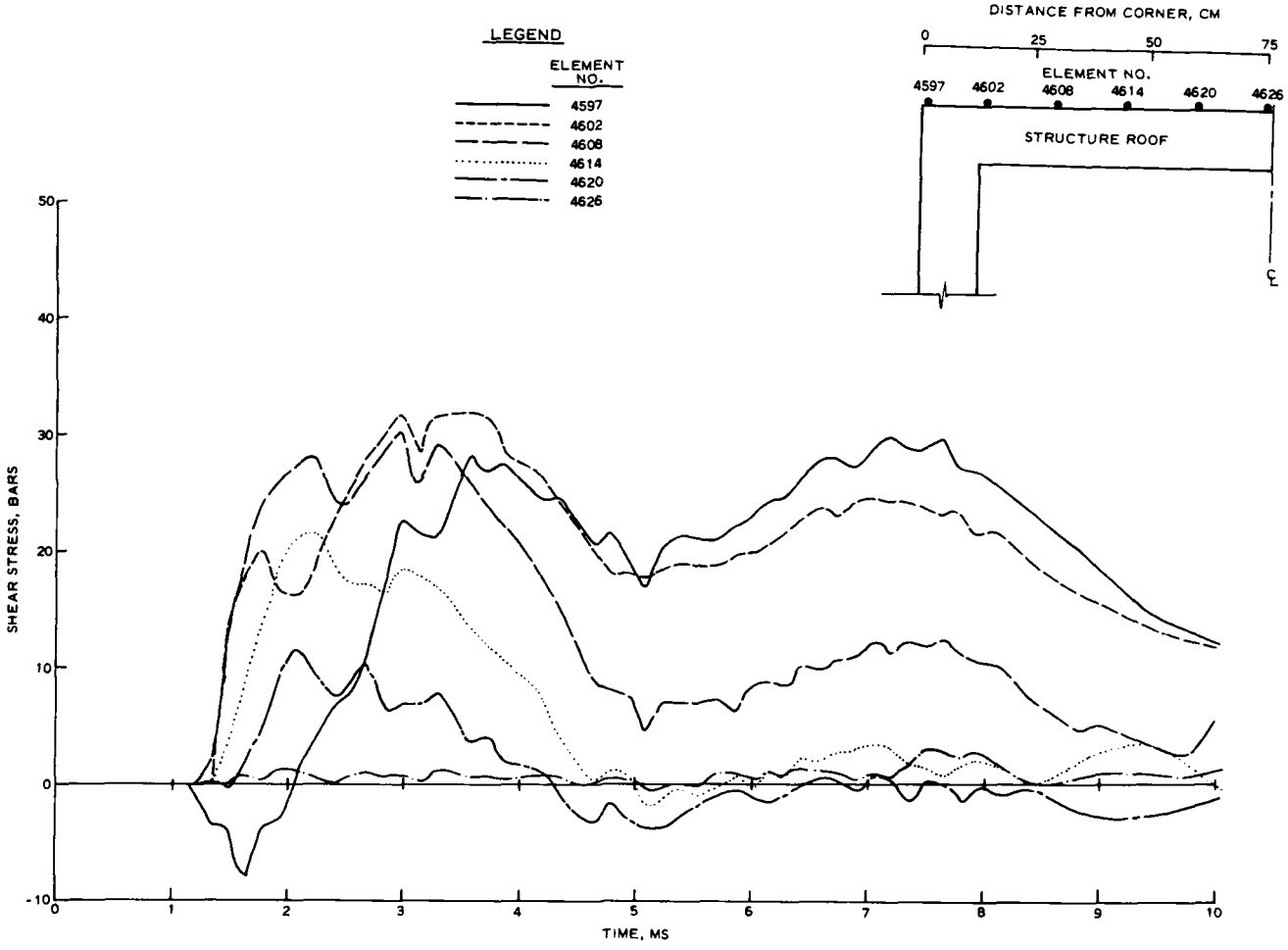

Figure 4.8 Shear stress-time histories for six locations along the structure roof (sand backfill).

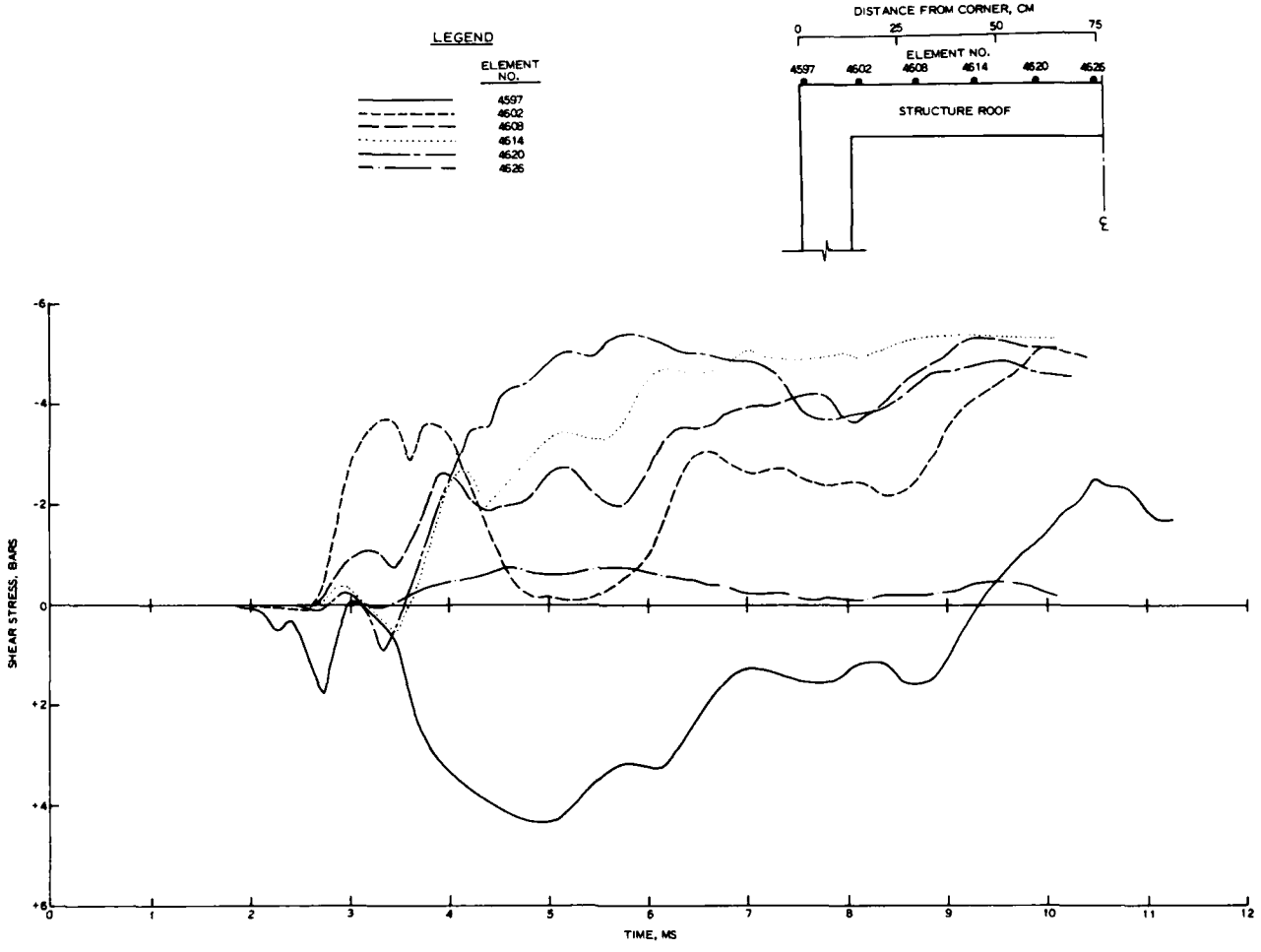

Figure 4.9 Shear stress-time histories for six locations along the structure roof (clay backfill).

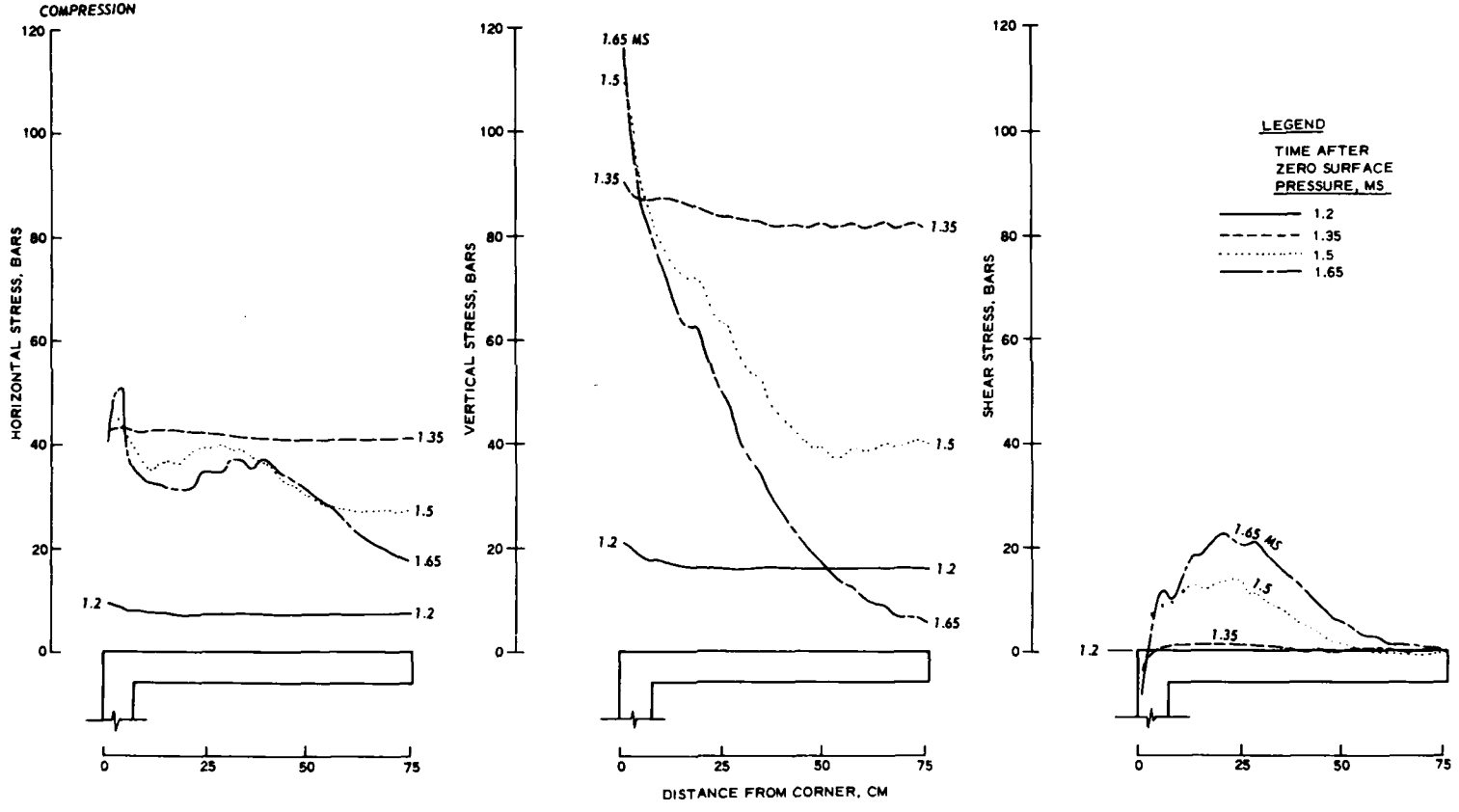

Figure 4.10 Isochrones of stress above the roof just after initial loading (sand backfill).

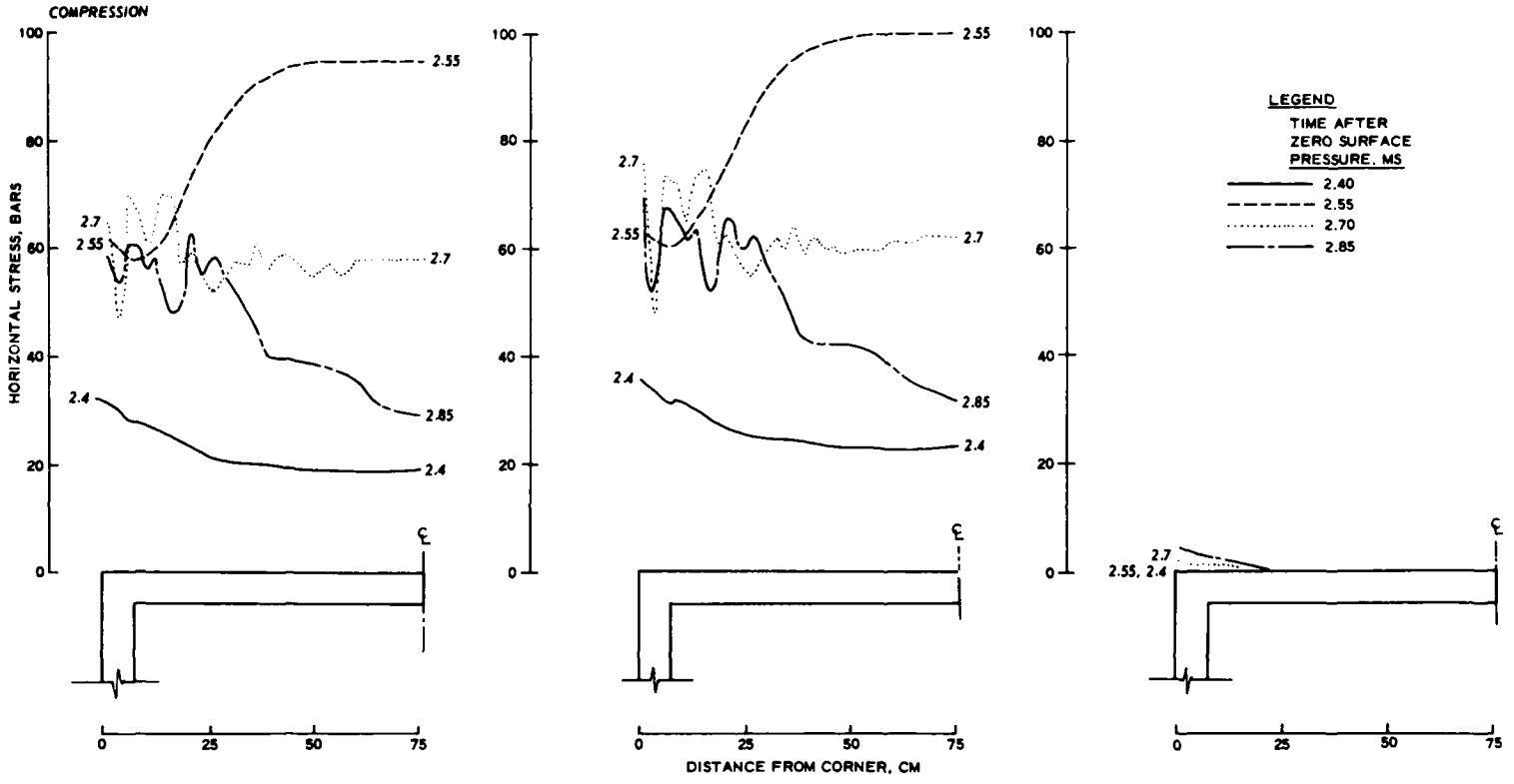

Figure 4.11 Isochrones of stress above the roof just after initial loading (clay backfill).

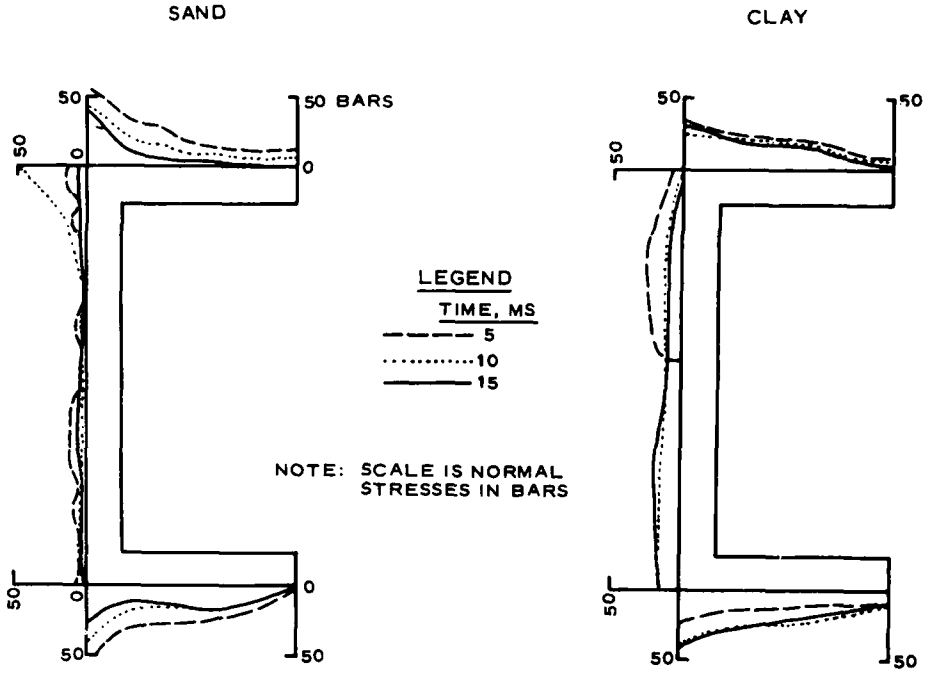

a. INSTANTANEOUS NORMAL STRESSES

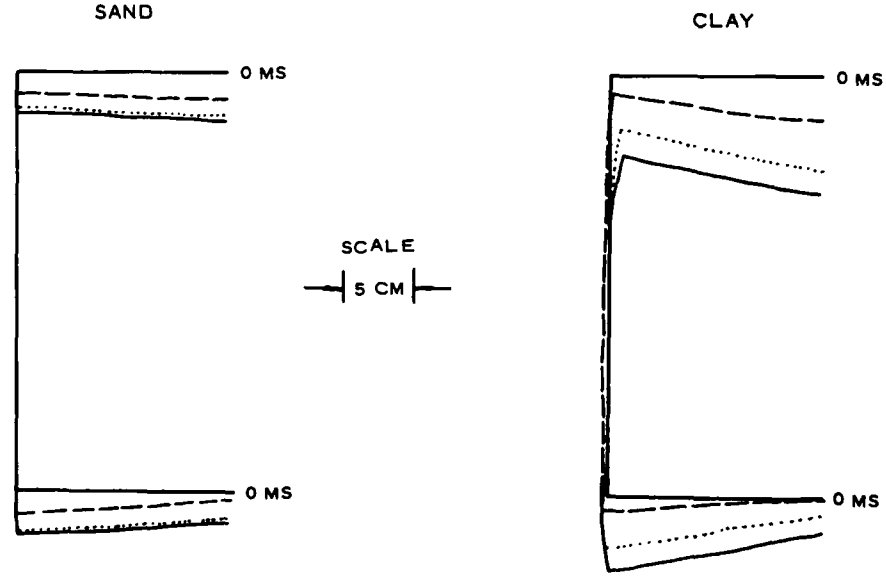

b. INSTANTANEOUS DEFLECTIONS OF NEUTRAL AXIS

Figure 4.12 Late-time isochrones of normal stress on the structure and neutral axis deflections.

CHAPTER 5

EFFECT OF 1D VERSUS 2D GEOMETRY ON CALCULATED STRESSES

In order to determine the extent to which 1D simulations can be used in lieu of 2D simulations for predicting stresses associated with shallow-buried structure tests, 1D sand and clay calculations were performed for a section through the Foam HEST 1 backfill, a section through the center of the roof, and a section through the sidewall, as shown in Figure 2.3. The airblast loading, material properties, FE grid, and time step were identical to those used in the previously-described 2D calculations.

5.1 STRESSES IN THE BACKFILL

The backfilled excavation adjacent to the structure was 8 feet deep and was underlain by sand; a rigid calculational boundary was inserted at 14 feet. Figure 5.1 shows vertical stress-time histories computed at nominal depths of 1, 2, 4, and 6 feet for a 1D sand backfill section with those obtained from elements in the 2D calculation located 5.5 feet from the sidewall of the structure and 1.5 feet from the edge of the backfill excavation. Agreement is excellent at the 1- and 2-foot depths and is still quite good at 6 feet up to about 12 ms. First reflections off the bottom boundary arrive at the 6-foot-deep output location at 13.1 ms in the 1D calculation and at 11.1 ms in the 2D calculation due to the faster downward path provided by the concrete structure. There is no influence from the excavation wall since the properties of the native soil were assumed to be identical to those of the sand backfill.

Figure 5.2 compares stress-time histories for the clay backfill case. Again the agreement is excellent at the 1- and 2-foot depths, but at greater depths the stresses are arriving earlier in the 2D calculation than in the 1D calculation. First arrival paths to the output stations at 4 feet and 6 feet in the 2D run are through the native soil which has an initial P-wave speed of 1.68 feet/ms as opposed to 0.81 feet/ms for the clay backfill.

5.2 STRESSES ABOVE THE CENTER OF THE ROOF

The 6-inch-thick concrete roof slab was covered with 2 feet of compacted soil. Figure 5.3 shows vertical stress-time histories computed at nominal depths of 0.5, 1, 1.5, and 2 feet in the sand backfill for a section through the center of the roof. For at least 3 ms of calculation time, the 1D results are in excellent agreement with the 2D results; comparisons at later times are meaningless due to the low stress levels and the oscillatory nature of the calculations. As a matter of practical application, however, 3 ms is still a much longer period than indicated by the early-time stress isochrones previously presented in Figure 4.10, which clearly shows that an essentially 1D plane wave loading condition for the roof only lasts about 0.3 ms after initial impact. Impulse applied to the center of the roof was obtained by integrating the stress-time histories from the 2-foot-deep output location; results are shown in Figure 5.4. Overall agreement is quite good but may be fortuitous after the brief plateau which occurs at about 3 ms.

Figure 5.5 compares results from calculations using the clay backfill. Again, the agreement is very good up to 3 ms at all four output locations even though the isochrones in Figure 4.11 indicate a much shorter plane wave loading period. The calculations of impulse applied to the center of the roof shown in Figure 5.6 begin to deviate substantially about 1 ms after initial arrival of the vertically-propagating stress wave.

5.3 STRESSES ABOVE THE SIDEWALL

Figure 5.7 compares vertical stresses from the 2D sand backfill calculation at nominal depths 0.5, 1, 1.5, and 2 feet directly over the sidewall of the concrete structure with those from a 1D simulation. It is obvious from the calculation geometry sketches that the 1D section is a poor representation of the 2D problem; the calculation results only prove it. Stress and impulse applied to the top corner of the roof are shown in Figure 5.8; peak stresses compare favorably, but the poor impulse comparisons should dispell any urge to use 1D approximations for this location.

Stress-time histories from the clay backfill calculations are shown in Figure 5.9. The early-time portions are not particularly bad, but they are not particularly good either. Comparisons of stress and impulse applied to the roof are shown in Figure 5.10. In this case the impulse comparison is better than the peak stress comparison, which only reinforces the conclusion that results from 1D runs can be misleading for locations near structure corners.

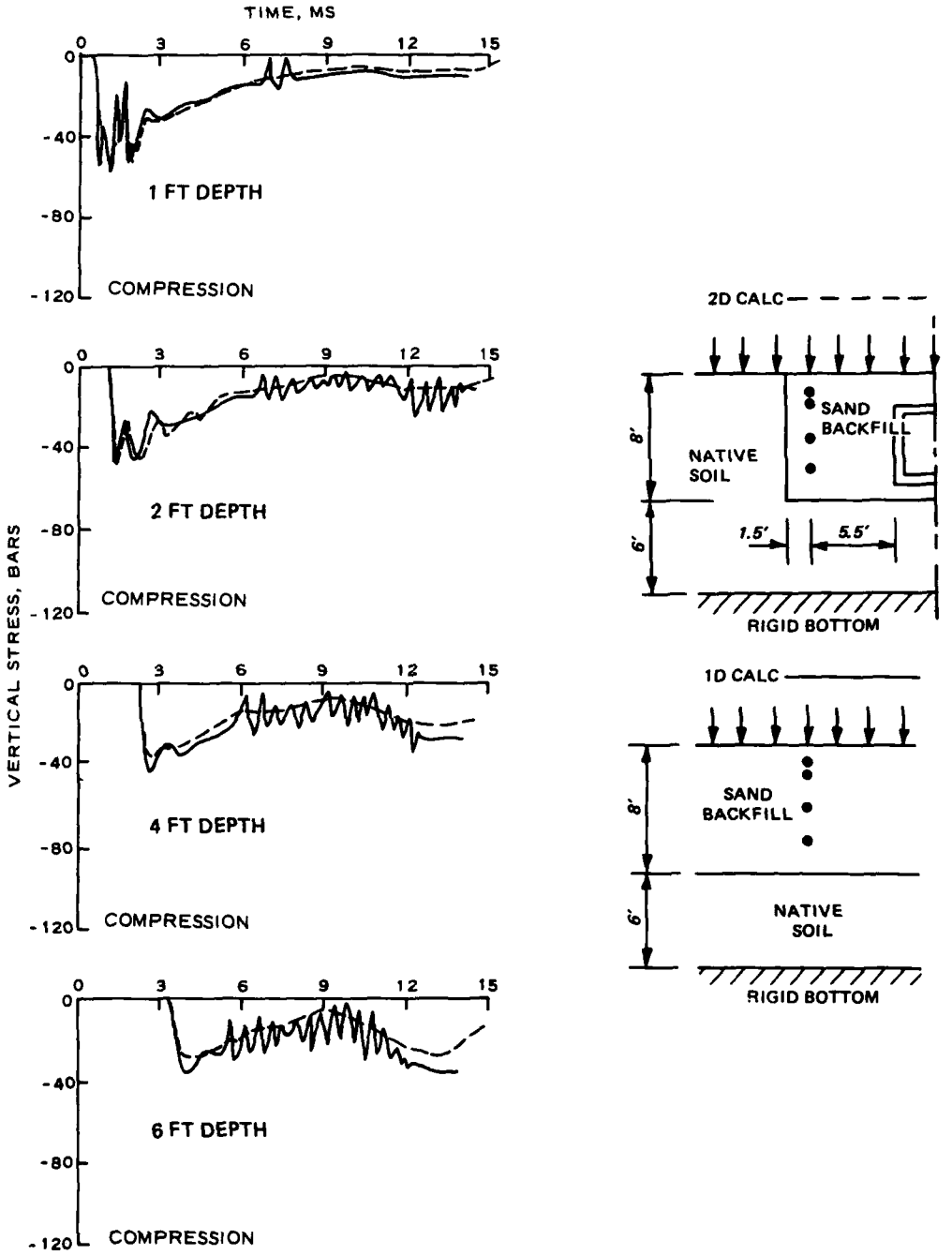

Figure 5.1 Comparison of vertical stress-time histories from 2D calculation with results from 1D calculation of sand backfill section.

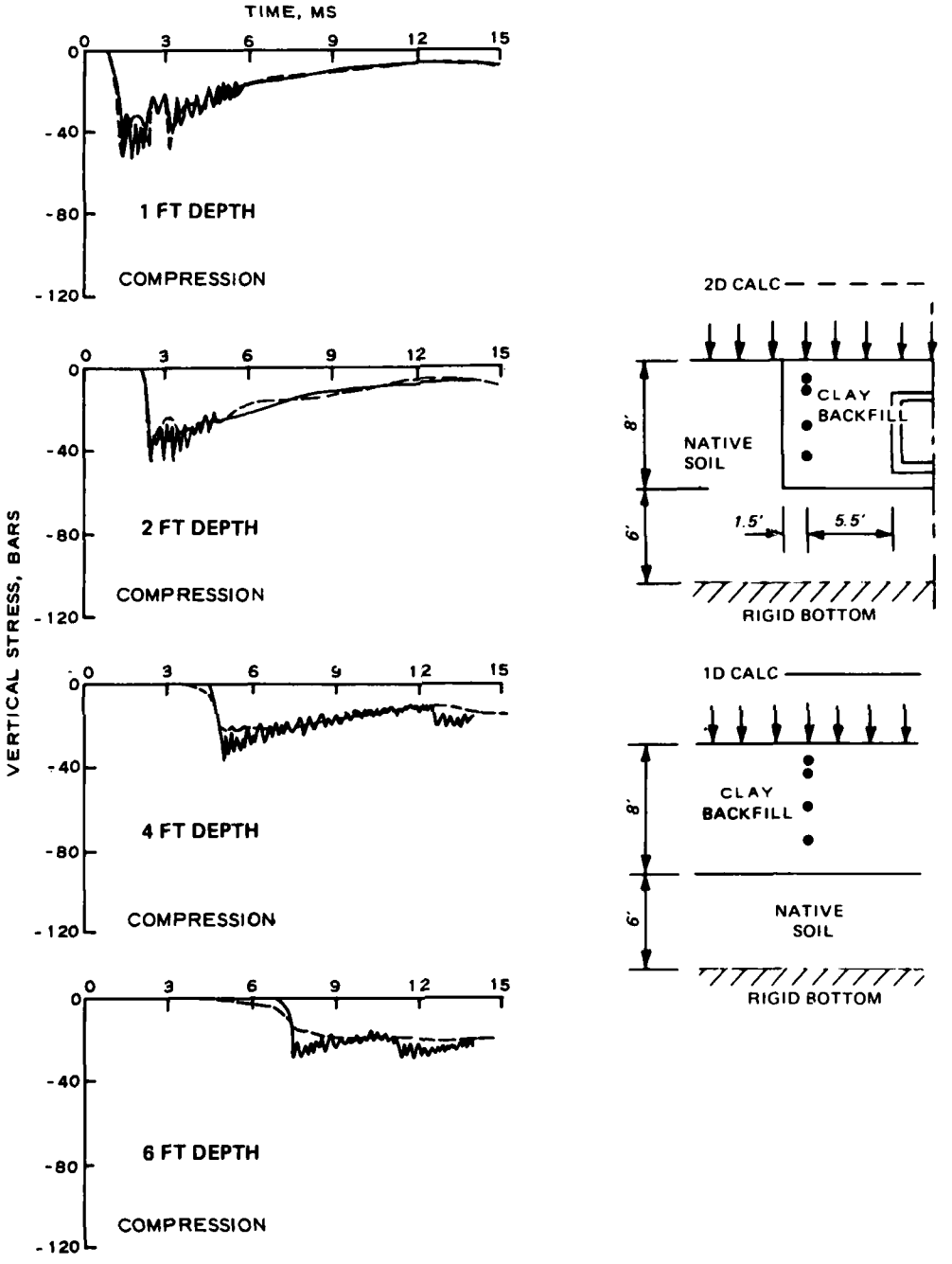

Figure 5.2 Comparison of vertical stress-time histories from 2D calculation with results from 1D calculation of clay backfill section.

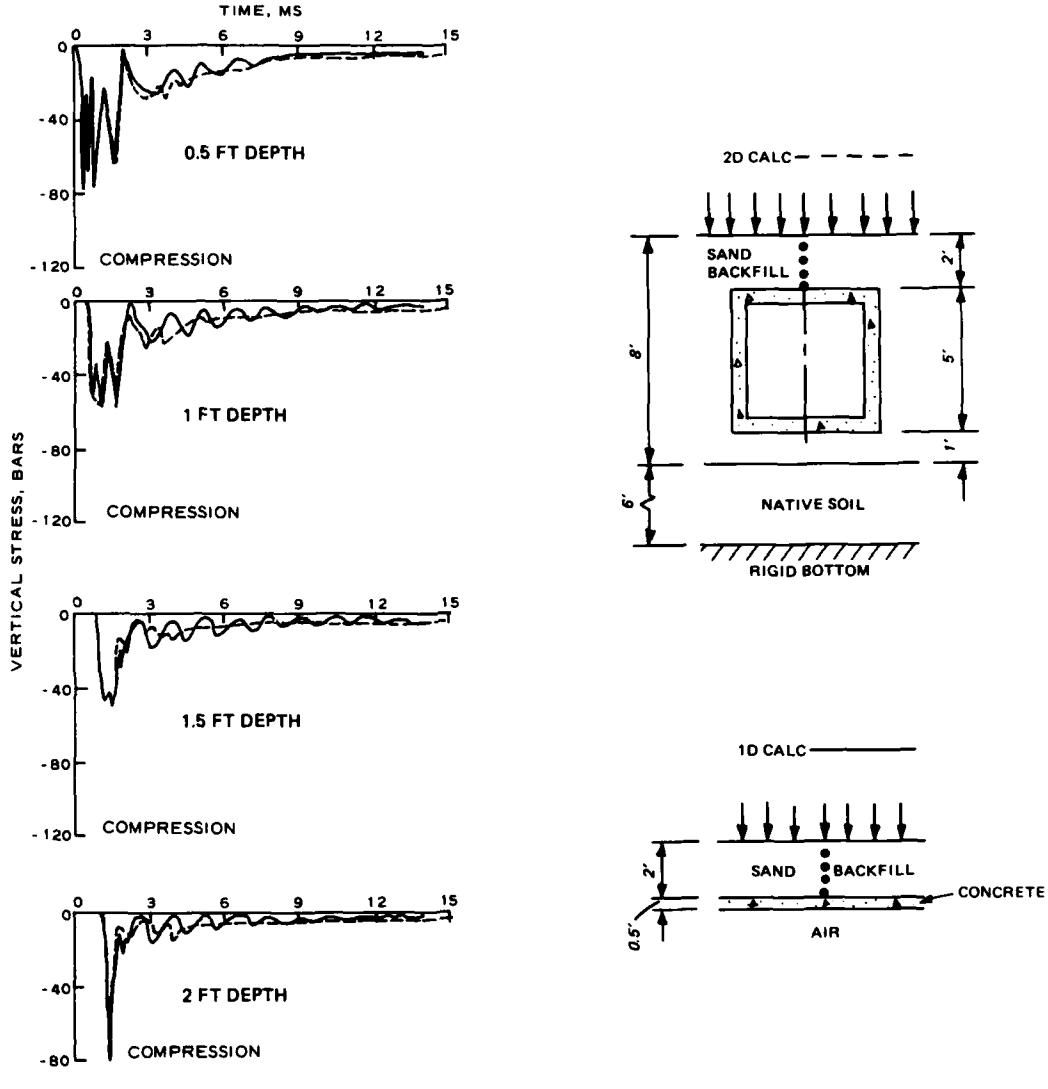

Figure 5.3 Comparison of vertical stress-time histories from 2D calculation with results from 1D calculation of sand backfill/roof center section.

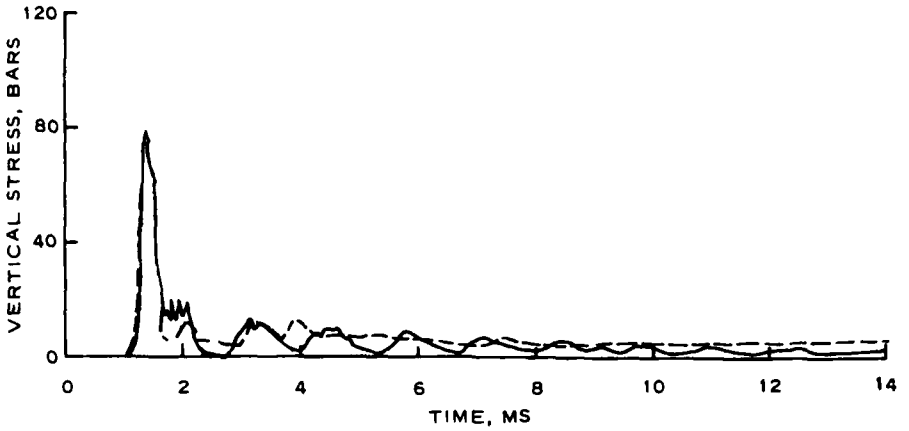

a. VERTICAL STRESS OVER CENTER OF ROOF

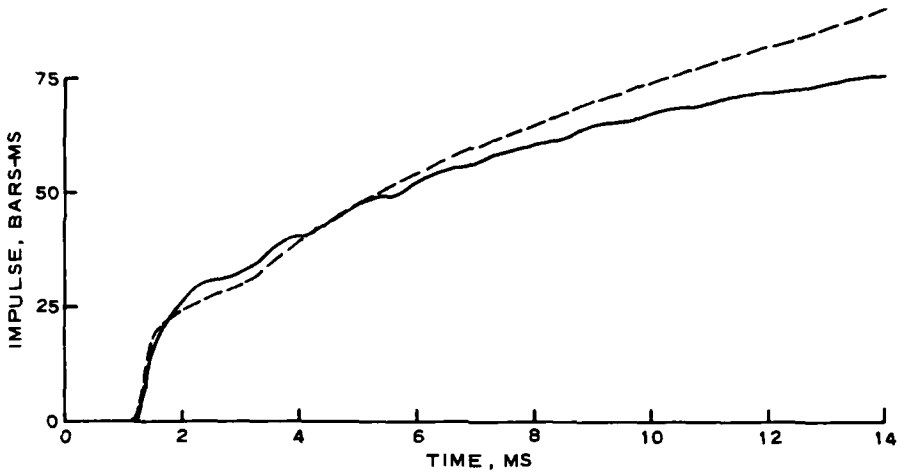

b. IMPULSE APPLIED TO CENTER OF ROOF

LEGEND

1D RESULTS

2D RESULTS

Figure 5.4 Vertical stress and impulse applied to center of roof from 1D and 2D calculations with sand backfill.

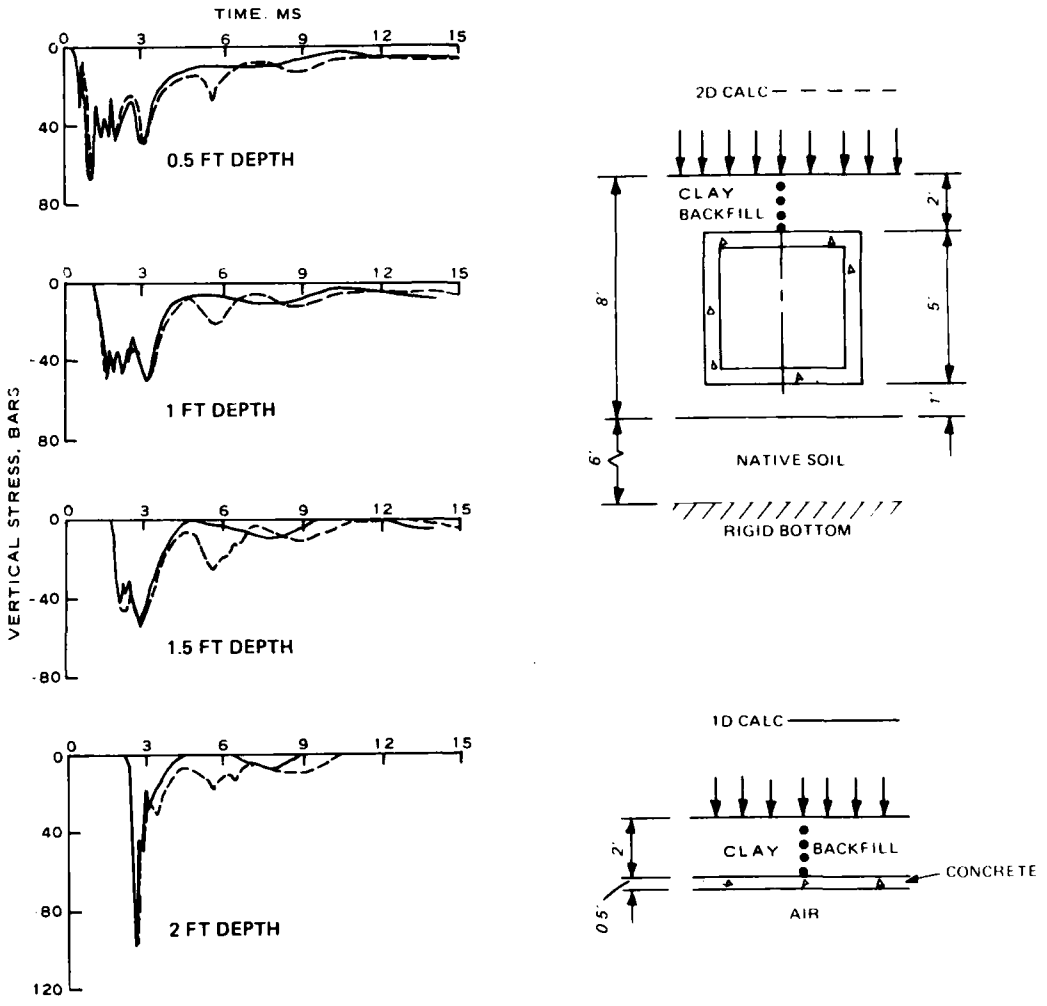

Figure 5.5 Comparison of vertical stress-time histories from 2D calculation with results from 1D calculation of clay backfill/roof center section.

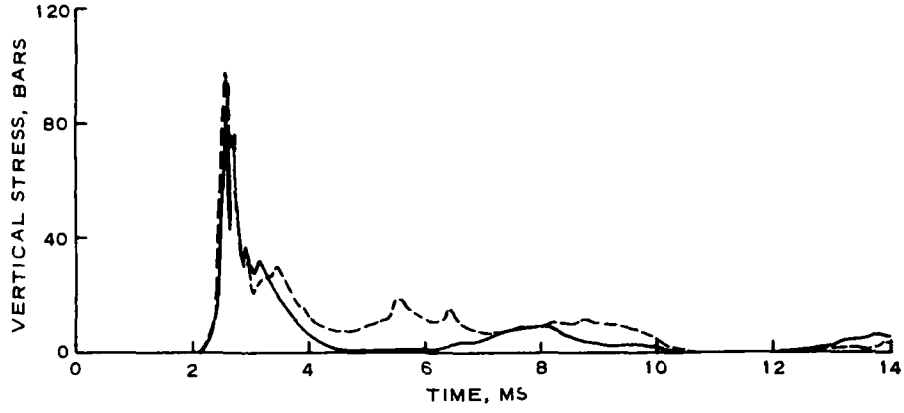

a. VERTICAL STRESS OVER CENTER OF ROOF

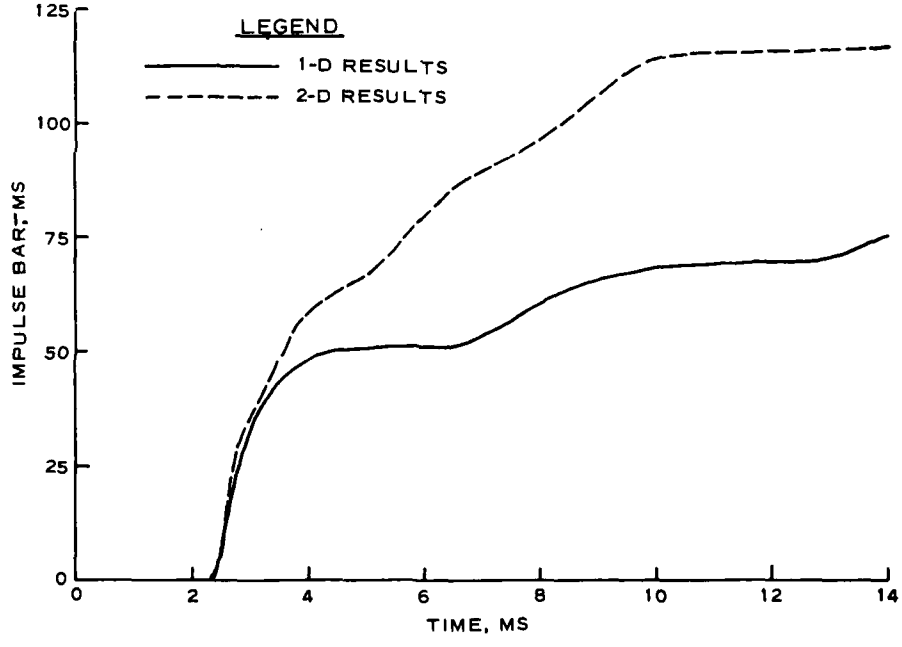

b. IMPULSE APPLIED TO CENTER OF ROOF

Figure 5.6 Vertical stress and impulse applied to center of roof from 1D and 2D calculations with clay backfill.

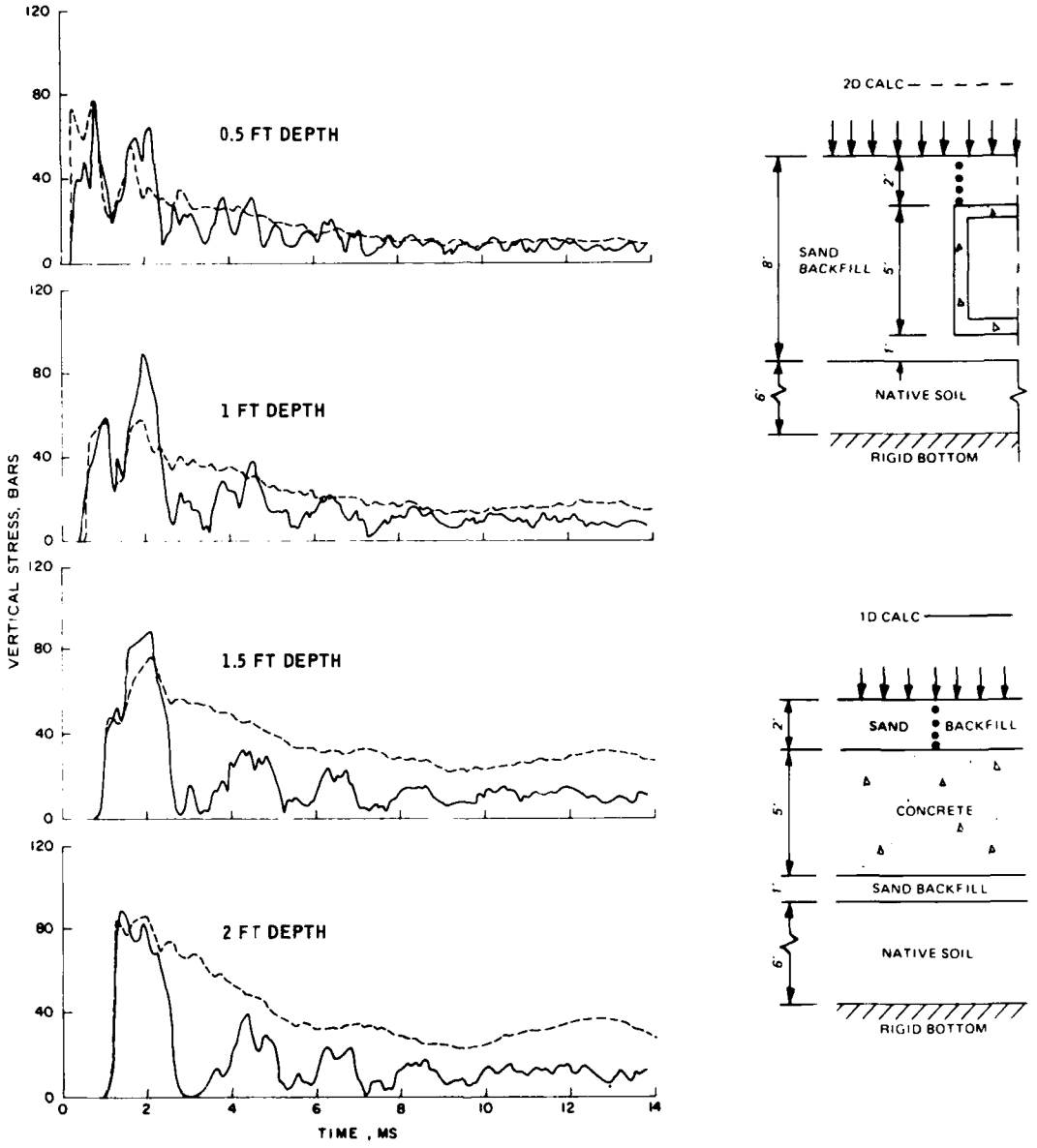

Figure 5.7 Comparison of the vertical stress-time histories from 2D calculation with results from 1D calculation of said backfill/sidewall section.

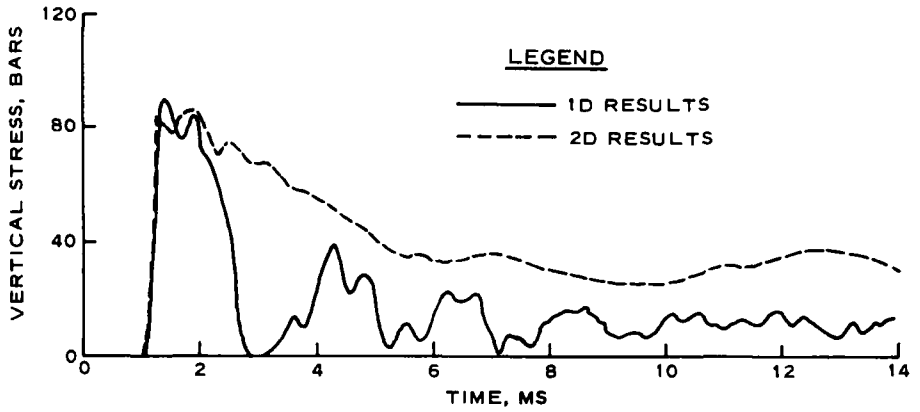

a. VERTICAL STRESS OVER THE CORNER OF THE ROOF

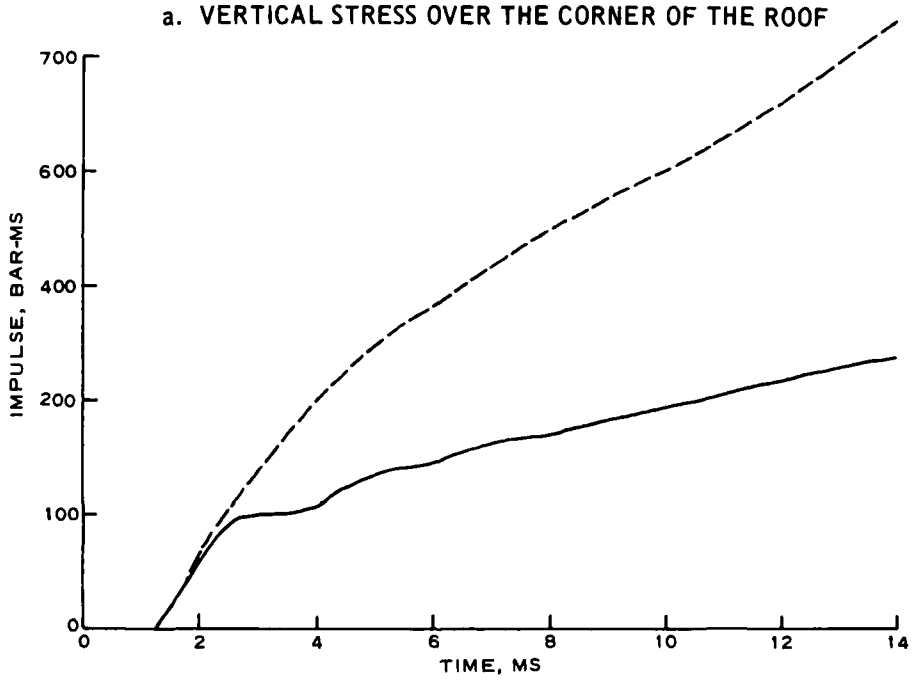

b. VERTICAL IMPULSE APPLIED TO THE TOP CORNER OF THE ROOF

Figure 5.8 Vertical stress and impulse applied to top corner of roof from 1D and 2D calculations with sand backfill.

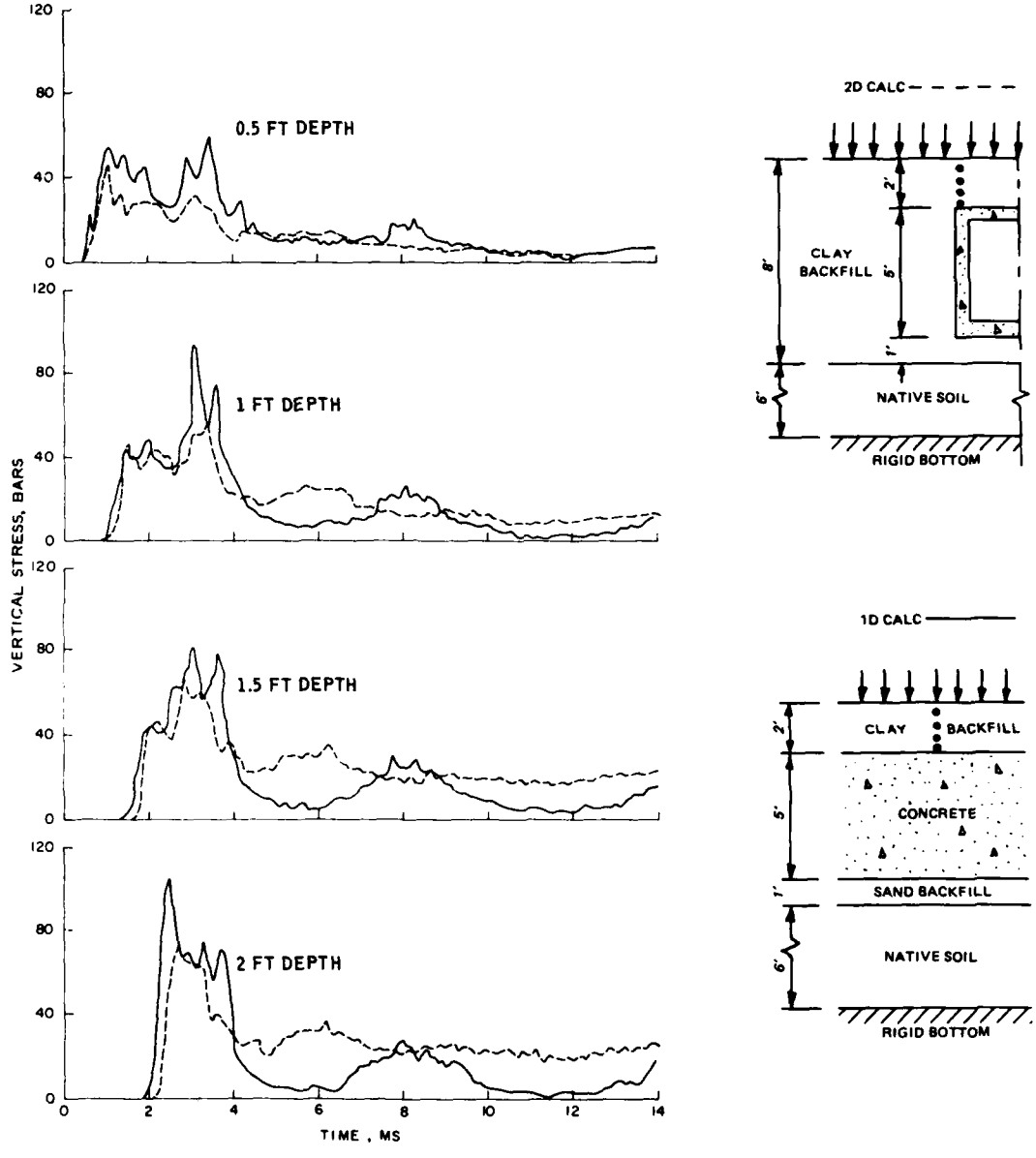

Figure 5.9 Comparison of the vertical stress-time histories from 2D calculation with results from 1D calculation of clay backfill/sidewall section.

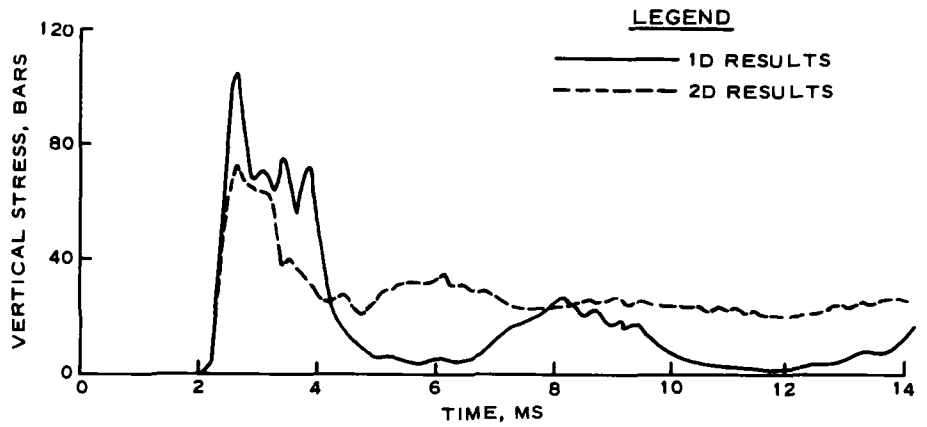

a. VERTICAL STRESS OVER THE CORNER OF THE ROOF

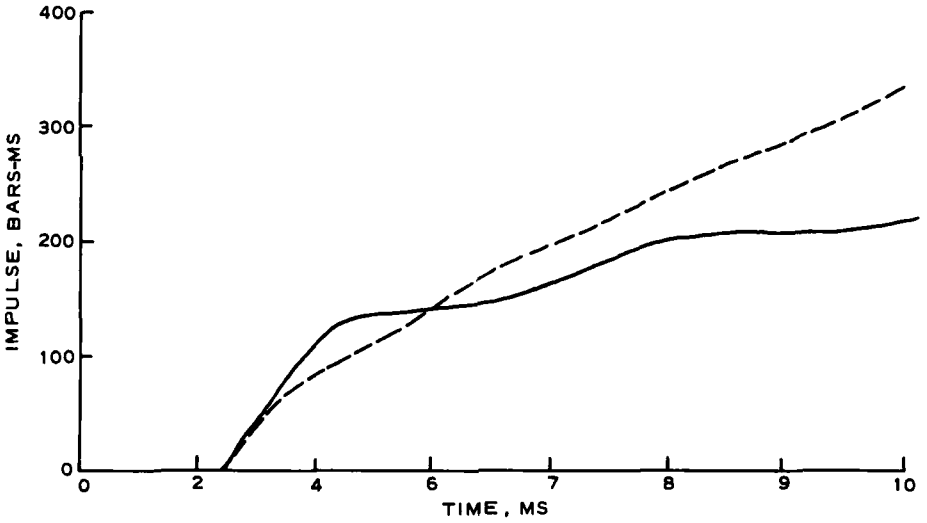

b. VERTICAL IMPULSE APPLIED TO THE TOP CORNER OF THE ROOF

Figure 5.10 Vertical stress and impulse applied to top corner of roof from 1D and 2D calculation with clay backfill.

CHAPTER 6

CONCLUSIONS

The calculations were conducted to support the DNA Shallow-Buried Structures Program. They were designed to (1) assess the credibility of a dynamic FE technique employing nonlinear elastic-ideally plastic soil models for predicting the loads transmitted from a surface overpressure to the roof of a shallow-buried structure, (2) determine how these loads would be affected by changing the type of soil used as backfill around the structure (i.e., from a dry cohesionless sand to a low shear strength clay), and (3) provide a better understanding of the loading histories by separating "early-time" stress wave reflections due to impedance mismatch from "late-time" stress redistributions due to soil arching.

6.1 CREDIBILITY OF CALCULATIONAL TECHNIQUE

For locations in the backfill above and/or well away from the structure, the calculated arrival times and the general character of the stress-time histories are in excellent agreement (for at least 8 ms and probably longer) with those measured by the SE gages in Foam HEST 1. Peak stresses were approximately 40 percent less than those measured; this could have been due to gage overregistration but probably resulted from uncertainties associated with the surface overpressure. At deeper locations near the structure, the calculation initially detected a vertical Poisson effect due to horizontal waves radiating out from the sidewall that was not detected by the vertically-oriented SE gage. On the other hand, the gage appears to have detected a relief wave caused by an impedance mismatch between the backfill and the underlying soil that was not modeled in the calculation.

The calculation did a very good job of replicating the intense stress pulse which initially loaded the center of the roof. This loading arrived at 1.2 ms and had a duration of about 0.8 ms; differences after 2 ms are probably due to the fact that the soil/concrete

interface is bonded in the calculation while free to separate in the experiment. Up to a time of 2.3 ms, the calculation also did a very good job of replicating the vertical stresses measured on the roof near the sidewalls, but the wave forms differed distinctly after this time; causes for this late-time difference in wave character are not readily apparent.

Early-time particle velocity comparisons at two locations in the sand backfill were reasonably good, but the measurements after about 5 ms appear to have been significantly influenced by relatively compressible native soil materials beneath the backfill which were not modeled as such in the calculation. Displacement at the 2-foot depth, for example, peaked at 40 ms and measured 18 cm, whereas the calculated peak was only 2.5 cm and occurred at about 12 ms. The calculated displacement of the center of the roof agrees very well with the measured response up to 8 ms; however, the calculated displacement reached a maximum of 3.4 cm at 12 ms while the measured maximum was approximately 20 cm at 35 ms.

6.2 EFFECT OF CLAY VERSUS SAND BACKFILL

For locations in the backfill, the arrival times computed for the clay were greater and the peak stresses were smaller than those computed for the sand. Because the ratio of structure to backfill initial wave speeds is greater for the clay, the influence of the structure on both arrival times and rise times of the stress waves is more pronounced than with the sand.

Although stresses within the sand backfill were higher than those in the clay, the peak stress and impulse delivered to the center of the roof were higher for the clay calculation. Stress and impulse over the sidewall, however, were greater for the sand backfill case. Stresses around the structure at late times were more uniform in the clay calculation whereas in the sand calculation they still tended to concentrate near the corners. The differences noted in stress and impulse distribution patterns result solely from the change in backfill.

The maximum relative deflection of the center of the roof for the clay backfill case was 3.2 cm and occurred at 8.5 ms while that for the sand was only 0.6 cm and occurred at 3.2 ms. The neutral axis deflections all around the structure at late times were greater for the clay backfill.

6.3 EFFECT OF 1D VERSUS 2D CALCULATIONAL GEOMETRY

Vertical stress calculations were compared at depths of 1, 2, 4, and 6 feet in the backfill for elements located 5.5 feet from the sidewall of the structure and 1.5 feet from the edge of the excavation. Agreement at all depths was excellent for the sand backfill case. The same was true for the clay backfill at the 1- and 2-foot depths, but at greater depths the 2D calculation histories were significantly altered by waves coming through the native soil ahead of those traveling directly through the backfill.

For a 1D section through the center of the roof, stresses computed in both the sand and the clay backfills were in excellent agreement with the 2D results for at least 3 ms. This was true in spite of the fact that both 2D calculations clearly showed that 1D plane wave loading condition only lasted over the roof for a much shorter time, i.e., about 0.3 ms after initial impact or less. For practical purposes, 1D calculations of stress and impulse applied to the center of the roof appear to be quite adequate for the first 1 ms of loading after impact.

A 1D section through the sidewall of the structure is a very poor representation of actual geometry. Results from 1D calculations can be misleading for locations near the structure corners.

REFERENCES

1. Sam A. Kiger and Jim Getchell; "Vulnerability of Shallow Buried Flat Roof Structures; Report 1, FOAM HEST 1 and 2"; WES report in prepaation; U. S. Army Engineer Waterways Experiment Station, CE, Vicksburg, MS.

2. J. E. Windham; "One-Dimensional Wave Propagation Calculations and Analyses Related to Possible Tensile Wave Phenomena in a HEST Test of a Shallow-Buried Rectangular Box Structure"; WES informal report to DNA, Oct 1977; U. S. Army Engineer Waterways Experiment Station, CE, Vicksburg, MS.

3. S. W. Key; "HONDO--A Finite Element Computer Program for the Large Deformation Dynamic Response of Axisymmetric Soils"; SLA-74-0039, Apr 1974; Sandia Laboratories, Albuquerque, NM.

4. J. O. Curtis; "Modification and Evaluation of HONDO: A Dynamic, Axisymmetric Finite Element Code"; Miscellaneous Paper S-76-3, Apr 1976; U. S. Army Engineer Waterways Experiment Station, CE, Vicksburg, MS.

5. R. W. Young, et al; "HONDO Code UPGRADE"; Report No. UCID-17611, Prepared for the U. S. Army Engineer Waterways Experiment Station under Contract No. WES 77-05 through ERDA under Contract No. W-7405-Eng-48, Oct 1977; Lawrence Livermore Laboratory; Livermore, CA.

6. R. D. Crowson and S. A. Kiger; "The Effect of Earth Cover on the Dynamic Response of Hardened Reinforced Concrete Structures"; The Shock and Vibration Bulletin No. 47, Part 4, Structural Dynamics System Identification, Computer Applications, Sep 1977; The Shock and Vibration Information Center, Naval Research Laboratory, Washington, D. C.

7. Sam A. Kiger; "Static Test of a Hardened Shallow-Buried Structure"; Technical Report N-78-7, Oct 1978; U. S. Army Engineer Waterways Experiment Station, CE, Vicksburg, MS.

8. I. S. Sandler, F. L. DiMaggio, and G. Y. Baladi; "Generalized Cap Model for Geological Materials," Journal of the Geotechnical Engineering Division, GT7, Jul 1976; American Society of Civil Engineers, New York.

9. U. S. Department of Defense, "Unified Soil Classification System for Roads, Airfields, Embankments, and Foundations"; Military Standard MIL-STD-619B, Jun 1968; Washington, D. C.

10. J. Q. Ehrgott; "Project HARDPAN, Laboratory Material Property Test Data"; WES unpublished report; U. S. Army Engineer Waterways Experiment Station, CE, Vicksburg, MS.

11. J. G. Jackson, Jr.; "Physical Property and Dynamic Compressibility Analysis of the Watching Hill Blast Range"; Technical Report S-77-4, Apr 1977; U. S. Army Engineer Waterways Experiment Station, CE, Vicksburg, MS.

12. J. E. Windham and J. O. Curtis; "Effect of Backfill Property and Airblast Variations on the External Loads Delivered to Buried Box Structures"; Technical Report S-78-5, Jun 1978; U. S. Army Engineer Waterways Experiment Station, CE, Vicksburg, MS.

13. P. F. Hadala; "The Effect of Placement Method on the Response of Soil Stress Gages"; Technical Report No. 3-803, Nov 1967; U. S. Army Engineer Waterways Experiment Station, CE, Vicksburg, MS.

APPENDIX A

ANALYSES TO DETERMINE MATERIAL PROPERTIES FOR THE CONCRETE STRUCTURE

A.1 INTRODUCTION

Prior to performing finite-element (FE) backfill/structure interaction calculations for Foam HEST 1, continuum properties for the concrete elements in the FE grid needed to be chosen so as to simulate the load-deformation response of the actual reinforced concrete box structure. The decision was made, after contacting a number of consultants involved with modeling reinforced concrete structures in FE calculations and considering the lack of time available for implementing a new model into the HONDO code, to use a linear elastic-ideally plastic model already incorporated in the code. The properties needed for the model are Young's modulus E, Poisson's ratio ν (assumed to be 0.25), and a limiting value of elastic stress f_y.

The results of a forced vibration test and a three-dimensional (3D) eigenvalue analysis of the uncovered box structure are presented in Reference 6* along with structural details and dimensions. The results of the vibration test indicated a natural frequency of 150 Hz; the 3D eigenvalue analysis produced a natural frequency of 144 Hz for the same mode. A value of E was determined for the two-dimensional (2D) backfill/structure interaction FE calculations by conducting 2D eigenvalue or modal analyses of the uncovered structure and varying E until the natural frequency measured during the forced vibration test was produced.

Reference 7 presents the results of a static test on a one-half scale model of the Foam HEST 1 structure. The results of this test were subsequently used to determine the bending moment (24,360 inch-pounds) and axial thrust (5000 pounds) at failure for the full-scale structure.** These values were used in a subsequent analysis to determine a

---

* Numbered references in the appendices of this report indicate references cited in the main text.

** Values extracted from briefing chart furnished by Sam A. Kiger, Structures Laboratory, WES.

value of f_y for the elastic-plastic model of the structure elements in the FE calculations.

A.2 DETERMINATION OF E

The modal analyses were performed with the SAP IV elastic FE code;* they were designed to simulate the structure placed in the excavation but uncovered. The FE grid of the structure is shown in Figure A.1; the same grid spacing was used to model the structure in the 2D backfill calculations. The actual box structure has outside dimensions of 4.93 feet (1.5 metres) and has a wall thickness of 5.6 inches (14.2 centimetres); the structural representation used in the modal analyses has outside dimensions of 5 feet (1.52 metres) and a wall thickness of 6 inches (15.2 centimetres). The element size used in the structure was 1.5 inches (3.8 centimetres). The concrete used in the structure had a f'_c of 5700 psi (393 bars). From the ACI code**

$$E = W^{1.5} \cdot 33 \sqrt{f'_c} \qquad (A.1)$$

where E = Young's modulus and W = unit weight of concrete = 150 pcf (2.4 gm/cc). Young's modulus of the concrete is calculated to be 4.58×10^6 psi (3.16×10^5 bars). Eigenvalue analyses were conducted for this structural representation using E values of 4.0×10^6 psi (275.9 bars) and 5.0×10^6 psi (344.9 bars). A ν value of 0.25 was used for both analyses.

Only the bottom of the structure was in contact with the soil during the forced vibration test. For the eigenvalue analyses the soil was modeled by horizontal and vertical springs attached to the bottom nodes of the structure. The values of the vertical spring constants

---

* E. L. Wilson, et al; "Computer Programs for Static and Dynamic Analyses of Linear Structural Systems"; EERC Report No. 72-10, Nov 1972; Department of Civil Engineering, University of California, Berkeley, CA.

** ACI Standard Building Code Requirements for Reinforced Concrete, ACI 318-63, Jun 1963; American Concrete Institute, Detroit, MI.

K_v were determined by multiplying the constrained modulus of the soil (62 ksi or 4276 bars) by the distance between the nodes (1.5 inches or 3.8 centimetres), which gives K_v = 90 ksi (6207 bars). The values of the horizontal spring constants K_H were assumed to be 5 ksi (345 bars).

The first ten modes and corresponding natural frequencies were determined from the eigenvalue calculations. The mode shapes and frequencies are presented in Figures A.2 and A.3 for the eigenvalue calculations with E of 4.0×10^6 psi and 5.0×10^6 psi, respectively. The natural frequencies for the structure from both calculations are presented in Table A.1. The second structural mode from both calculations matched the mode shape measured during the vibration test on the structure; the calculated frequencies were 145.9 and 161.0 Hz. As discussed earlier, the experimentally determined frequency for this mode shape was 150 Hz. Interpolation between the calculated frequencies gave a Young's modulus of 4.2×10^6 psi (2.9×10^5 bars) for the 150-Hz frequency.

A.3 DETERMINATION OF f_y

As previously described, the ultimate moment and thrust for the Foam HEST 1 roof slab were determined to be 24,360 inch-pounds and 5000 pounds, respectively. For the purpose of determining a value of f_y for the model, the roof of the structure was assumed to behave as an elastic-plastic beam having a simple linear thrust-moment diagram which would pass through the above failure point, as shown in Figure A.4. The maximum thrust for a 6-inch-deep beam of unit width is given by

$$T_m = f_y A = 6 f_y \qquad (A.2)$$

The plastic section modulus Z for such a beam equals $bd^2/4$ or 9; therefore, the maximum plastic moment for the beam is

$$M_m = f_y Z = 9 f_y \qquad (A.3)$$

The equation for a linear thrust-moment line is

$$T = T_m - \left(\frac{T_m}{M_m}\right) M \qquad (A.4)$$

Substituting Equations A.2 and A.3 intc A.4 gives

$$f_y = \frac{3T + 2M}{18} \qquad (A.5)$$

Thus, in order to pass through the point $T = 5000$ pounds and $M = 24{,}360$ inch-pounds, f_y must equal 3540 pounds/inch^2.

Table A.1 Calculated Natural Frequencies from the Modal Analyses of the Uncovered Box Structure

Mode No.	Frequency, Cycles/Second	
	$E = 4.0 \times 10^6$ psi (2.76×10^5 bars)	$E = 5.0 \times 10^6$ bars (3.45×10^5 bars)
1	37.44	41.09
2	145.90	161.00
3	185.90	193.00
4	271.50	301.00
5	295.80	315.50
6	344.50	368.40
7	369.70	393.40
8	560.80	622.50
9	599.90	667.10
10	800.10	882.30

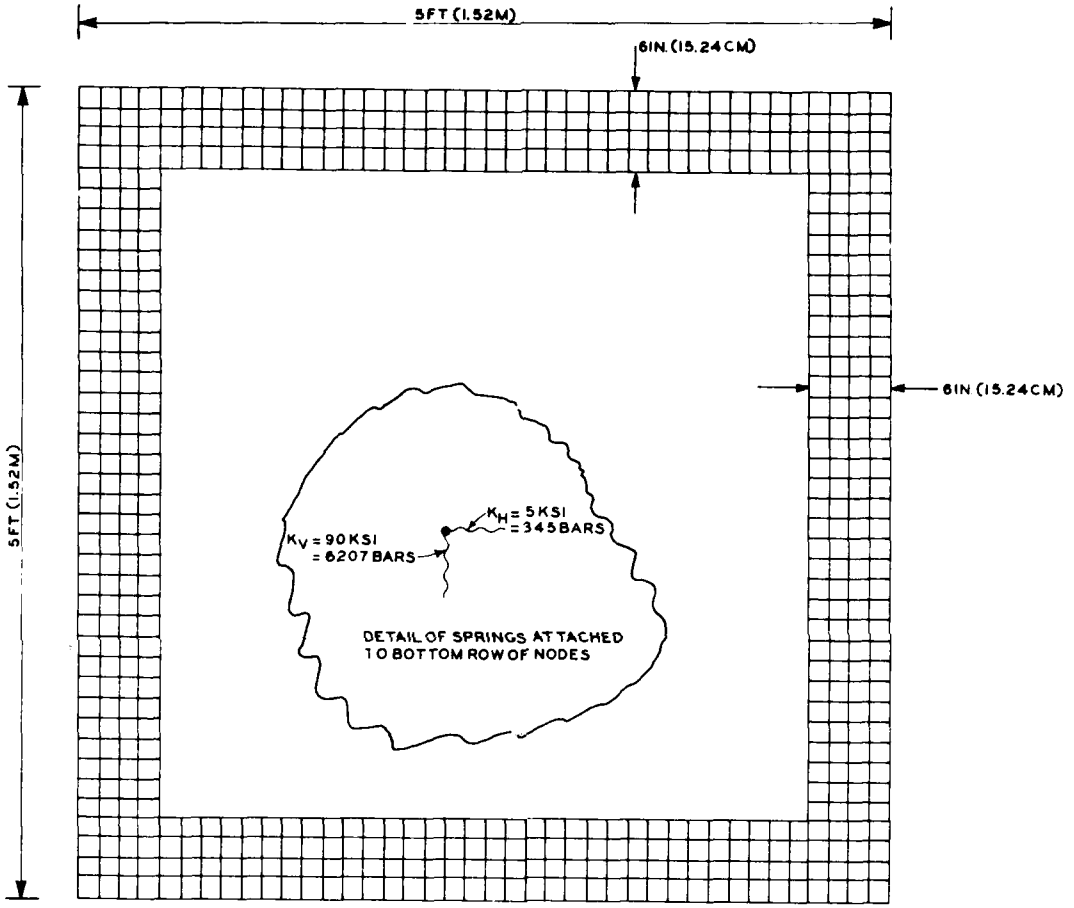

Figure A.1 Geometry used for modal analyses.

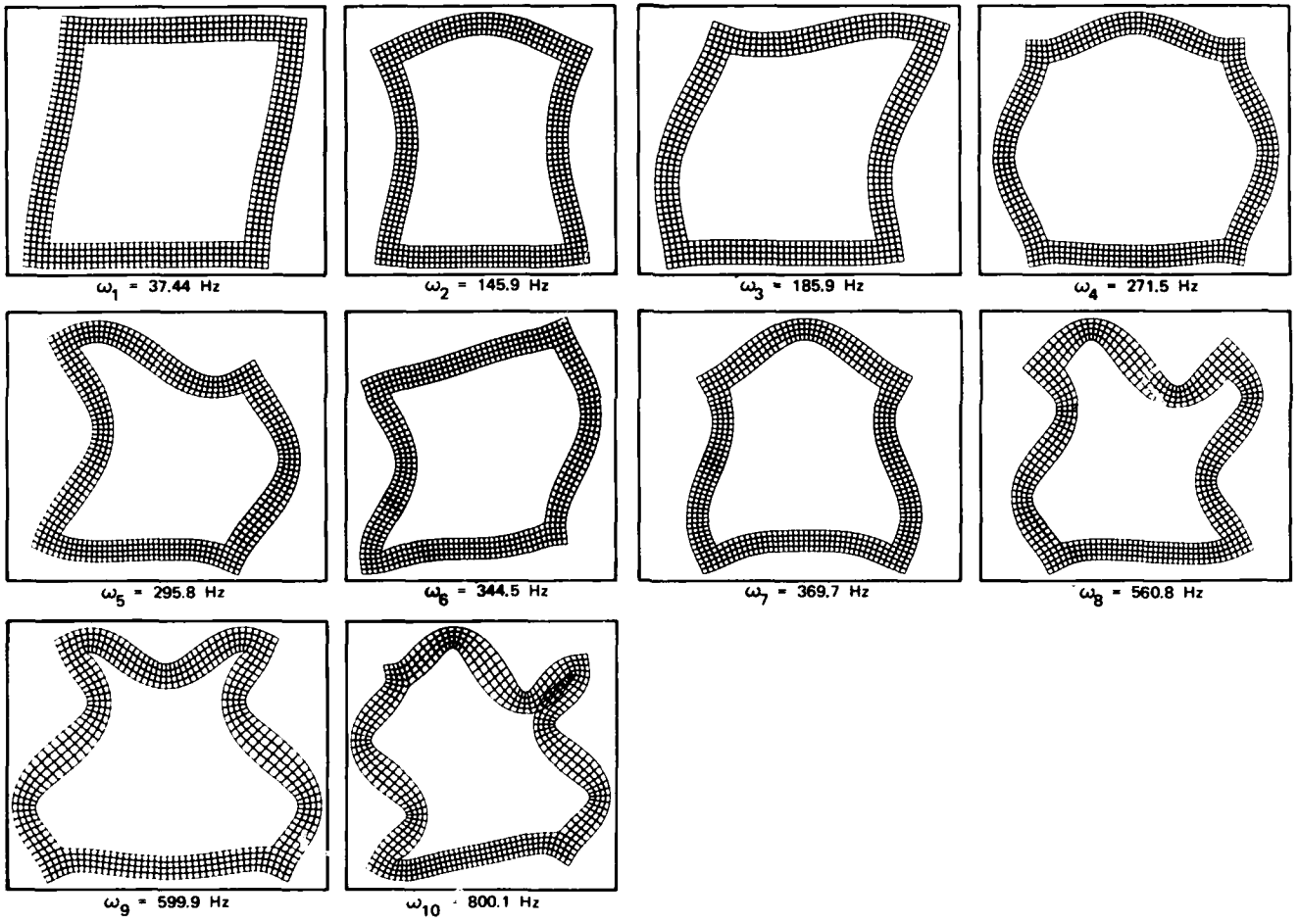

Figure A.2 Mode shapes and corresponding natural frequencies from the eigenvalue calculations with $E = 4 \times 10^6$ psi (2.76×10^5 bars) for the structure.

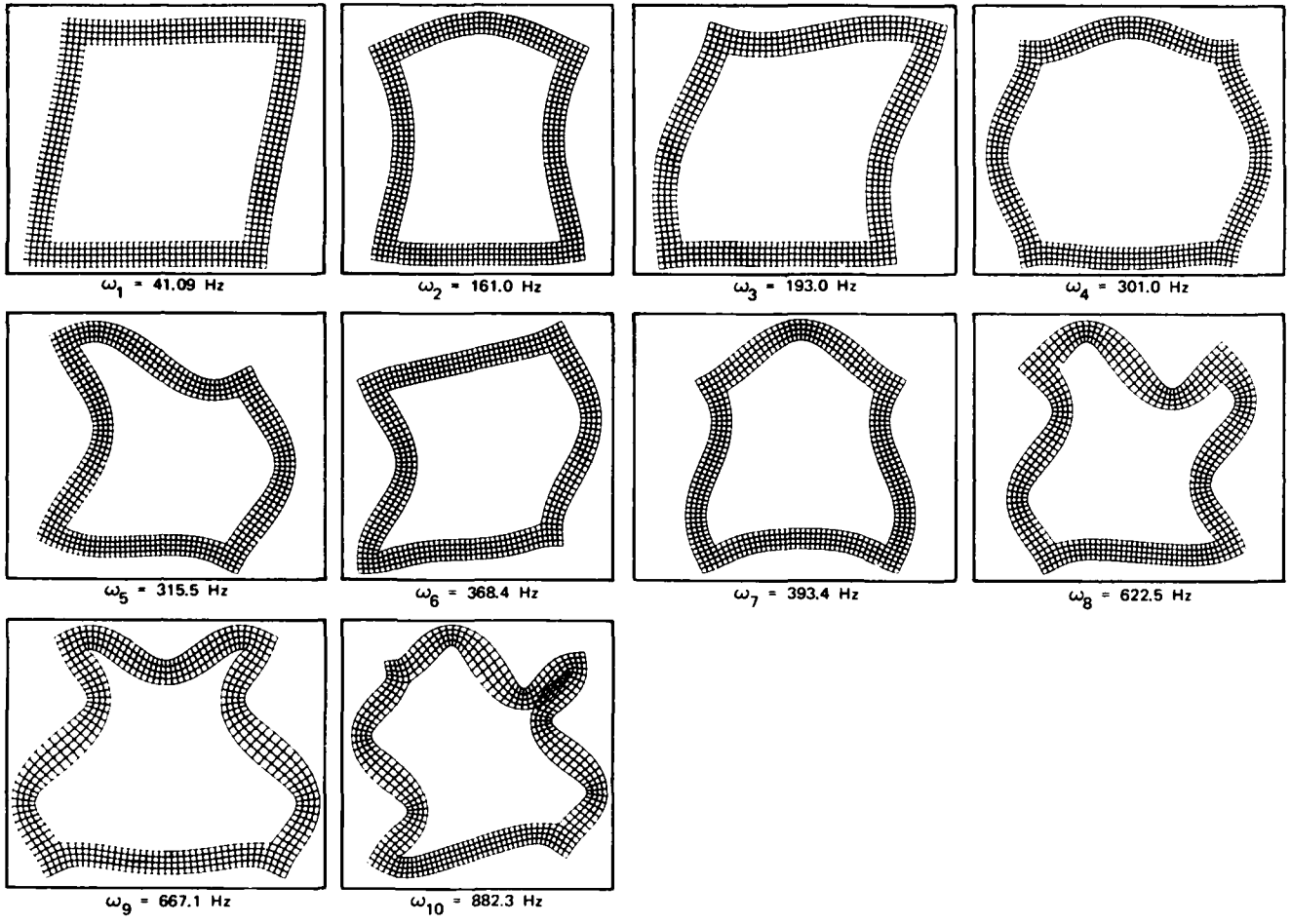

Figure A.3 Mode shapes and corresponding natural frequencies from the eigenvalue calculations with $E = 5 \times 10^6$ psi (3.45×10^5 bars) for the structure.

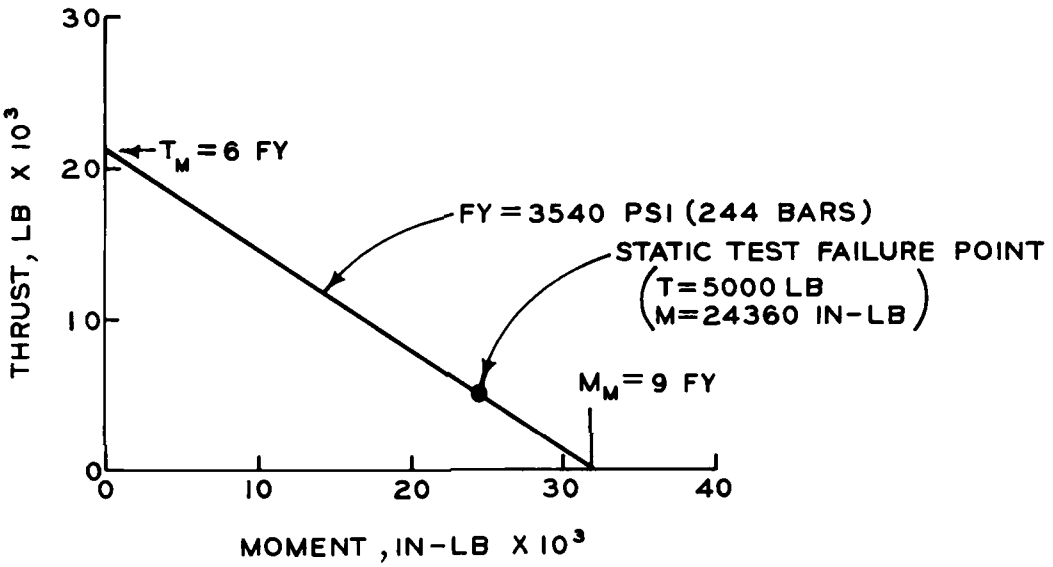

Figure A.4 Moment-thrust diagram for concrete model.

APPENDIX B

SOIL PROPERTY TESTS AND ANALYSES

In order to perform the FE calculations described in the main text, mechanical property estimates were required for three soil materials, i.e., the sand actually used to backfill the Foam HEST 1 (FH1) structure excavation, the undisturbed native soils at the test site located immediately adjacent to and beneath the excavation, and a hypothetical (yet realistic) clay backfill whose limiting shear strength envelope would be appreciably lower and in marked contrast to that of the FH1 sand. Only the sand was available for laboratory testing; results from a limited series of tests on this material are presented herein, along with the analyses and assumptions used in making property recommendations for all three soil materials.

B.1 FH1 SAND BACKFILL

The FH1 backfill was a locally purchased, poorly graded sand (SP). Laboratory classification tests indicated a specific gravity of 2.66 and a grain-size distribution as shown in Plate B.1. Measurements made during construction indicate an average water content of 3.2 percent and a dry unit weight of 102 pcf (1.63 gm/cc), i.e., an "as-placed" wet density of 105.3 pcf (1.69 gm/cc).

Blast pressure gages BP-2, BP-3, and BP-5 recorded peak pressures on the backfill surface of 105.5, 146.9, and 175.2 bars, respectively, at about 0.18 ms, i.e., a loading rate on the order of 600 to 1000 bars/ms. The arrival time versus distance data shown in Figure B.1 indicate that the airblast was traveling with a velocity of 20 feet/ms. Arrival times are also shown in Figure B.1 for the three roof interface pressure gages (IF-1, IF-2, and IF-3) and two soil stress gages (SE-3 and SE-6) that were located at a depth of 2 feet. Approximately 1.2 ms was required for the stress wave to travel this distance, indicating an initial P-wave velocity of 1.67 feet/ms. This velocity appears to be relatively constant to a depth of 7 feet, i.e., the SE gage records

plotted in Figure B.2 depict an arrival velocity of 1.63 feet/ms. A wet density of 105.3 pcf and an average wave speed of 1.65 feet/ms imply a constrained modulus of 61.8 ksi (4260 bars).

One static and three dynamic uniaxial strain (UX) tests were conducted with a gas-driven ram loader on 6.30-centimetre-high by 13.40-centimetre-diameter remolded specimens of FH1 sand. The maximum vertical stress in static test FH.1 was 140 bars and was applied in about 1 minute; complete results are plotted in Plate B.2. As shown in Plates B.3, B.4, and B.5, 100-bar dynamic loads were applied in 5 to 8 ms, i.e., a loading rate of about 15 bars/ms. Dry sands are generally considered to be rate-independent for practical applications in which the loading times are on the order of several milliseconds or longer. These data are no exception, i.e., stress-strain curves for all four tests are essentially identical. Strain at 100 bars averaged 5.9 percent, representing a secant modulus of only 24.6 ksi.

Another series of UX tests was conducted on 1.27-centimetre-high by 9.14-centimetre-diameter specimens using a new exploding-bridgewire device in order to determine if the compressibility of the FH1 sand was sensitive to submillisecond loadings. Results from five tests are shown in Plate B.6; loading rates to 100 bars ranged from static to about 300 bars/ms. Strains at 100 bars ranged from 4.1 percent for static test FH.16 to 0.78 percent for dynamic test FH.14, representing a change in secant modulus from about 35 ksi to about 186 ksi. While 300 bars/ms is still a much slower loading rate than was actually applied to the sand backfill during FH1, comparison of one-dimensional wave propagation calculation results with the FH1 stress measurements indicated that 186 ksi was much too stiff to recommend for a UX loading modulus. Instead, the dynamic UX stress-strain relation shown in Figure B.3, which has the field-inspired linear loading modulus of 61.8 ksi (4260 bars), was recommended for the proposed FE calculations. The questions raised regarding rate-dependent versus rate-independent and laboratory-measured versus field-measured sand backfill properties are referred to "future research."

In order to obtain paths of principal stress difference ($\sigma_z - \sigma_r$) versus mean normal stress $P = (\sigma_z + 2\sigma_r)/3$ for a state of uniaxial strain, two static K_o tests (FH.9 and FH.10) were conducted on 7.6-centimetre-high by 5.6-centimetre-diameter specimens in a triaxial test device. Results are plotted in Plates B.7 and B.8. The slope of the UX stress path at any point is $2G/K$, where G is the shear modulus and K is the bulk modulus. The assumption was made (due to a lack of data more than anything else) that the rate effects on G and K are the same and, hence, that the dynamic and static stress paths are the same. The path recommended for the FE calculations is shown in Figure B.4; initial loading and unloading values of Poisson's ratio ν are noted.

Static triaxial compression (TX) tests FH.5A, FH.6, FH.7, and FH.8 were conducted on 12.7-centimetre-high by 5.3-centimetre-diameter specimens with constant confining pressures of 6.9, 34.5, 69.0, and 103.4 bars, respectively. Results are presented in Plates B.9, B.10, B.11, and B.12. Failure was defined as the maximum principal stress difference or the stress difference at 20 percent strain difference, whichever occurred first. The failure envelope derived from these tests is plotted in Figure B.4; and since the literature available at the time indicated that failure relations for dry sands are relatively insensitive to loading rate, this envelope was also assumed to represent the dynamic behavior of FH1 sand.

B.2 UNDISTURBED NATIVE SOILS

FH1 was conducted at a remote site south of Hineston, Louisiana, on the Fort Polk reservation. A limited subsurface exploration program was conducted by the Baton Rouge office of Woodward-Clyde Consultants.* Three borings were drilled and logged to a depth of 30 feet (9.1 metres) based on visual classifications; the excavation for the structure was also logged. Standard penetration blow-counts were recorded in cohesionless materials; estimates of unconfined compressive strength for the

---

* Woodward-Clyde Consultants letter report to WES dated 28 July 1977 re soil borings drilled under purchase order No. DACW39-77-M-4313.

cohesive materials were made from pocket penetrometer readings. The material down to about 12 feet is described as a very stiff-to-hard, tan, light gray, and red sandy clay with a UC strength of about 4.5 tsf; a dense, orange, fine-to-coarse sand with an SPT resistance of 26 to 30 blows/foot was encountered at the 12-foot depth in two of the three borings. No groundwater was observed entering the boreholes.

Undisturbed samples suitable for laboratory compressibility and strength tests were not obtained. Even limiting compressibility estimates based on in situ air voids could not be made since there were no density or water content data. In the absence of any quantitative mechanical property data, the properties of the native site materials both adjacent to and beneath the structure excavation were assumed to be the same as those of the FH1 sand backfill given in Figures B.3 and B.4.

B.3 HYPOTHETICAL CLAY BACKFILL

The backfill placed around the structures in Project HARD PAN* was a plastic clay (CH) of relatively low strength. Compaction to a dry density of 96.0 pcf (1.54 gm/cc) at a water content of 20.7 percent requires about 97 percent of Standard Proctor effort; air voids would be 12.1 percent. Static and dynamic UX and TX test data for this material are available in Reference 10. Some data on the effect of loading rate on the compressibility of clays are also contained in Reference 11. Based on this information, clay backfill properties were postulated for the proposed FE calculations. The recommended dynamic UX stress-strain relation is given in Figure B.5; the UX stress path and TX failure envelope are given in Figure B.6.

---

* A series of high-explosive experiments conducted by AFWL at Trading Post Kansas, during 1974 and 1975.

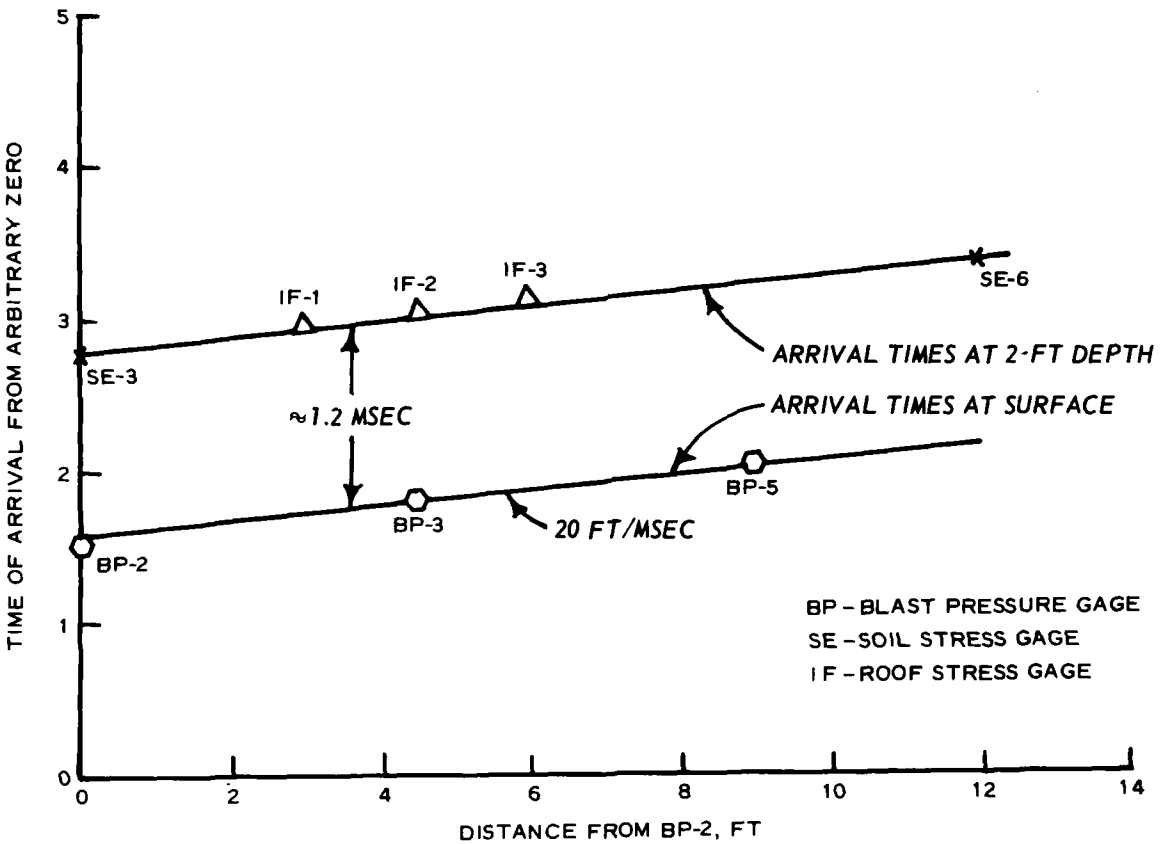

Figure B.1 Foam HEST 1 times of arrival from arbitrary zero versus distance from blast pressure gage BP-2.

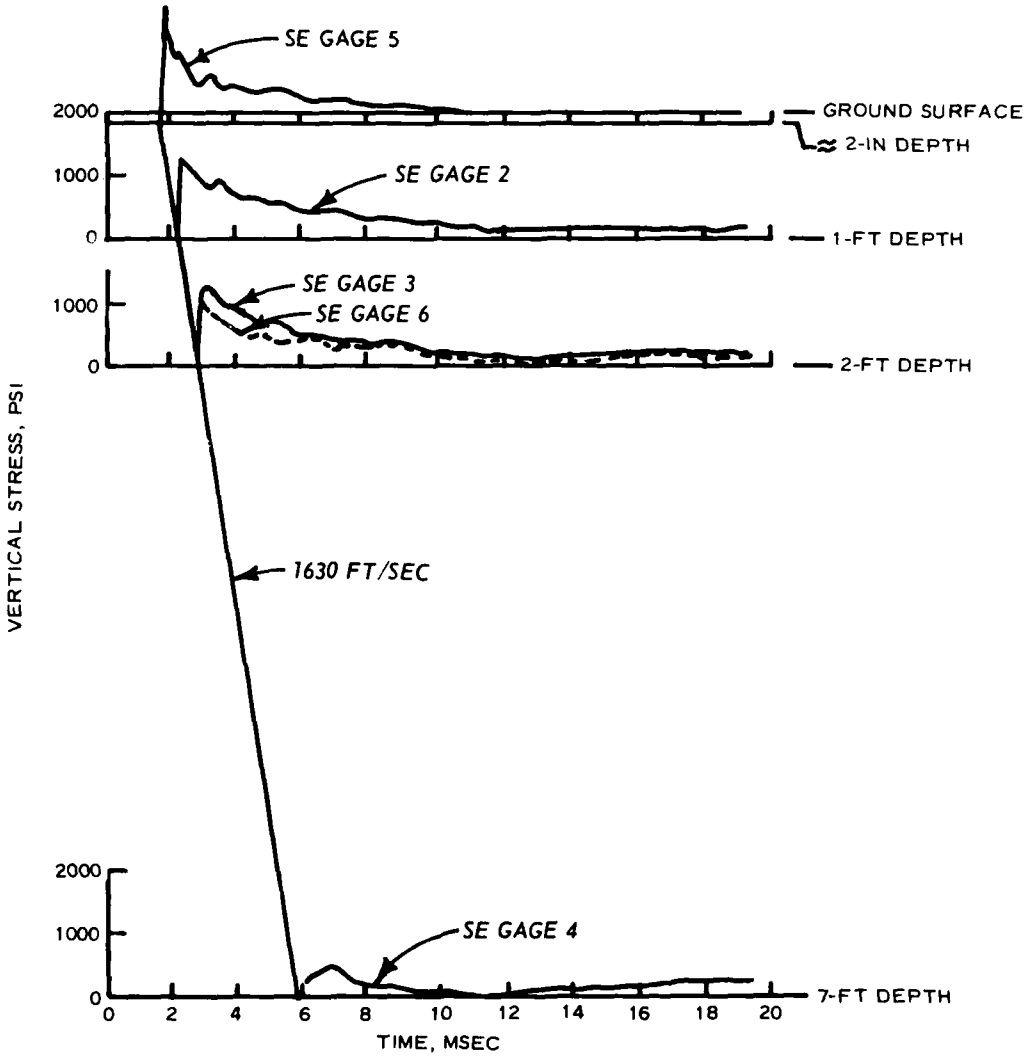

Figure B.2 Vertical stress-time histories measured in the Foam HEST 1 sand backfill.

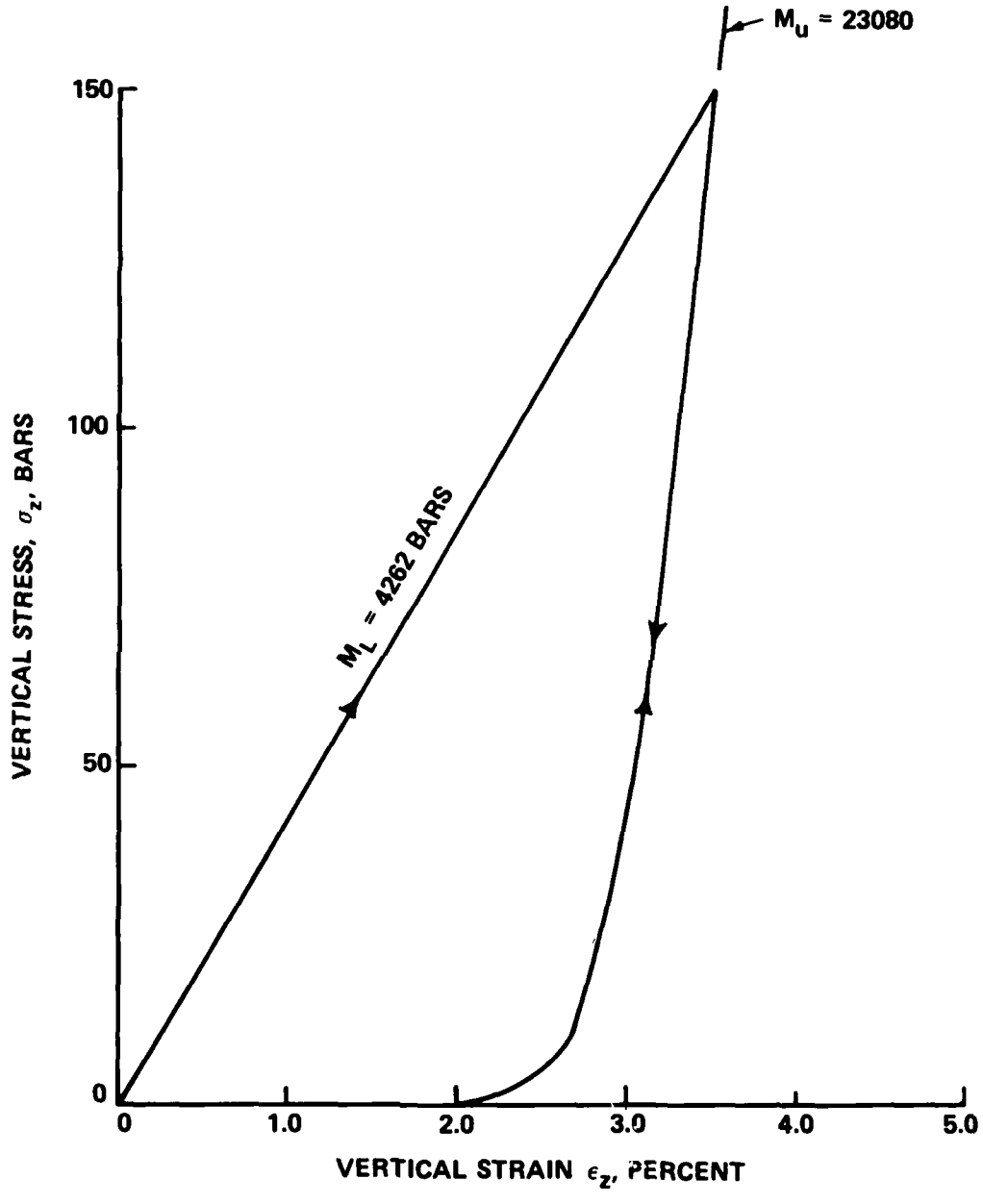

Figure B.3 Recommended dynamic UX stress-strain relation for Foam HEST 1 sand backfill.

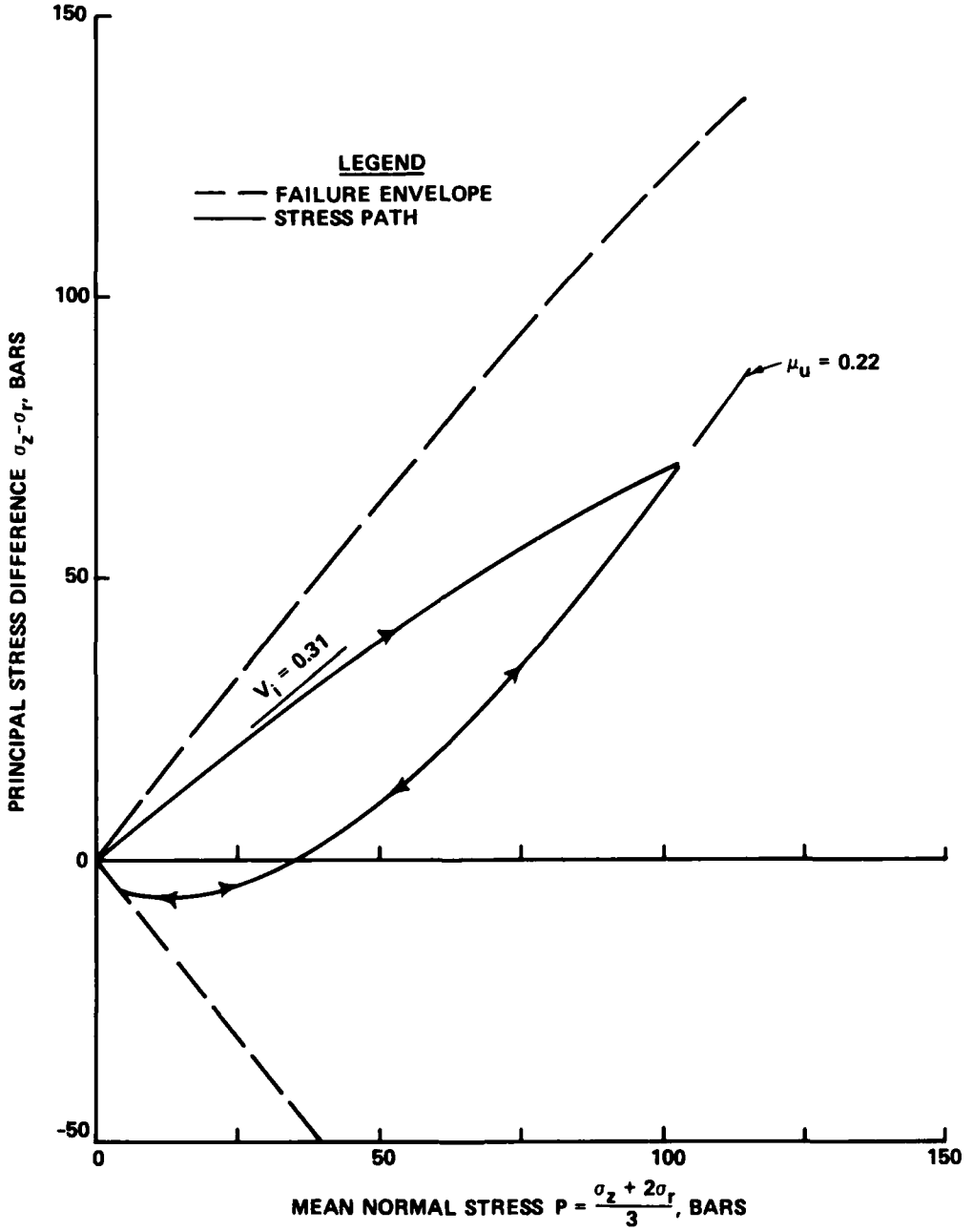

Figure B.4 Recommended dynamic UX stress-path and TX failure envelope for Foam HEST 1 sand backfill.

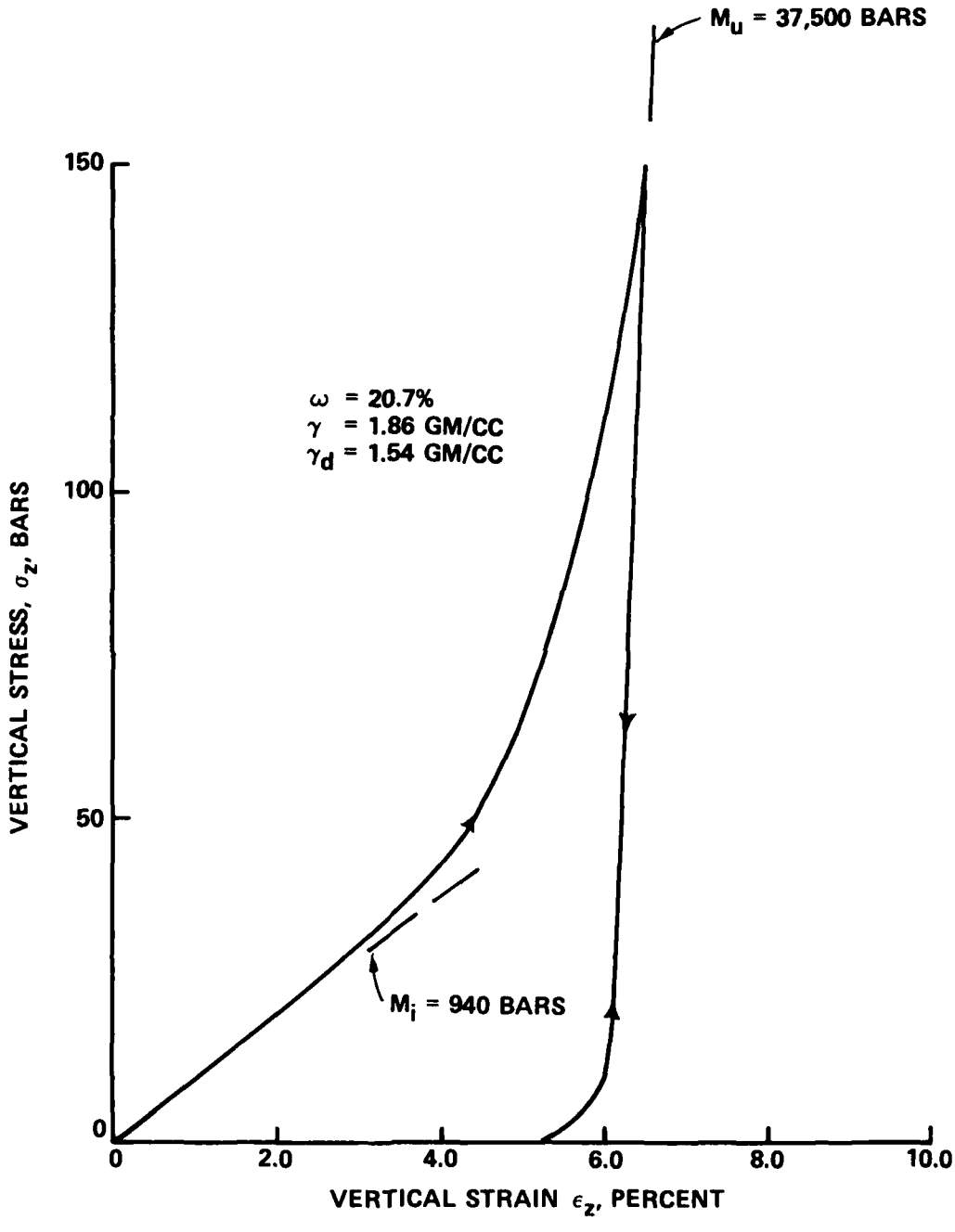

Figure B.5 Recommended dynamic UX stress-strain relation for clay backfill.

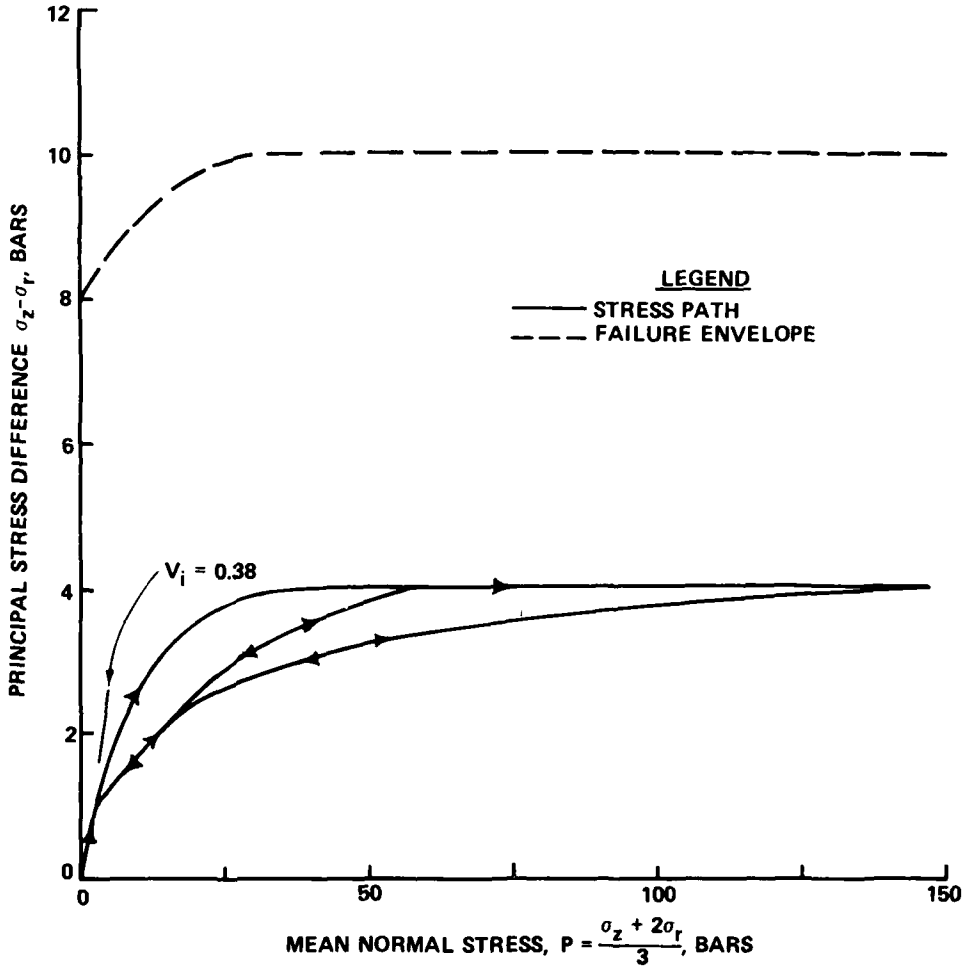

Figure B.6 Recommended dynamic UX stress-path and TX failure envelope for clay.

AD-A085 255 ARMY ENGINEER WATERWAYS EXPERIMENT STATION VICKSBURG--ETC F/G 18/3
FINITE-ELEMENT CALCULATIONS OF FOAM HEST 1.(U)
APR 80 J E WINDHAM
UNCLASSIFIED WES/MP/SL-80-1 NL

2 OF 2
AD
A085255

END
DATE FILMED
7-80
DTIC

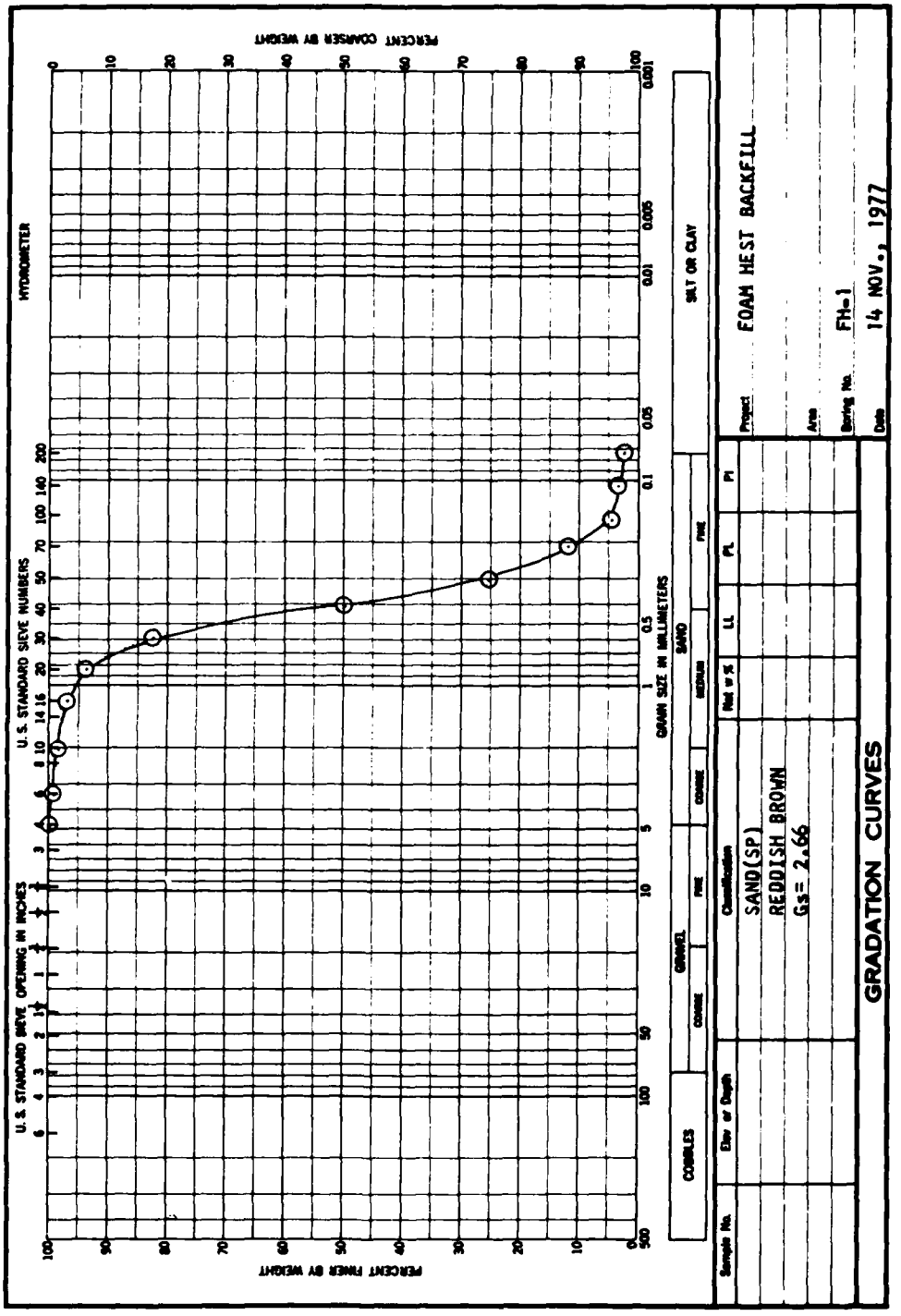
GRADATION CURVES
Project FOAM HEST BACKFILL
Boring No. FH-1
Date 14 NOV., 1977
Sample No.
Elev or Depth
Classification
SAND(SP)
REDDISH BROWN
Gs= 2.66
Nat w %
LL
PL
PI
COBBLES
GRAVEL
SAND
SILT OR CLAY
COARSE
FINE
COARSE
MEDIUM
FINE
U. S. STANDARD SIEVE OPENING IN INCHES
U. S. STANDARD SIEVE NUMBERS
HYDROMETER
GRAIN SIZE IN MILLIMETERS
PERCENT FINER BY WEIGHT
PERCENT COARSER BY WEIGHT

Plate B.1

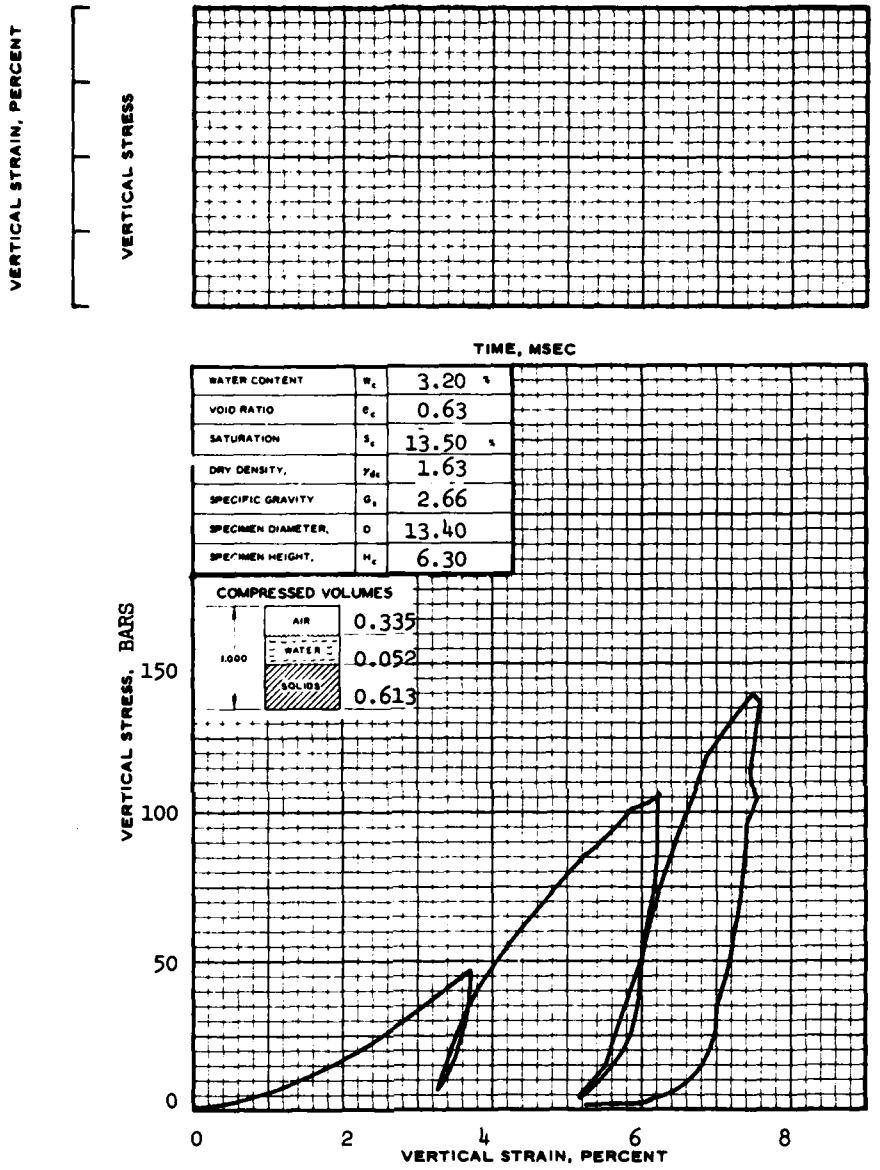

CLASSIFICATION Sand (SP)

LL = . PL = . PI =

e_o = 0.63 S_o = 13.5 %

REMARKS Remolded

PROJECT	FOAM HEST BACKFILL
AREA	
BORING NO.	SAMPLE NO.
DEPTH EL	DATE Nov. 1977

UNIAXIAL STRAIN TEST RESULTS

STATIC TEST FH.1

Plate B.2

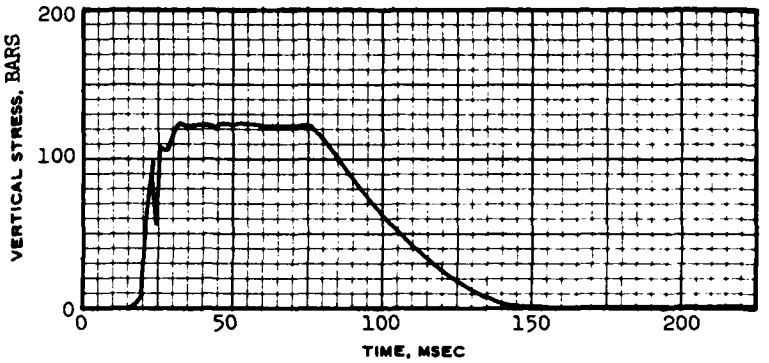

WATER CONTENT	w_c	3.20 %
VOID RATIO	e_c	0.63
SATURATION	S_c	13.50 %
DRY DENSITY, gm/cc	γ_{dc}	1.63
SPECIFIC GRAVITY	G_s	2.66
SPECIMEN DIAMETER, cm	D	13.40
SPECIMEN HEIGHT, cm	H_c	6.30

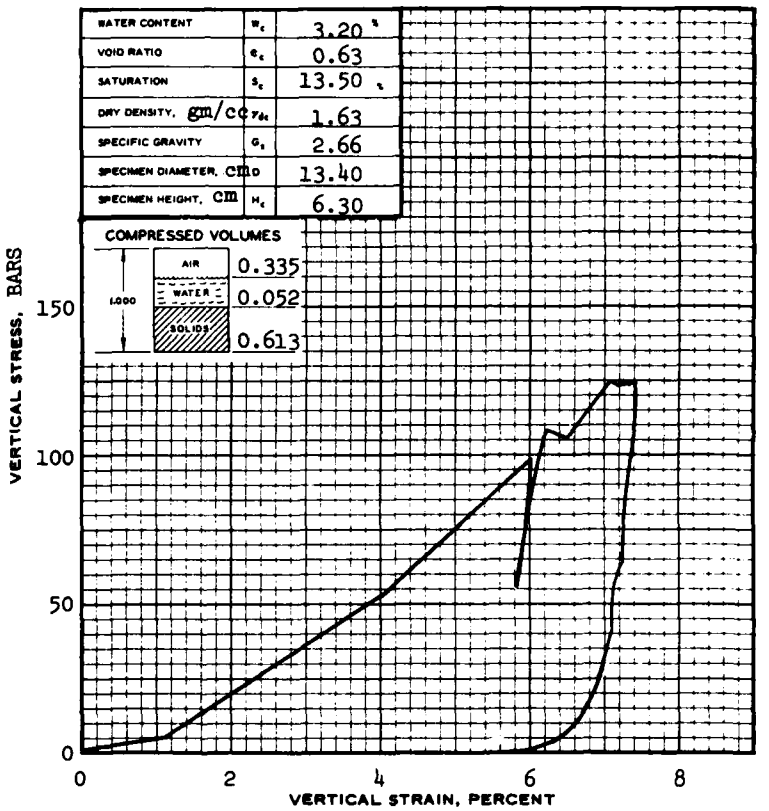

CLASSIFICATION Sand (SP)

LL = , PL = , PI =

e_o = 0.63 S_o = 13.5 %

REMARKS Remolded

PROJECT FOAM HEST BACKFILL	
AREA	
BORING NO.	SAMPLE NO.
DEPTH EL.	DATE Nov. 1977

UNIAXIAL STRAIN TEST RESULTS

DYNAMIC TEST FH.2

Plate B.3

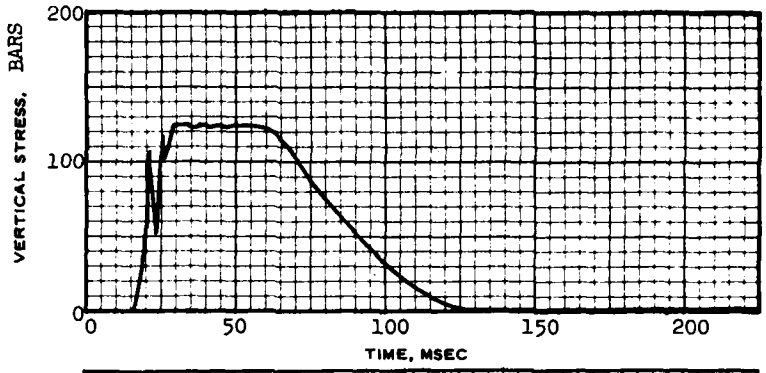

WATER CONTENT	w_c	3.20 %
VOID RATIO	e_c	0.63
SATURATION	S_c	13.50 %
DRY DENSITY, gm/cc	γ_{dc}	1.63
SPECIFIC GRAVITY	G_s	2.66
SPECIMEN DIAMETER, cm	D	13.40
SPECIMEN HEIGHT, cm	H_c	6.30

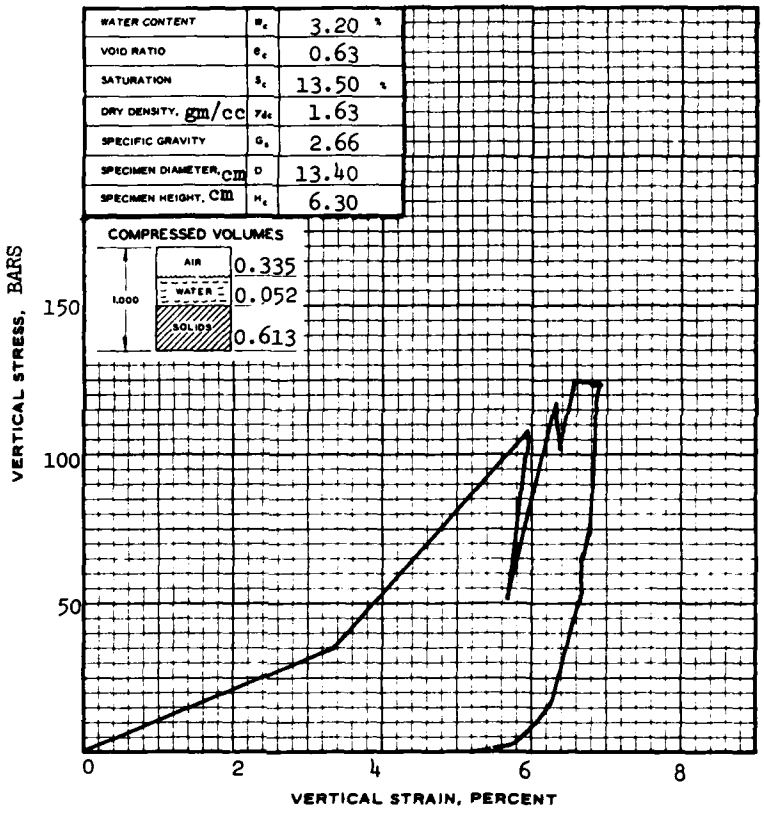

CLASSIFICATION Sand (SP)

LL = , PL = , PI =

e_o = 0.63 S_o = 13.50 %

REMARKS Remolded

PROJECT FOAM HEST BACKFILL	
AREA	
BORING NO.	SAMPLE NO.
DEPTH EL	DATE Nov. 1977

UNIAXIAL STRAIN TEST RESULTS

DYNAMIC TEST FH.3

Plate B.4

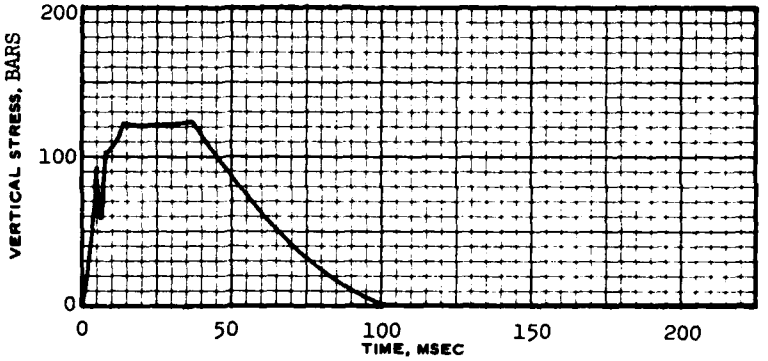

WATER CONTENT	w_c	3.20 %
VOID RATIO	e_c	0.63
SATURATION	S_c	13.50 %
DRY DENSITY, gm/cc	γ_{dc}	1.63
SPECIFIC GRAVITY	G_s	2.66
SPECIMEN DIAMETER, cm	D	13.40
SPECIMEN HEIGHT, cm	H_c	6.90

COMPRESSED VOLUMES

AIR	0.335
WATER	0.052
SOLIDS	0.613

1.000

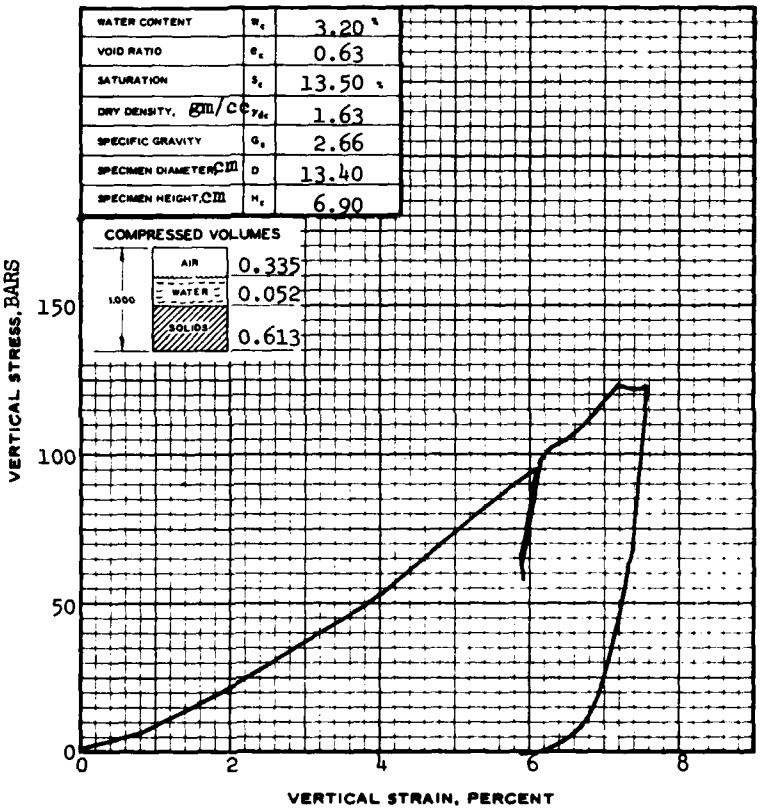

CLASSIFICATION Sand (SP)

LL = , PL = , PI =

e_o = 0.63 S_o = 13.5 %

REMARKS Remolded

PROJECT FOAM HEST BACKFILL	
AREA	
BORING NO.	SAMPLE NO.
DEPTH EL	DATE Nov. 1977

UNIAXIAL STRAIN TEST RESULTS

DYNAMIC TEST FH.4

Plate B.5

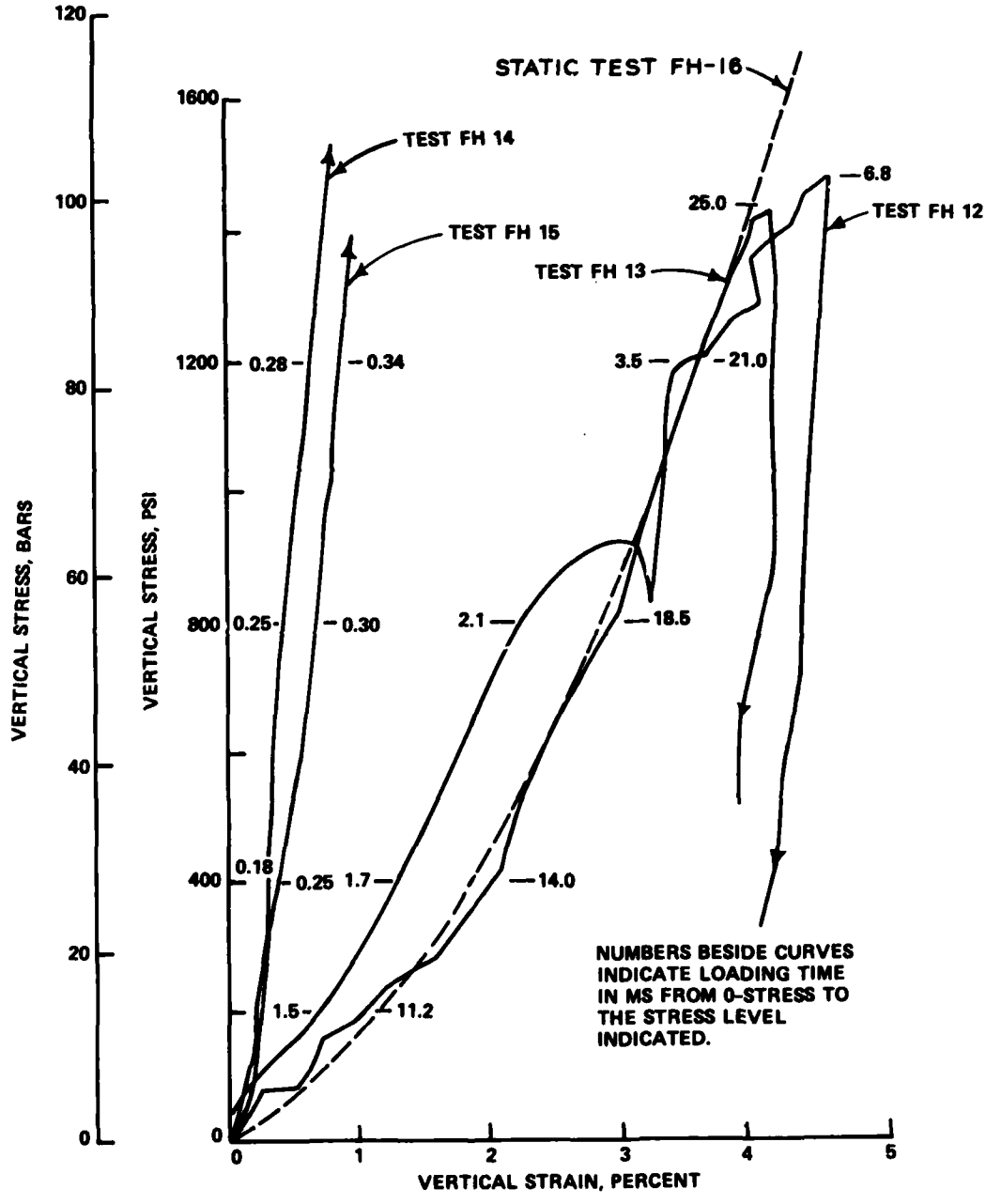
STATIC TEST FH-16
TEST FH 14
TEST FH 15
TEST FH 13
TEST FH 12
6.8
25.0
0.28
0.34
3.5
21.0
0.25
0.30
2.1
18.5
0.18
0.25
1.7
14.0
1.5
11.2
NUMBERS BESIDE CURVES INDICATE LOADING TIME IN MS FROM 0-STRESS TO THE STRESS LEVEL INDICATED.
VERTICAL STRESS, BARS
VERTICAL STRESS, PSI
VERTICAL STRAIN, PERCENT
120
100
80
60
40
20
0
1600
1200
800
400
0
1
2
3
4
5

Plate B.6

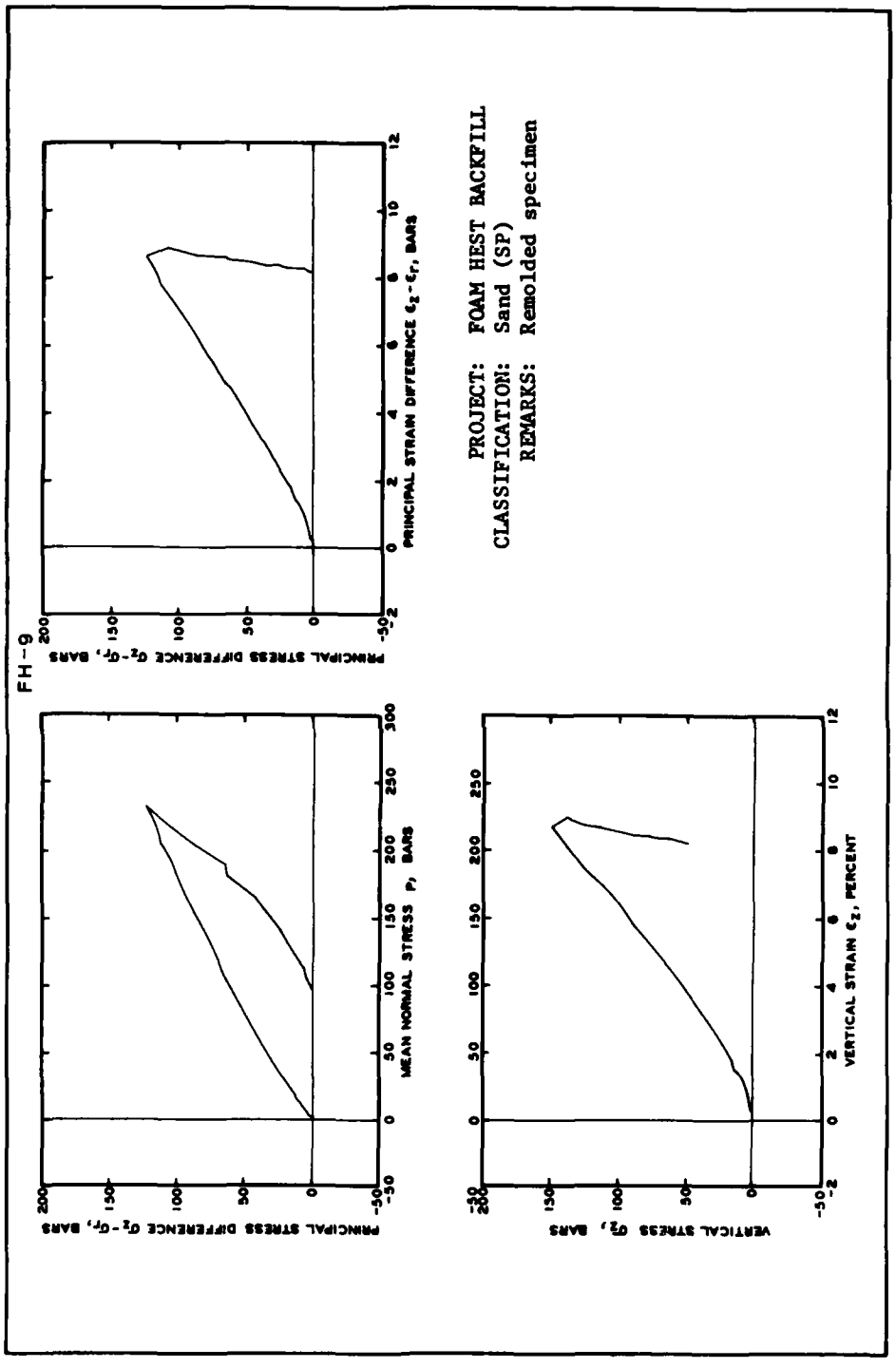

Results of static TX K_o test FH.9.

Plate B.7

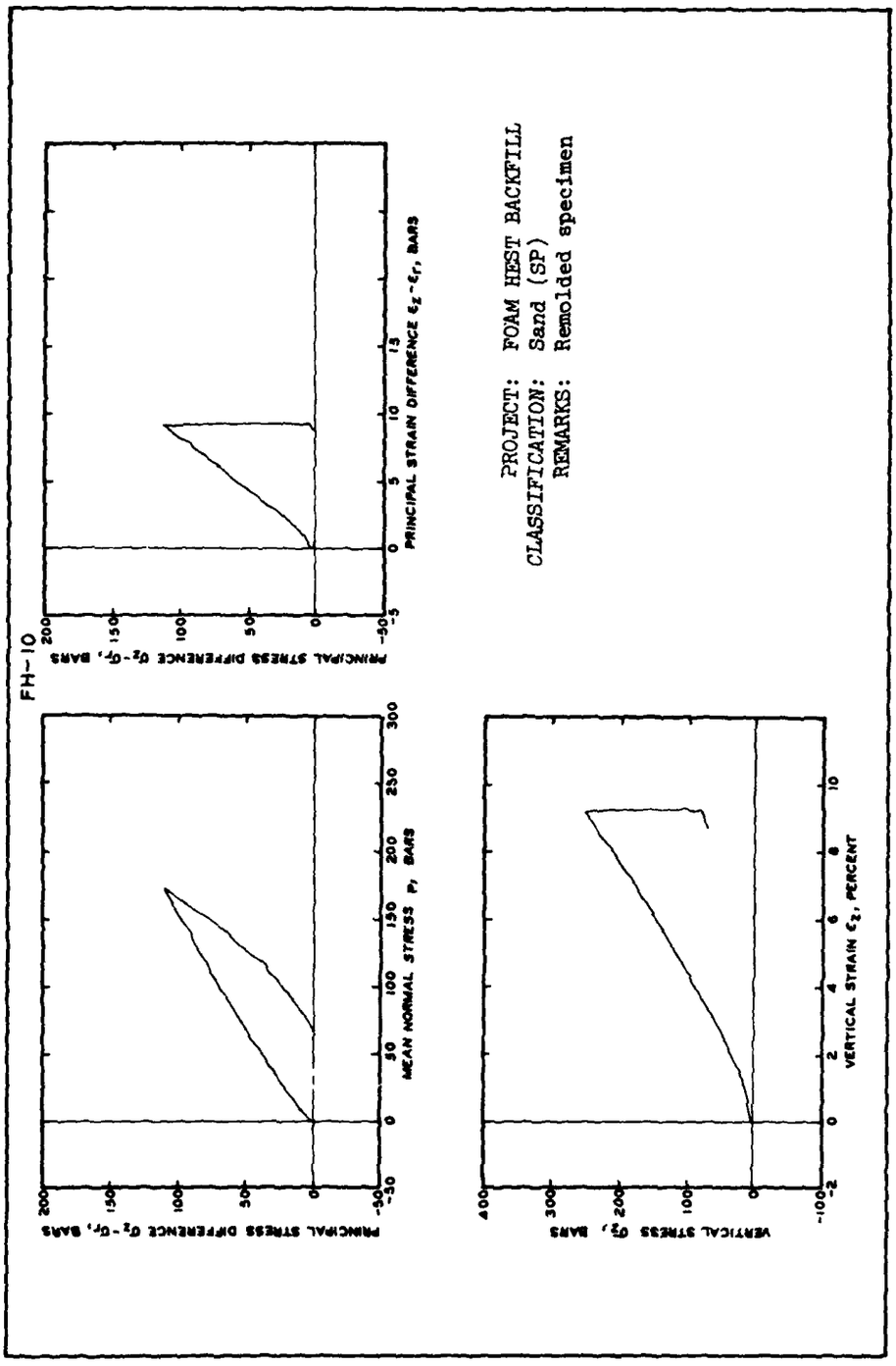

Results of static stress controlled K_o test FH.10

Plate B.8

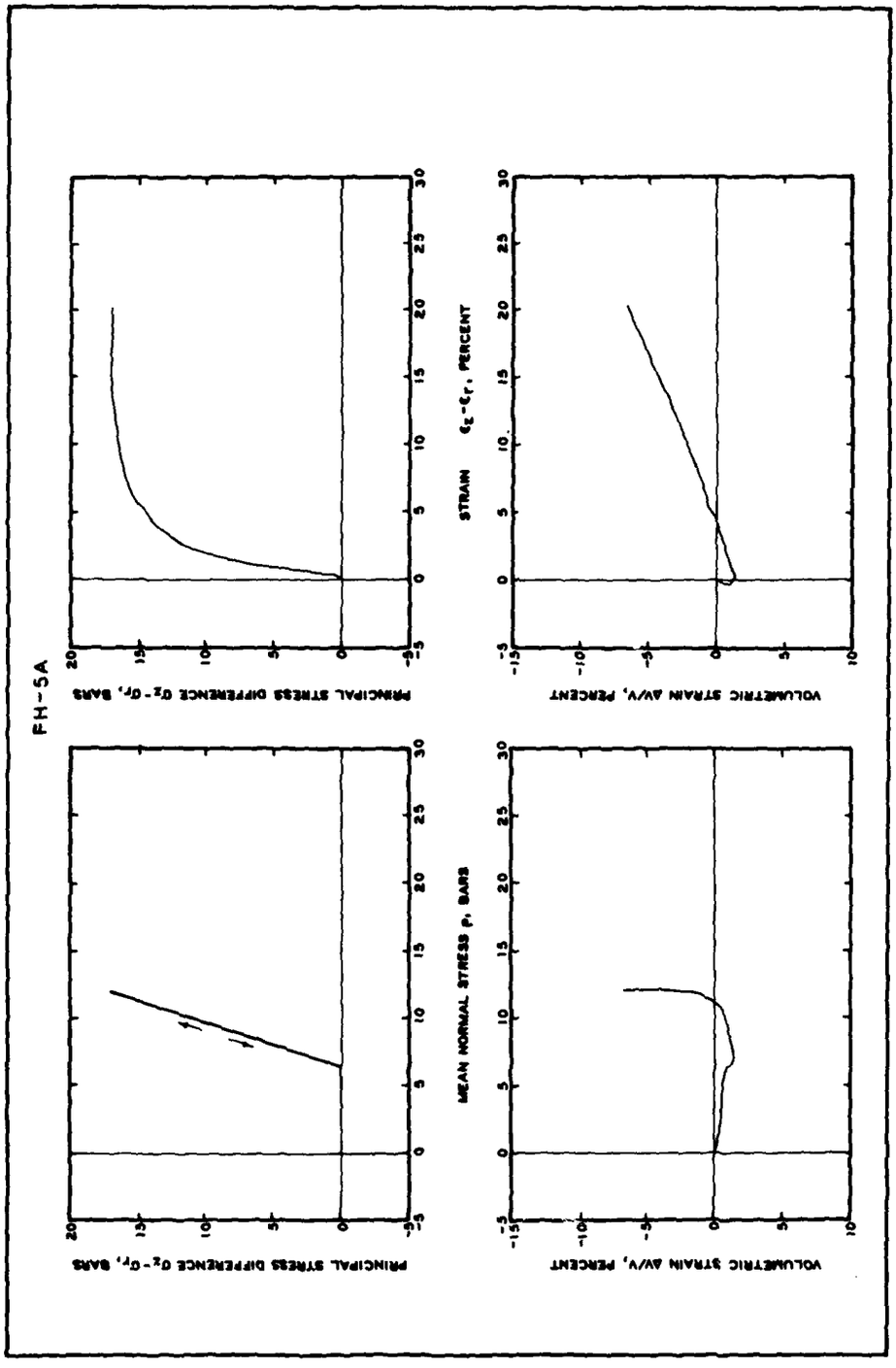

Results of static stress contress controlled, constant σ_r test FH.5A

Plate B.9

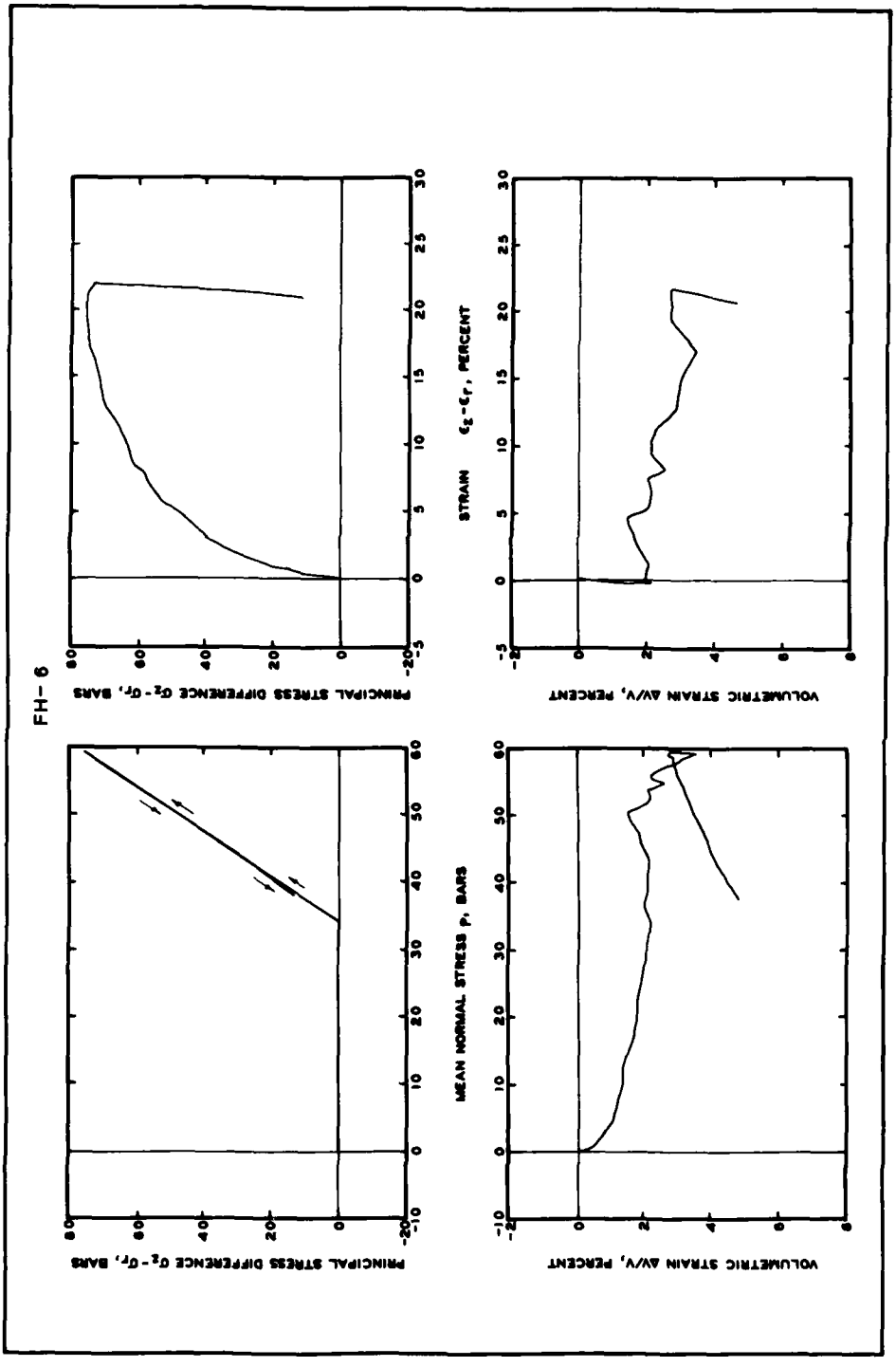

Results of static stress controlled, constant σ_r test FH.6

Plate B.10

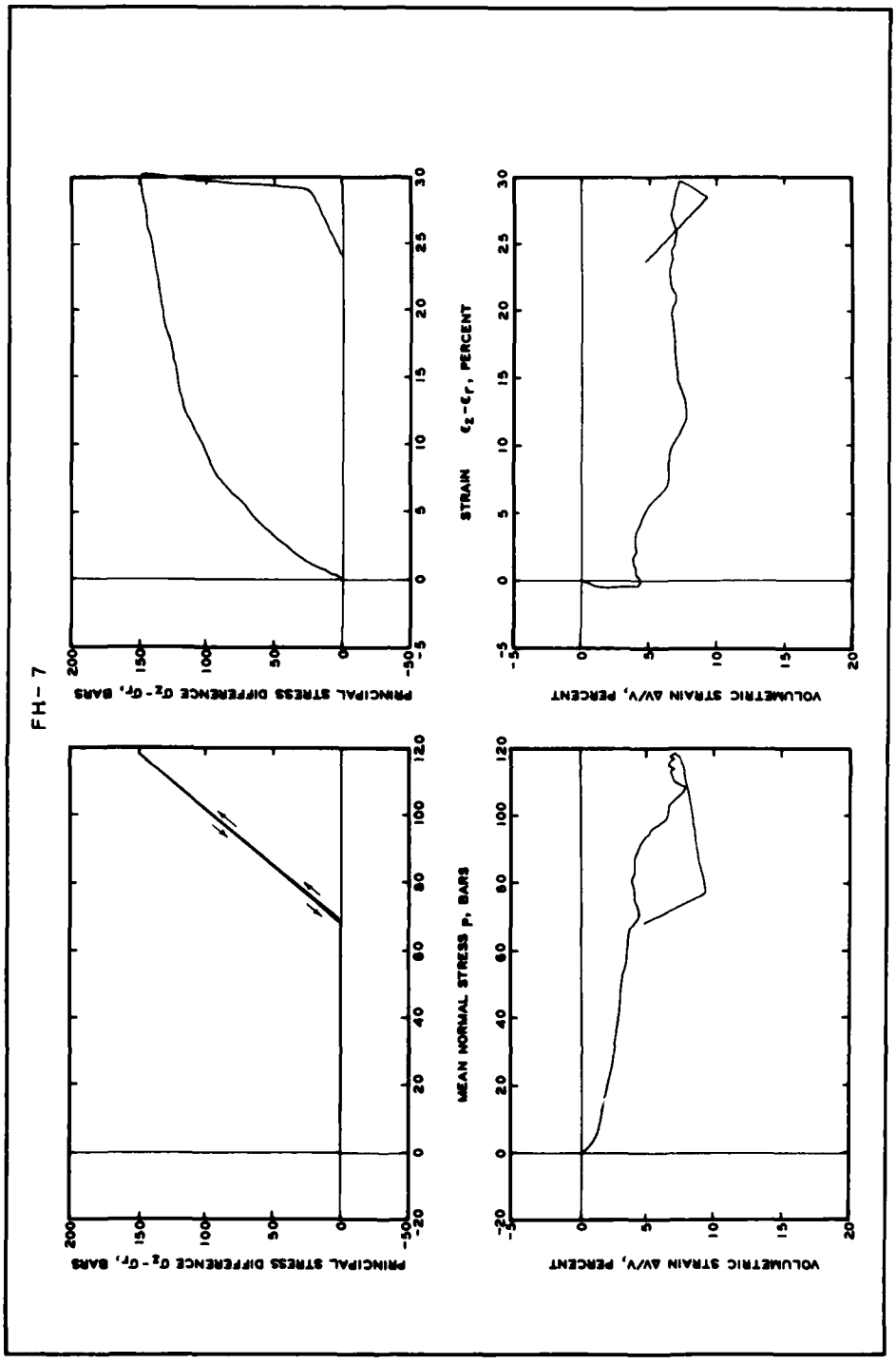

Results of static stress controlled, constant σ_r test FH.7

Plate B.11

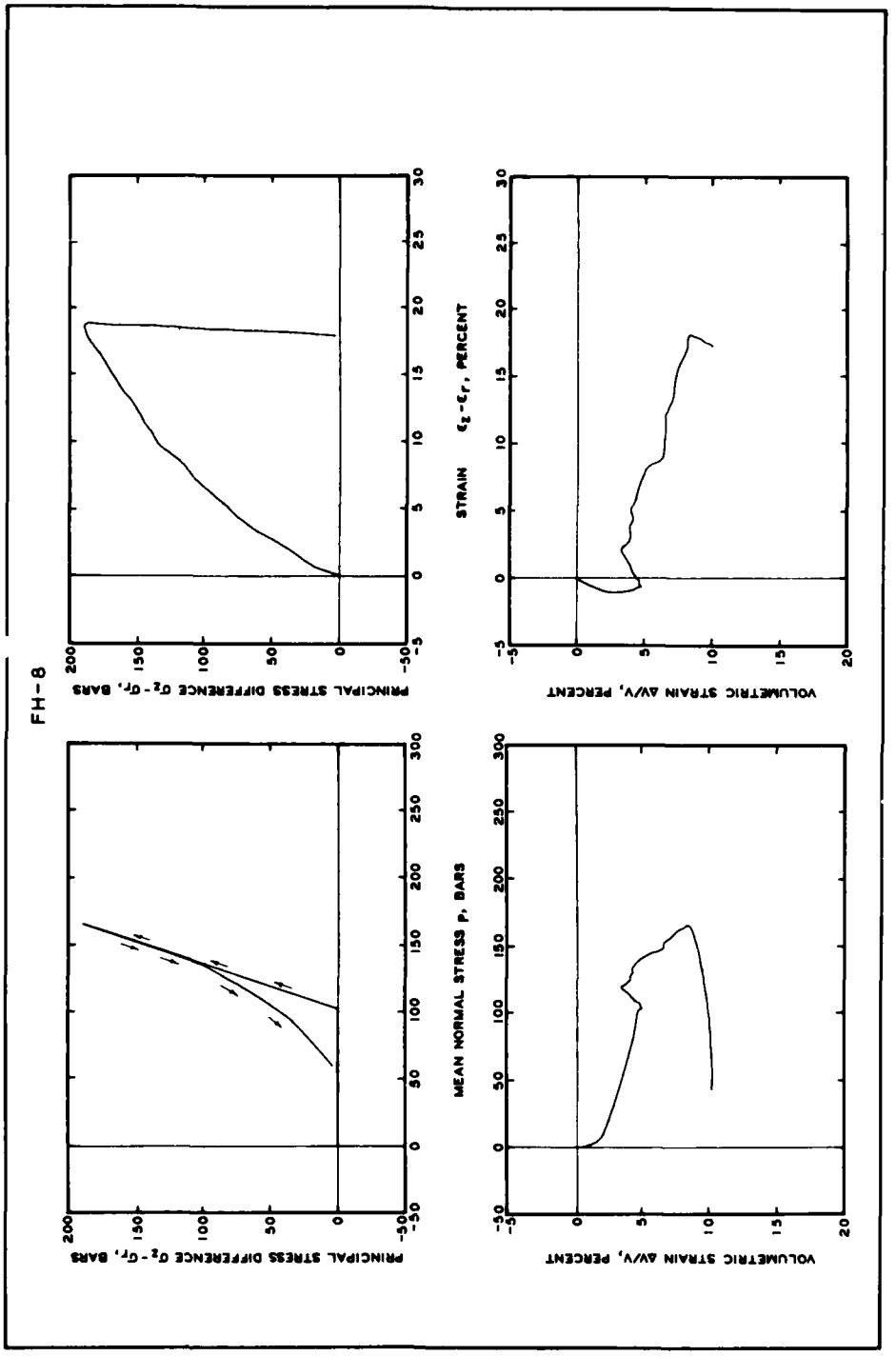

Results of static stress controlled, constant σ_r test FH.8

Plate B.12

APPENDIX C

CAP MODEL EQUATIONS AND FITS TO SOIL MATERIALS

Mechanical response of the soil materials represented in the FE calculations described in the main text was simulated by a nonlinear elastic/nonideally plastic (cap) model.[8] The fundamental or general functional equations of the cap model are given in Figure C.1. Property parameters, mathematical functions, and fitting constants for the specific cap model subroutine incorporated in the HONDO FE code for the proposed calculations are given in Figure C.2. Numerical values for the various constants that were derived in fitting the model to properties recommended for the FH1 sand backfill and the hypothetical clay backfill (see Appendix B) are listed in Table C.1. Values for the native soil materials outside the backfilled excavation are the same as those listed for the FH1 sand.

Comparisons of the cap model fits with the UX stress-strain relations recommended for the sand and clay are shown in Figures C.3 and C.4, respectively. Figures C.5 and C.6 show comparisons for UX stress paths and TX failure envelopes.

Table C.1 Values of Constants from Cap Model Fits to Recommended Soil Properties

Constant	Unit	Sand	Clay
A	bars	404.145	5.7735
B	$bars^{-1}$	0.000625	0.04
C	bars	404.145	1.1547
R_0	---	3.35	8.5
R_1	---	-0.35	0.0
RR	$bars^{-1}$	0.005	0.0
W	---	0.5	0.048
D	$bars^{-1}$	0.00015	0.015
α	---	0.0	1.0
D_1	$bars^{-1}$	0.0	0.035
D_2	$bars^{-2}$	0.0	0.0
W_F	$bars^{-2}$	0.0	-0.0000115
D_F	$bars^{-1}$	0.0	0.02
W_K	bars	12,033.162	697.419
B_K	---	0.7759	0.0
D_K	$bars^{-1}$	0.1	0.0
D_{K1}	$bars^{-2}$	0.0	0.0
D_{K4}	bars	1,500.0	50,000.0
D_{K5}	$bars^{-2}$	0.02	0.00003
G_{max}	bars	8,500.0	181.935
G_R	---	0.8619	0.0
G_1	$bars^{-1}$	5.0	0.0
ρ	g/cc	1.63	1.54

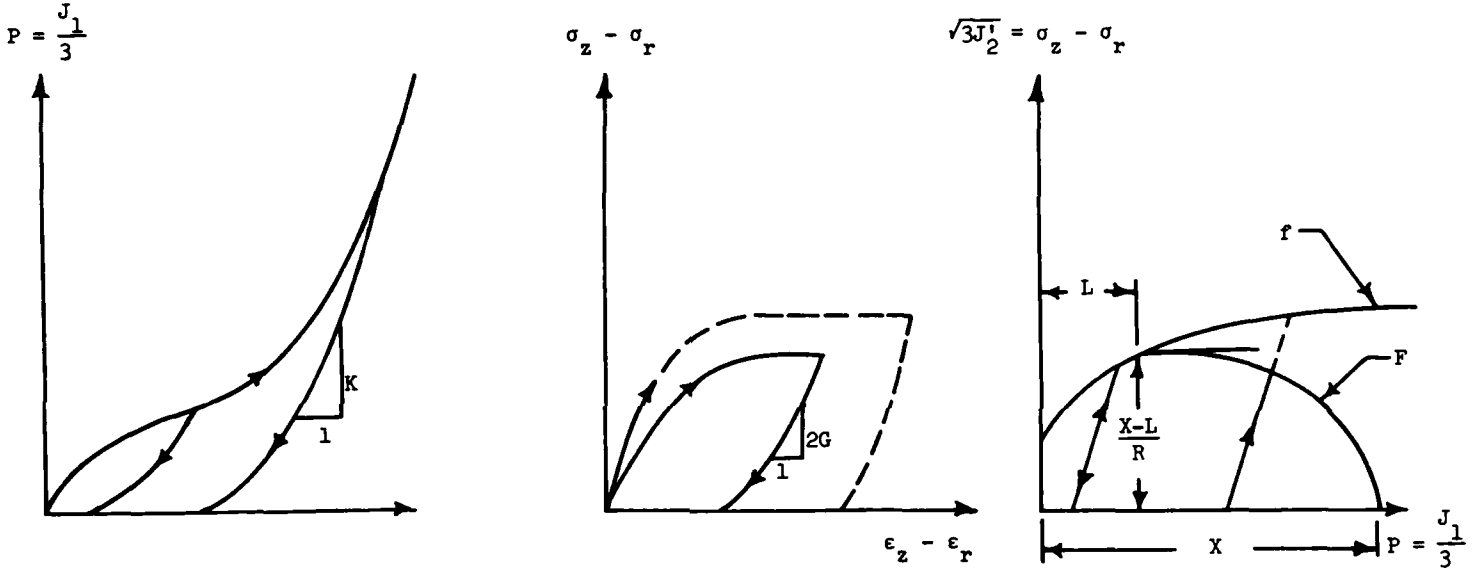

ISOTROPIC COMPRESSION TEST

TRIAXIAL COMPRESSION TESTS

ELASTIC BULK MODULUS

$K = K(J_1 , \varepsilon^P_{KK})$

HARDENING FUNCTION

$\varepsilon^P_{KK} = \varepsilon^P_{KK}(J_1) = \varepsilon^P_{KK}(X)$

ELASTIC SHEAR MODULUS

$G = G(\sqrt{J_2'} , \varepsilon^P_{KK})$

FAILURE ENVELOPE

$f = f(J_1 , \sqrt{J_2'}) = 0$

ELLIPTICAL CAP

$F = (J_1 - L)^2 + R^2 J_2' - (X-L)^2 = 0$

CAP SHAPE FUNCTION

$R = R(L)$

Figure C.1 Fundamental equations of the cap model.

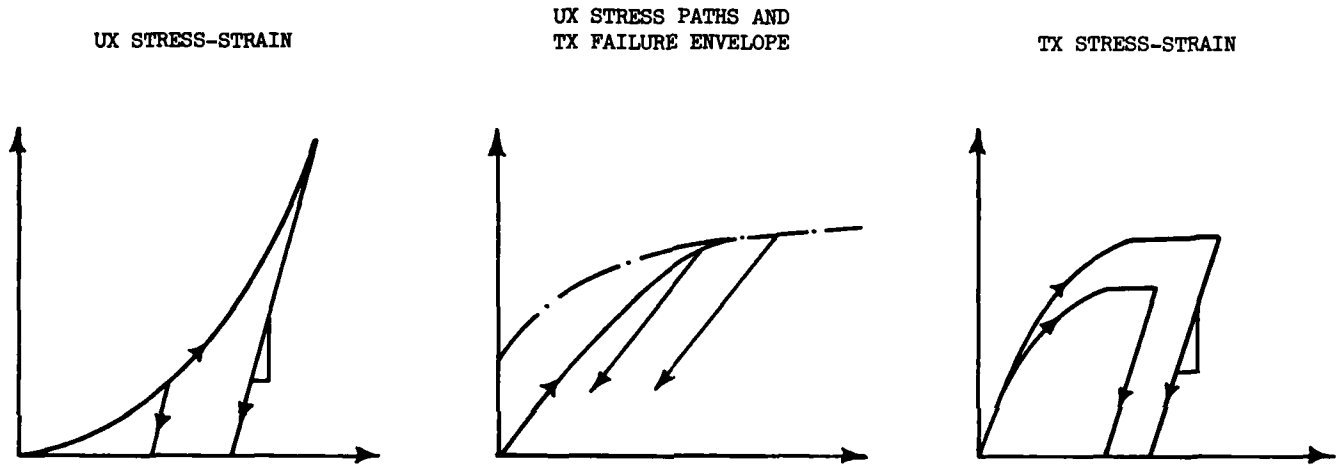

Parameter	Mathematical Functions (Compression +)	Fitting Constants
Elastic Bulk Modulus	$K = W_K[1 - B_K \exp(-D_K J_1 - D_{K1} J_1^2)] + D_{K4}[1 - \exp(-D_{K5} J_1^2)]$	W_K, B_K, D_K, D_{K1}, D_{K4}, D_{K5}
Elastic Shear Modulus	$G = G_{max}[1 - G_R \exp(-G_1 \sqrt{J_2'})]$	G_{max}, G_R, G_1
Failure Envelope	$f = \sqrt{J_2'} = C - A \exp(-BJ_1)$	C, A, B
Hardening Function	$\varepsilon_{KK}^P = -W[\exp(-DX) - 1 - \alpha DX \exp(-D_1 X - D_2 X^2)] + W_F X^2 \exp(-D_F X)$	W, D, α, D_1, D_2, D_F, W_F
Cap Shape Function	$R = R_0[1 + R_1 \exp(-RR \cdot L)]$	R_0, R_1, RR

Figure C.2 Property parameters, mathematical functions, and fitting constants for cap model used in finite-element calculations.

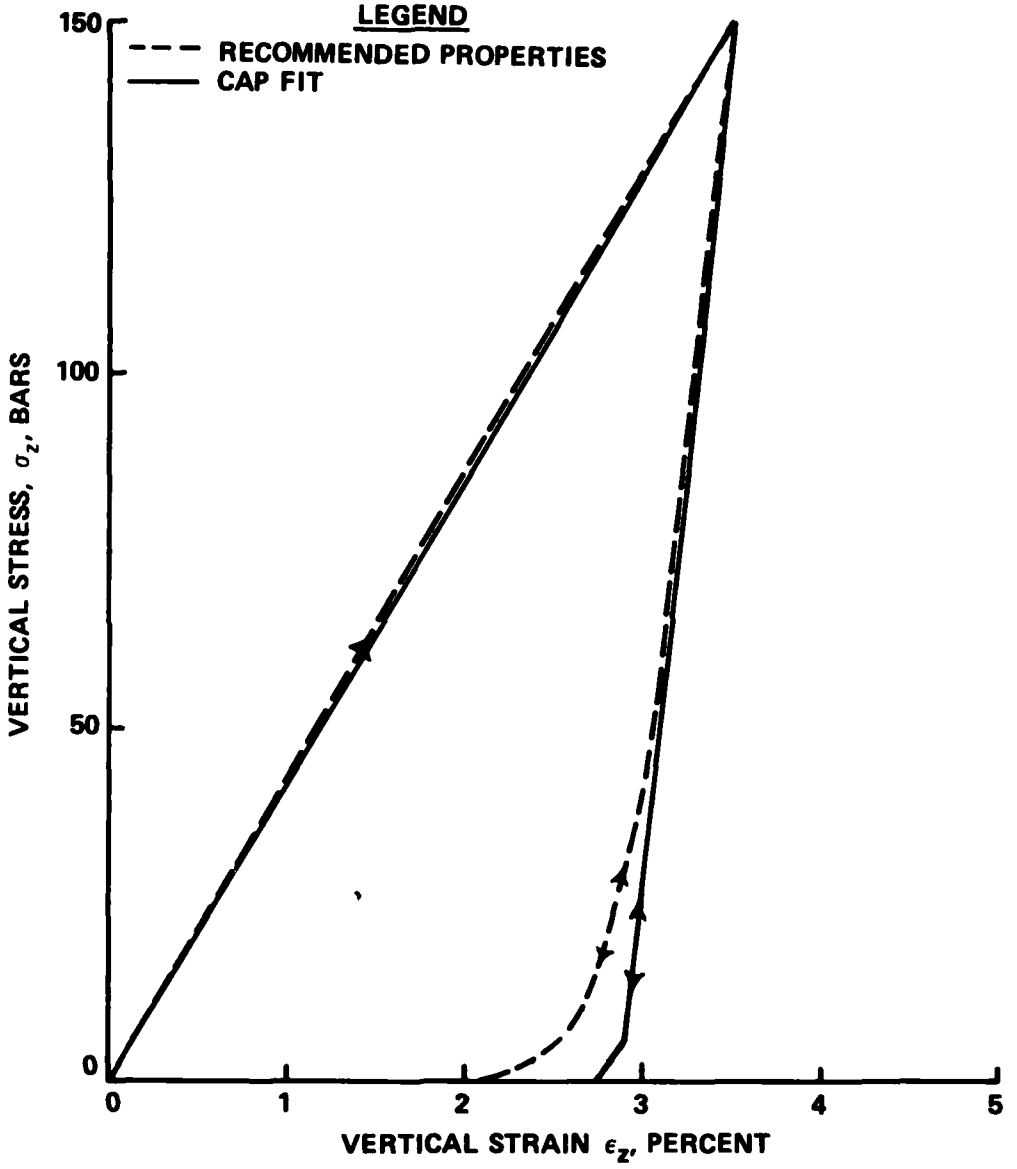

Figure C.3 Comparison of cap model fit with recommended UX stress-strain relation for sand backfill.

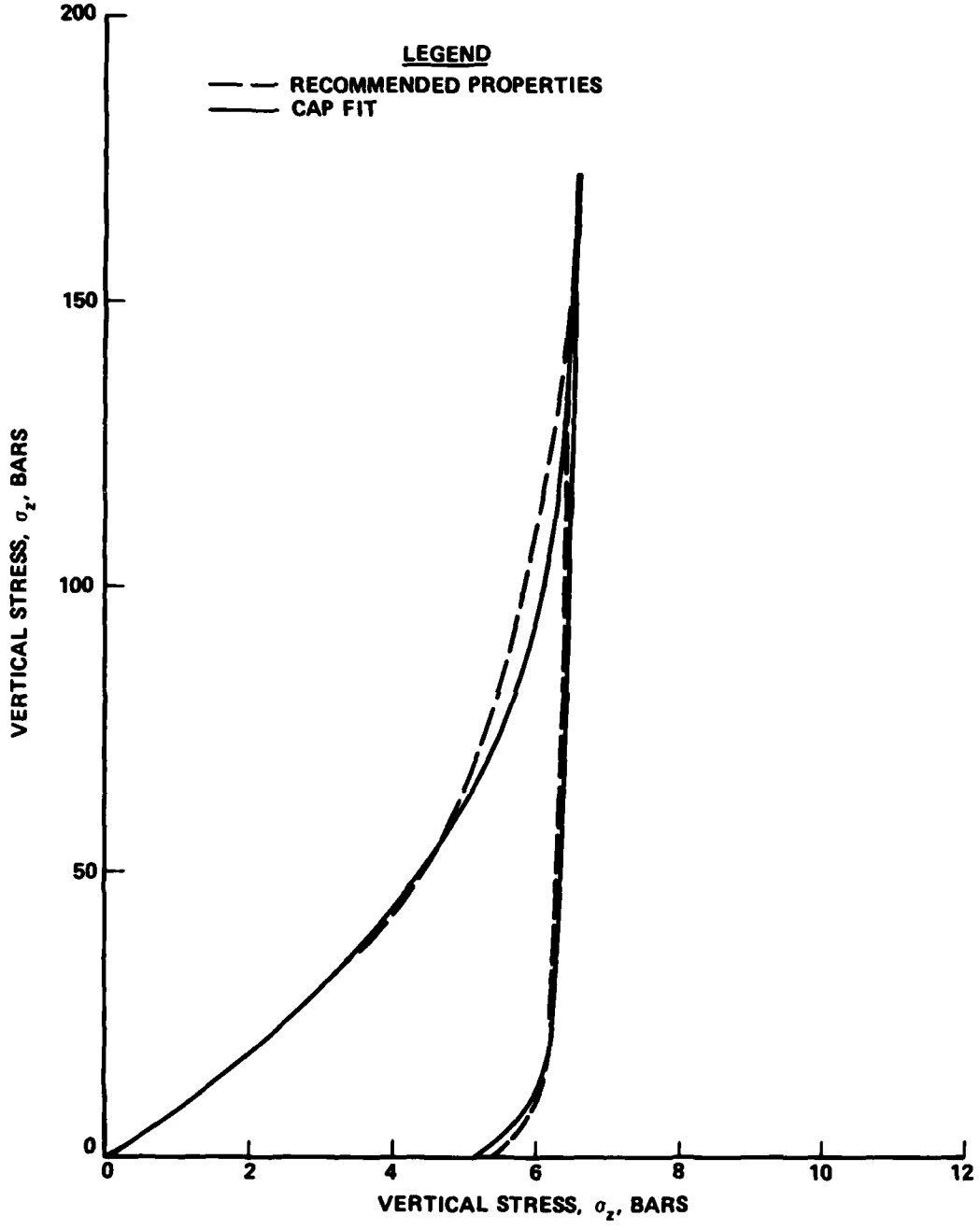

Figure C.4 Comparison of cap model fit with recommended UX stress-strain relation for clay backfill.

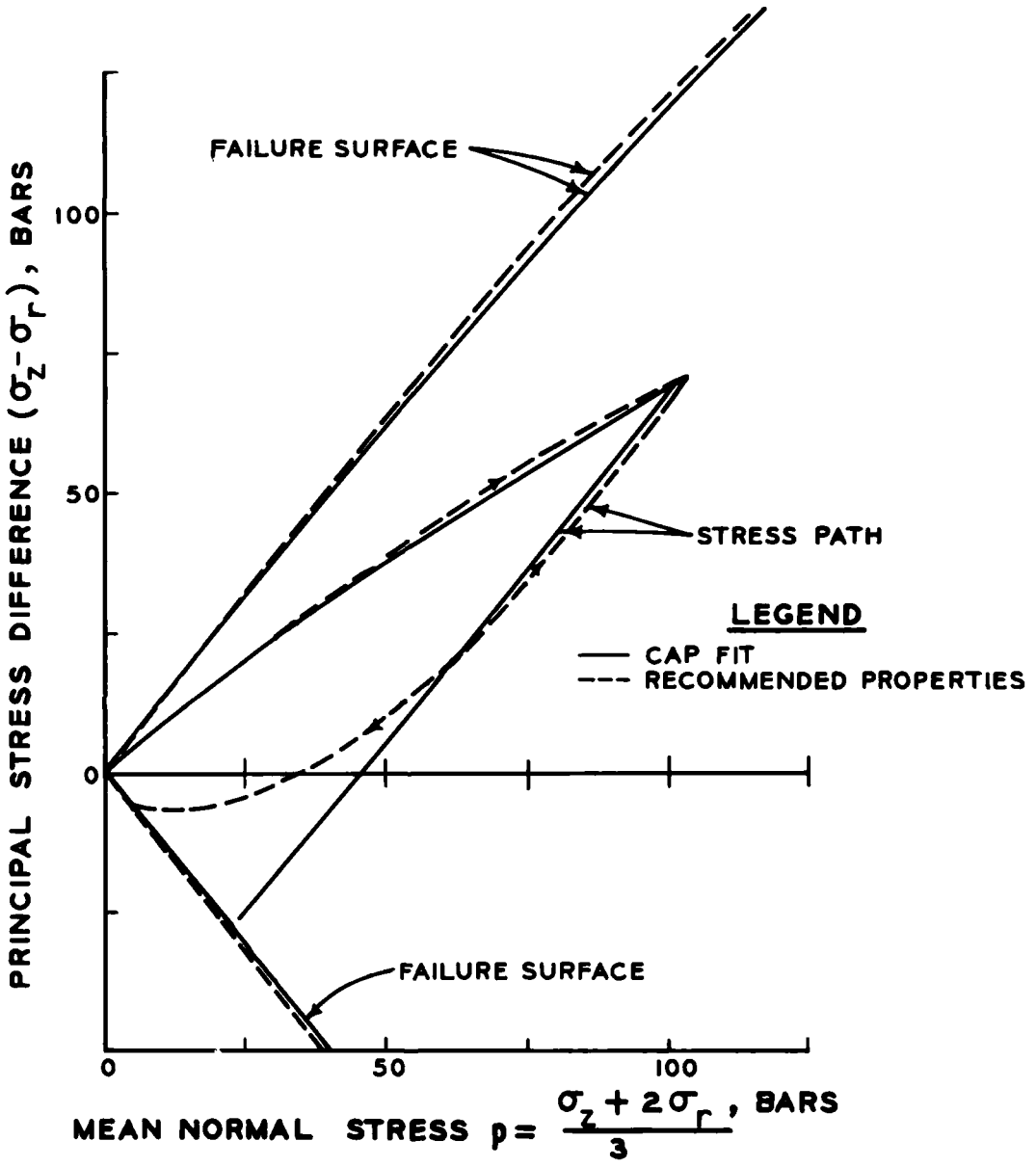

Figure C.5 Comparison of cap model fit with recommended UX stress-path and TX failure surface for sand backfill.

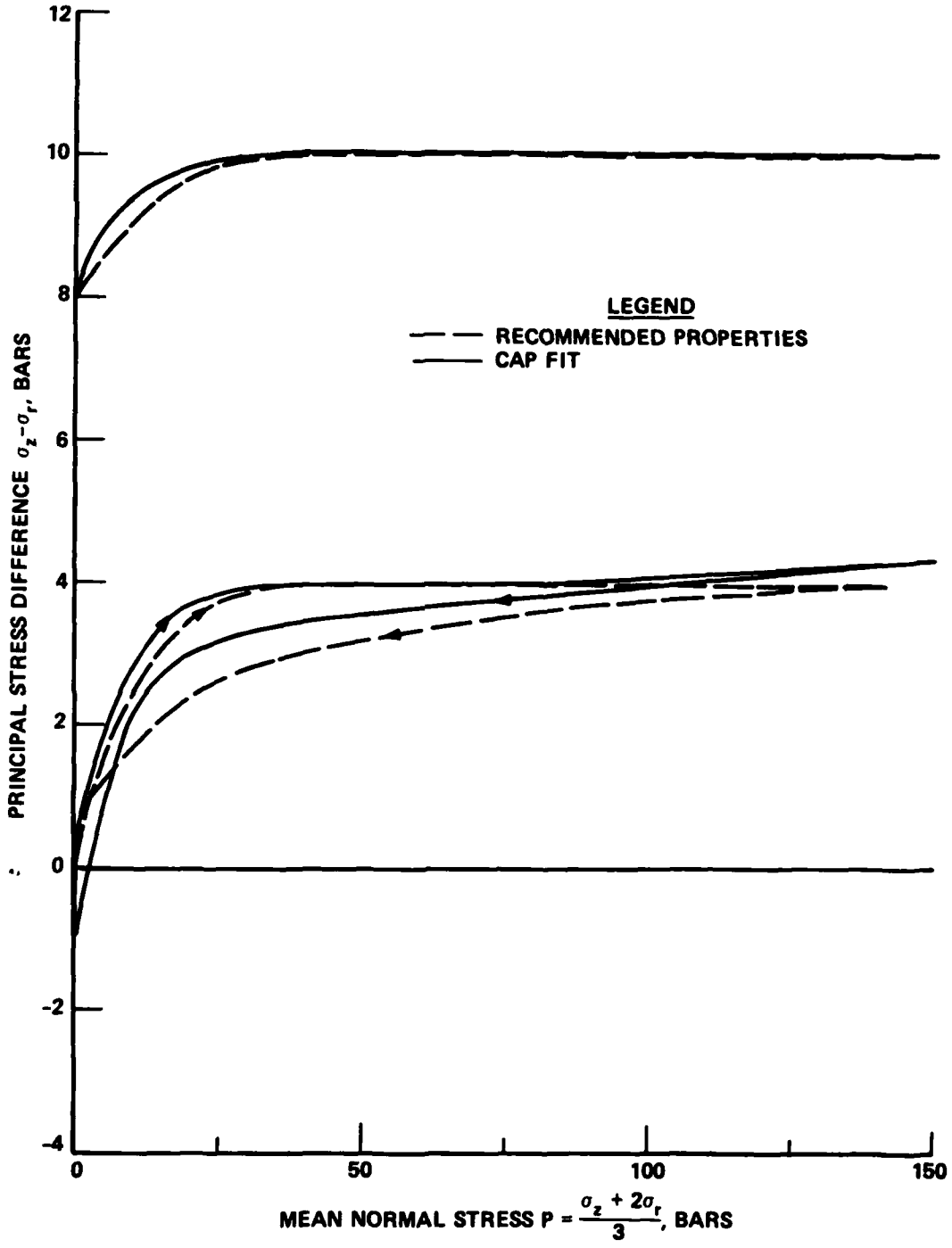

Figure C.6 Comparison of cap model fit with recommended UX stress-path and TX failure surface for clay backfill.

DISTRIBUTION LIST

DEPARTMENT OF DEFENSE

Director, Defense Advanced Research Project Agency
ATTN: Technical Information Office

Defense Technical Information Center
12 cy ATTN: TC/Mr. Meyer B. Kahn

Director, Defense Intelligence Agency
ATTN: Technical Library
DB-4C/J. Burfening
B. Morris

Director, Defense Nuclear Agency
ATTN: TITL
DDST
SPSS/J. Galloway
2 cy SPSS/K.Goering
SPSS/G.Ullrich
SPSS/E. Furbee

Under Secretary of Defense for Research and Engineering
ATTN: Strategic and Space Systems (OS)

Commander, Field Command, Defense Nuclear Agency
ATTN: FCTMOT/J. Strode

Director, Joint Strategic Targeting Planning Staff
ATTN: JLTW/R. Carpenter

DEPARTMENT OF THE ARMY

Director, BMD Advanced Technology Center
ATTN: ATC-T

Office, Chief of Engineers
ATTN: DAEN-MPE-T/D. Reynolds
DAEN-RDL
2 cy DAEN-ASI-L

Commander, U. S. Army Engineer Center
ATTN: DT-LRC

Division Engineer, U. S. Army Engineer Division, Huntsville
ATTN: HNDED-SR

Commander, U. S. Army Nuclear and Chemical Agency
ATTN: Library

Commander/Director, U. S. Army Cold Regions Research and Engineering Laboratory
ATTN: Library

Director, U. S. Army Construction Engineering Research Laboratory
ATTN: Library

DEPARTMENT OF THE NAVY

Officer-in-Charge, Naval Construction Battalion Center
ATTN: Code LO8A/Library
Code L51/J. Crawford

Commander, Naval Facilities Engineering Command
ATTN: Code 09M22C/Technical Library

Office of Naval Research
ATTN: Code 715/Technical Library

DEPARTMENT OF THE AIR FORCE

Air Force Weapons Laboratory, AFSC
ATTN: NTE/M. Plamondon
NTES/R. Jolley
NTED/E. Seusy

Deputy Chief of Staff, Research, Development, and Acquisition
ATTN: AFRDQSM

Ballistic Missile Office, AFSC
ATTN: MNNXH/D. Gage
MNNXH/M. Del Vecchio

Vela Seismological Center
ATTN: C. Ullrich

DEPARTMENT OF ENERGY

Nuclear Regulatory Commission, Directorate of Licensing Regulations
ATTN: Site Analysis Branch/L. Heller

Sandia Laboratories
ATTN: Div 5521/S. Key

DEPARTMENT OF DEFENSE CONTRACTORS

Aerospace Corporation
ATTN: T. Alley
L. Selzer

Agbabian Associates
ATTN: M. Agbabian

Applied Theory, Inc.
ATTN: J. Trulio

Boeing Company
ATTN: Aerospace Library

California Research and Technology, Inc.
ATTN: Library

Electromechanical Systems of New Mexico, Inc.
ATTN: R. Shunk

DEPARTMENT OF DEFENSE CONTRACTORS (Continued)

Civil Systems, Inc.
ATTN: J. Bratton

Eric H. Wang, Civil Engineering Research Facility
ATTN: J. Lamb

General Electric Company, TEMPO-Center for Advanced Studies
ATTN: DASIAC

IIT Research Institute
ATTN: R. R. Robinson

Higgins, Auld & Associates
ATTN: N. Higgins

University of Illinois, Consulting Services
ATTN: W. Hall
J. Haltiwanger

Karagozian & Case, Structural Engineers
ATTN: J. Karagozian

J. H. Wiggins Co., Inc.
ATTN: J. Collins

Merritt Cases, Inc.
ATTN: J. Merritt

DEPARTMENT OF DEFENSE CONTRACTORS (Continued)

R&D Associates
ATTN: R. Port
J. Lewis

SRI International
ATTN: A. Florence
J. Gran

Dr. Ted Belytschko

Terra Tek, Inc.
ATTN: Library

TRW Defense and Space Systems Group
ATTN: Technical Information Center
N. Lipner

TRW Defense and Space Systems Group
ATTN: G. Hulcher

Weidlinger Associates, Consulting Engineers
ATTN: M. Baron
J. Wright

Weidlinger Associates, Consulting Engineers
ATTN: J. Isenberg
H. Levien

In accordance with letter from DAEN-RDC, DAEN-ASI dated 22 July 1977, Subject: Facsimile Catalog Cards for Laboratory Technical Publications, a facsimile catalog card in Library of Congress MARC format is reproduced below.

Windham, Jon Enrique

Finite-element calculations of Foam HEST 1 / by Jon E. Windham. Vicksburg, Miss. : U. S. Waterways Experiment Station ; Springfield, Va. : available from National Technical Information Service, 1980.

115 p. : ill. ; 27 cm. (Miscellaneous paper - U. S. Army Engineer Waterways Experiment Station ; SL-80-1)

Prepared for Defense Nuclear Agency, Washington, D. C., under DNA Subtask X99QAXSC062, Work Units 14 and 30, and DNA Subtask H19HAXSX337, Work Unit 15.

References: p. 72-73.

1. Backfills. 2. Finite element method. 3. Foam HEST I. 4. HE explosions. 5. Shallow buried structures. 6. Simulation. 7. Soil-structure interaction. 8. Underground tests. I. United States. Defense Nuclear Agency. II. Series: United States. Waterways Experiment Station, Vicksburg, Miss. Miscellaneous paper ; SL-80-1.

TA7.W34m no.SL-80-1


FILM